12-18-2020

MICRO-PHYSIOLOGICAL MODELS TO MIMIC MUCOSAL BARRIER COMPLEXITY OF THE HUMAN INTESTINE IN VITRO

Abhinav Sharma
University of Massachusetts Amherst

MICRO-PHYSIOLOGICAL MODELS TO MIMIC MUCOSAL BARRIER COMPLEXITY OF THE HUMAN INTESTINE IN VITRO

A Dissertation Presented

by

ABHINAV SHARMA

Submitted to the Graduate School of the
University of Massachusetts Amherst in partial fulfillment
of the requirements for the degree of

DOCTOR OF PHILOSOPHY

September 2020

Department of Chemical Engineering

MICRO-PHYSIOLOGICAL MODELS TO MIMIC MUCOSAL BARRIER COMPLEXITY OF THE HUMAN INTESTINE IN VITRO

A Dissertation Presented

by

ABHINAV SHARMA

Approved as to style and content by:

_____
Neil S. Forbes, Co-chair

_____
Jungwoo Lee, Co-chair

_____
Jeffrey L Blanchard, Member

_____
Jessica D. Schiffman, Member

_____
John Klier, Department Head
Department of Chemical Engineering

DEDICATION

To parents Satya and Melaram Sharma, and my wife Priyanka Itkar.

‘This is your win more than it is mine’

‘Perseverance is the key to a successful **PhD**’

ACKNOWLEDGMENTS

I am grateful to my advisors Dr. Neil Forbes and Dr. Jungwoo Lee for giving me the opportunity to work on this project. I am thankful to both for supporting me and providing access to resources throughout my stay here. I would like to thank Dr. Jessica Schiffman and Dr. Jeffrey Blanchard for serving on my thesis committee, being available when needed and providing useful feedback. I am also thankful to Dr. Shelly Peyton and Dr. John Klier for their help and advice at critical times. I have been fortunate to have met academic advisors at every stage of my life that have helped me take the next step and I cannot thank them enough. Dr. Ramesh Sharma during high school, Dr. S.V. Dharwadkar during undergrad and Dr. Dipankar Bandyopadhyay during Masters'. I am very thankful for all the good times and the moral support from lab mates Nele, Vishnu, Ryan, James, Shane, Shoshana, Yongkuk, and Jun-Goo. I am also thankful to have found great people to enjoy life with outside the lab including Kiran, Pranav, Priyaa, Koushik, Ronak, Sagar, Sampada, Nihar, and Gaurav. I would also like to thank the families in the US that made me feel at home away from home, Ravi and Radhika for inviting us over for holidays, Ryan's family for the skiing trips, Vishnu's family for cooking great Indian food during their visits to Amherst, and James and Chelcie for being kind and supportive.

I would not have reached this far without the sacrifices and unconditional support from my parents. Along the way, I have also received a lot of love and support from my sister Archana, her husband Dayaram Sharma and her family, my in-laws Rajashree, Sudhir, Pritam and Priyanka Itkar, my extended family including grandparents, cousins, uncles and aunts. I am most grateful to have my wife Priyanka beside me in this humbling PhD journey. No words can explain what she has done for me in the past ten years.

ABSTRACT

MICRO-PHYSIOLOGICAL MODELS TO MIMIC MUCOSAL BARRIER COMPLEXITY OF THE HUMAN INTESTINE IN VITRO

September 2020

ABHINAV SHARMA

B.E., BABASAHEB AMBEDKAR MARATHWADA UNIVERSITY

M.Tech., INDIAN INSTITUTE OF TECHNOLOGY GUWAHATI

Ph.D., UNIVERSITY OF MASSACHUSETTS AMHERST

Directed by: Professor Neil S. Forbes and Dr. Jungwoo Lee

The mucosal barrier in the intestine is vital to maintain selective absorption of nutrients while protecting internal tissues and maintaining symbiotic relationship with luminal microbiota. This bio-barrier consists of a cellular epithelial barrier and an acellular mucus barrier. Secreted mucus regulates barrier function via in situ biochemical and biophysical interaction with luminal content that continually evolves during digestion and absorption. Increasing evidence suggests that a mucus barrier is indispensable to maintain dynamic homeostasis of the gastrointestinal tract. However, the importance of mucus barrier has been largely underrated for in vitro mucosal tissue modeling. The major gap is the lack of experimental material (i.e. functional mucins) and platforms to integrate a relevant thickness of mucus layer with an epithelium under physiological conditions.

Here we report our progress on developing human-relevant models of the mucosal barrier in physiological settings by using natural mucins derived from a porcine small intestine (PSI). To overcome limited availability of functional mucus, we first developed a simple and scalable protocol for natural mucus extraction by directly solubilizing a

relatively sterile inner mucus layer from PSI that is readily accessible. Subsequently, functional separation of mucin proteins was performed by exploiting pH-dependent reversible sol-gel transition. Under optimized alkaline condition (0.01M NaOH), the mucus layer was selectively solubilized from the mucosal surface with a 72% yield (1275 mg/m PSI). The extracted and purified natural mucins retained essential biophysical and biochemical characteristics. The in vitro mucus barrier model enabled us to discover ionic (Ca^{2+}) environment dependent mucus barrier and its transport properties.

The mucus barrier was successfully integrated with human epithelial cell layer (HT-29), which allowed the studies of bi-directional crosstalk between luminal content and tissue immune cells through a physiologically relevant mucosal interface. The applied mucus barrier did not cause any cytotoxic or immunogenic effects to human intestinal and immune cells. As expected, mucus prevents the transmigration of probiotic bacteria VSL#3. In the absence of mucus, these bacteria caused epithelial damage, immune cell differentiation and induced production of pro-inflammatory cytokines IL-8 and TNF-α. The most intriguing result from these studies was that mucus increased the transmigration of pathogenic Salmonella. Similar to the transmigration of probiotic bacteria, breach of the mucosal barrier by Salmonella induced production of IL-8 and TNF-α. The importance of bacterial motility was confirmed by showing that Salmonella with a knockout that prevents flagella formation does not penetrate the barrier. Co-cultures of VSL#3 and Salmonella in the mucosal barrier platform demonstrated the differences in epithelial and immune cell responses under symbiosis or dysbiosis like conditions.

Taking bioengineering approaches, we have developed mucosal barrier models of intestines. Established models represent cellular and extracellular complexities in a

controlled and accessible manner. We envision that in vitro mucosal barrier models will serve as an enabling tool for understanding basic biology and disease progression in the intestines. Technologies, methods, and protocols developed here lay the foundation for future clinical applications and personalized medicine.

GRAPHICAL ABSTRACT

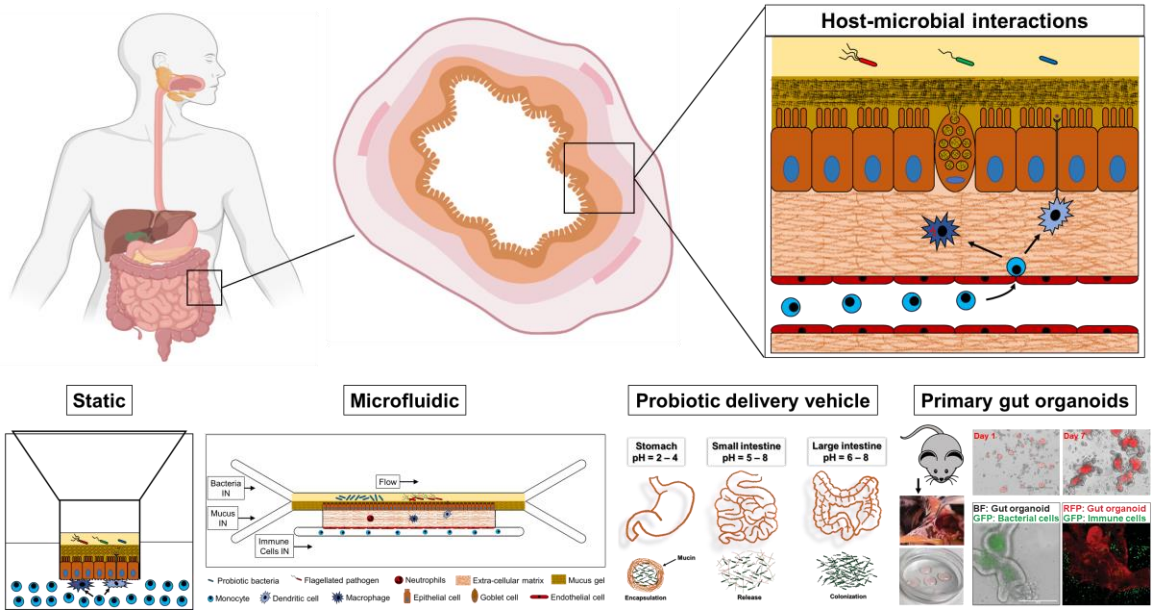

TABLE OF CONTENTS

Page

LIST OF FIGURES

Figure **Page**

ADDITIONAL FIGURES

Figure **Page**

CHAPTER 1

INTRODUCTION

The gastro-intestinal tract (GIT) performs essential functions in the human body. GIT is responsible for the processing and digestion of food and absorption of essential nutrients for survival. Apart from nutrient absorption, GIT maintains physiological homeostasis by protecting the internal tissue from persistent chemical, physical, and microbial insults while facilitating passage of desired molecules [1-3]. GIT is the largest reservoir of bacteria in the body with bacterial density as high as 10^{12} cfu/g [4] and houses almost 70% of the immune system in the form of gut-associated lymphoid tissue (GALT) [5]. The mucosal barrier along the luminal side of GIT is essential for protection against the harsh luminal environment along with development of the host immunity [6]. This bio-barrier is composed of a cellular epithelial barrier and an acellular mucus barrier. Acellular mucus barrier is the first line of defense and physically separates the acid and digestive enzymes in the stomach and small intestines, and dense bacterial population in the large intestines from underlying tissue.

The GIT mucosal barrier is unique due to its strategically modified anatomical structure, cellular composition, mucus layer thickness and complex biochemical milieu. These features are key to maintain the balance between absorption and protection from the luminal compartment [7-9]. The structural and environmental complexity, difficulty to access the GIT, and dissimilar microbiota population have limited the use of live animal models for studying dynamic interaction of mucosal barrier with luminal components that affect the barrier function [10]. As a consequence, great progress has been made to recreate intestinal cellular physiology [11], three-dimensional (3D) morphology [12-13], mechanically

active environment [14], and microenvironment compatible for host-microbe interactions [12, 15-17] in vitro. The in vitro systems allow the study of fundamental interactions between different cell types of the intestine by eliminating biological complexity inherently present in the tissue in vivo. In vitro functional human mucosal barrier models serve as an enabling tool for understanding basic biology and disease progression in the gastrointestinal tract. Recently, these models are becoming invaluable pre-clinical testing platforms for orally administrated drug compounds and probiotics since they provide an effective, low cost and high throughput way to gain useful information before performing cost-intensive animal and human trials.

Intestinal epithelium is a monolayer of cells that are highly polarized and consist of the absorptive enterocytes and the secretory goblet cells as major cell populations. In vitro, Caco-2 cells are the most commonly used model system for mimicking the epithelium as they spontaneously differentiate into mature enterocytes in culture that express morphological features such as the brush border expression, tight junctions and surface microvilli [18] that are similar to small intestine in vivo [19]. HT-29 colon adenocarcinoma cells cultured in medium without glucose also undergo enterocytic differentiation [20]. Further advancement in this field was achieved by treating HT29 cell line with chemotherapeutic drugs methotrexate and 5-fluorouracil. Treatment with these drugs caused differentiation of HT29 cells into a goblet cell phenotype and with further selection stable mucus producing cell lines HT29-MTX and HT29-FU were established [21-22]. Co-culture of Caco-2 and HT29-MTX cells at different cell ratios was shown to represent the in vivo like cell population of the intestines. For example, a ratio of (9:1) Caco-2:HT-29 MTX closely

matched the Caco-2 monocultures that best represent the small intestinal cell population [23]. Extracellular matrix proteins like collagen, gelatin and Matrigel are used to recreate the basement membrane that provides attachment sites and support for the epithelial cell growth. Furthermore, these provide stimulation for epithelial cell expansion, spreading, and differentiation [24].

For drug/nutrient absorption and transport studies, epithelial cells are seeded onto permeable membrane supports made of polycarbonate and allowed to cover the entire membrane as a monolayer [25]. These membrane supports known as transwell inserts fit inside commonly used multi-well plates and create the apical and basolateral compartments mimicking the luminal as well as the basal sections of the intestinal tissues. Caco-2 cell monolayers in transwell inserts are the most commonly used model for drug transport across intestinal epithelium [26]. These monolayers have been heavily used by researchers to mechanistically study transport of drugs, nutrients, etc. Caco-2 and Raji B cell co-culture was used for M-cell like differentiation in transwells by normal [27] and inverted [28] configurations. M-cell like differentiation was used to study the process of transcytosis across the monolayer which is commonly observed in the small intestine and important for development of immunity. Finally, to incorporate a mucus layer in this model a triple co-culture of Caco-2, HT29-MTX and Raji B was used [29]

Mucosal interfaces are a major target for drug delivery and mucus layer is the first barrier that a free drug or a drug delivery vehicle must overcome before reaching the cell surface [30-31]. Although there have been successful efforts in stimulating the cultured epithelial cell

lines to secrete mucus, the amount of mucus secreted is very small compared to in vivo. In most cases mucus is observed in patches and does not fully cover the surface of epithelial cell layer. Also, due to high variability in the culture conditions and the amount of mucus produced under different culture conditions, researchers have applied mucus extracted from excised tissues to cultured cell layers on transwell membranes [32]. This approach provides multiple benefits over mucus secreting cell lines. A uniform layer of mucus can be applied while most mucus secreting cell layers form non-uniform or patchy mucus layer. The thickness of the mucus layer can be controlled precisely, whereas thickness control is not feasible with the mucus secreting cell layers. The composition and the concentration of mucus can be defined according to the organ system being mimicked. Experimental variations can be reduced by pooling large quantities of extracted mucus or using commercially available mucins. However, a few drawbacks of this approach are limited availability of human derived tissues and therefore use of animal derived mucus and potential cytotoxic effects of animal derived mucus on human cells.

Mucins are available commercially from different organs of animals but have been shown to have significantly degraded properties compared to native mucus that may cause the results of the studies to deviate from in vivo [33]. Obtaining highly purified mucins require very sophisticated and expensive instrumentation and expertise, therefore, due to easy accessibility commercial mucins are used frequently in research studies. For example, an artificial intestinal mucus was developed using commercially available porcine gastric mucin and the rheological properties were matched with native pig intestinal mucus. Further optimization was carried out to reduce cell death and have no effect on the barrier

integrity of the Caco-2 cell monolayer [34]. The artificial mucus was applied to Caco-2 cell monolayer in a transwell platform and permeability of hydrophilic (mannitol, FD4, FD10 and fluorescein isothiocyanate-bovine serum albumin) and hydrophobic (testosterone) compounds was tested. Biosimilar mucus present on the epithelial cell layers acted as a barrier to hydrophobic compounds and introduced a lag time for the diffusion of hydrophilic compounds. Biosimilar mucus also showed more consistent results for creating a steric barrier in comparison to native porcine intestinal mucus validating this approach to model mucus barrier in vitro [35].

Three-dimensional cell cultures have been demonstrated to mimic organ physiology better than traditional two-dimensional culture [36]. Three-dimensional models of the intestine are enabled recently by the development of microfabrication techniques like photolithography, microcontact printing, and replica molding. These techniques have been coupled with biomaterials that mimic the basement membrane of the intestinal tissue. 3D villous like geometries have been created using collagen [31, 37], silicon [38], and poly lactic-glycolic acid (PLGA) [39]. These studies demonstrated that Caco-2 epithelial cell differentiation and polarization is dependent on the location along the villous like structures which mimic the in vivo conditions. The researchers further tested the application of these models for evaluation of probiotics Lactobacillus gasseri and E. coli Nissle 1917 in preventing adhesion of pathogenic bacteria Salmonella typhimurium and Pseudomonas aeruginosa [40]. The model enabled the dissection of mechanisms by which different probiotic bacteria exert their probiotic effect in a physiologically relevant environment.

Tubular constructs have been created using silk biomaterial that closely mimic the tubular structure of intestines by including three-dimensional folds on the luminal side of the constructs [12]. The silk scaffolds were seeded with human myofibroblasts within the bulk of the scaffold to add the mesenchymal cell component to support the epithelial cell growth in the lumen of the model. Caco-2 and HT29-MTX were co-cultured in the lumen of the scaffold. The tubular design and the three-dimensional luminal structure of the scaffold enabled the luminal oxygen tensions to stay in the anaerobic zone for long term. Long term (approx. 8 weeks) survival, mucus production and functional maintenance of cells in the silk scaffolds provided great advantages for chronic studies alongside co-culture of live anaerobic bacteria with epithelial cells. The system was utilized to study parasite-epithelial cell interactions using Cryptosporidium parvum as a model organism [41]. The diarrhea causing C. parvum successfully infected the model for 17 days and was serially transferred to three new scaffolds to re-establish infection. 3D silk scaffolds were also used to study toxic effects of Clostridioides difficile post germination and colonization [42]. Toxigenic C. difficile was significantly more toxic and caused higher epithelial cell death in the 3D model compared to 2D transwells.

A major advance was achieved in the field of in vitro intestine modeling with the development of ‘gut-on-a-chip’ platform. The microfluidic platform is made of polydimethylsiloxane (PDMS) with two microfluidic channels separated by a thin porous PDMS membrane. The porous PDMS membrane coated with Matrigel supported epithelial cell growth on the apical side and endothelial cells on the basolateral side. The apical and basolateral channels incorporated flows to mimic the luminal and vascular flow conditions.

Alongside flow, the system induced cyclic stretching of the PDMS membrane using a pneumatic system and the epithelial cells were subjected to in vivo like peristalsis. Epithelial (Caco-2) cells differentiated and polarized into villous like structures within 3 days compared to 3 weeks in transwell culture [11, 14]. The system enabled co-culture of live bacteria in the apical channel for more than 1 week without compromising epithelial cell viability and was further used as a model for inflammatory conditions in the intestines [15]. This was achieved by culturing vascular endothelial cells on the basolateral side of the PDMS membrane and flowing immune cells in the basolateral channel. By stopping the membrane stretching, the system successfully captured bacterial overgrowth on the epithelial cell layer leading to higher pro-inflammatory cytokine secretion and immune cell infiltration. This system has been recently adapted to incorporate biopsy derived stem cell organoids and induced pluripotent stem cell derived organoids that form the epithelial layer, therefore, demonstrating the ability to create personalized intestinal model [43-44].

Current in vitro models of intestines can be broadly classified as static and dynamic models. Static models such as transwell platforms and biomaterial scaffolds are commonly used for molecular and drug diffusion or absorption studies. These models do not provide the mechanically active environment that the cells experience in vivo. Also, static models are not suitable for performing host-microbial co-cultures due to lack of mucus, flow, and bacterial overgrowth. On the other hand, dynamic models can simulate in vivo like mechanical forces by incorporating fluid flow and stretching. Under these conditions long-term co-culture of bacteria with human epithelial and immune cells has been demonstrated either in the absence of mucus or using commercial porcine gastric mucin (PGM).

Despite significant progress in creating in vitro models of intestinal tissue with higher complexity there are few challenges that remain unmet.

- In vivo, a mucus layer tightly bound to epithelial cells physically separate bacteria from coming in contact with the epithelial cells and communication occurs via bacterial metabolites or host derived factors that diffuse across the mucus layer. Such selective barrier function has been challenging to demonstrate in vitro.
- Mucus secreting cell layers secrete very small amount of mucus compared to in vivo tissues. Mucus layer thickness is an important mechanism for separating bacteria and other luminal components that cause inflammation. The ability to recapitulate this phenomenon in vitro will significantly improve physiological significance of the in vitro mucosal barrier models.
- Commercially available mucus fails to recapitulate the properties of mucus due to enzymatic degradation and current mucus purification methods require extensive instrumentation producing low quantities of mucus. Therefore, development of methods for extraction of mucus that have intact functional properties will advance the engineering of intestinal mucosa models.

Taking into consideration the recent progress in the development of engineered intestinal models, current work aims to develop the basic technical strategies and platforms to address the above stated challenges.

CHAPTER 2

DEVELOPMENT OF A SCALABLE METHOD FOR MUCUS EXTRACTION AND IN VITRO RECONSTITUTION OF AN INTESTINAL MUCUS LAYER

2.1 Introduction

The role of mucus in the intestines is incompletely understood. The mucus layer functions as a selective biological barrier that permits transport of digested molecules while protecting the underlying epithelial tissue[1-3]. The content in the lumen is continually changing and the mucus layer must respond to its environment by being a barrier to some components while being permeable to others[2]. The rheology and microscopic structure of mucus affects its ability to prevent bacterial infiltration[45-46]. Many diseases involve dysfunction of the mucus barrier, such as inflammatory bowel diseases[47-49], cystic fibrosis[50], and colorectal cancer[51-52]. In diseased states, breakdown of the mucus microstructure increases bacterial infection[53-54]. Two factors that have been shown to affect these structural properties are the local pH and cation content[55]. An experimental model that can expand the understanding of these mechanisms would be an essential tool to address diseases of the intestines.

The mesh-like structure of the mucus barrier enables it to promote nutrient absorption while acting as a barrier to infection. Mucus is primarily made up of mucin proteins. In both the large and small intestine, mucus is composed predominantly of MUC2, one of the 21 known proteins in the MUC family[56-57]. In the small intestine, where most nutrient absorption occurs, the mucus barrier is thin (20-100 μm thick), which facilitates molecular transport while maintaining tissue sterility against luminal microbes[58-59]. In the large

intestine, the mucus barrier is thicker (700-1,000 μm), which physically shields the epithelial lining from the high density of the microbiota[60-62]. In the large intestine, the mucus layer is composed of a tightly bound inner layer and a loosely bound outer layer[63]. Secreted mucus traps invading bacteria which are eliminated with the luminal content[64-65].

The local environment around the mucus layer greatly affects its structural properties. The most well studied environmental factor is pH, which has a strong effect on the rheology of mucus[66-67]. In acidic environments, mucus is elastic and gel-like, but in neutral and basic environments, it behaves more like a liquid solution[66]. Mucin proteins have a bottlebrush-like structure with a protein backbone and glycan side chains[68] (Figure 2.1A). At acidic pH values, mucins change conformation and expose cysteine-rich hydrophobic regions on the protein backbone, which leads to hydrophobic interactions and gelation[69-70]. In addition to pH, other factors may affect the structure of mucus[71]. Calcium ions (Ca^{2+}) plays an important role in regulating intracellular mucin storage and secretion from goblet cells[55, 72]. The binding of Ca^{2+} with the glycan side chains causes dense packing of the mucin polymeric chains[55, 73-74]. In the intestines, where the luminal pH is neutral[75], dietary calcium may have a greater effect on mucus structure and its barrier function. After ingesting food, the availability of calcium and other ionic molecules in the gastro-intestinal tract is increased[76-77]. Depending on the fed state, the luminal Ca^{2+} concentration varies between 5-20 mM[76, 78].

Much of current in vitro research has used mucus extracted from the stomach[79-80]. It is plentiful, less contaminated with bacterial components, and its extraction is

straightforward. This material has been instrumental in demonstrating its pH dependent behavior and barrier function[67, 70, 81-83]. Commercially available gastro-intestinal mucus is derived from porcine stomachs. A limitation of this material is that gastric mucins have a different biochemical structure from intestinal mucins. Gastric mucus is mostly MUC5AC and MUC6[84], whereas the intestines is primarily MUC2[56]. In addition, commercial mucin has poor gel-forming capability[85]. This transition is an essential aspect of the primary barrier function of mucus.

In the absence of a commercial source, there are two predominant methods used to study intestinal mucus derived from rodent, large animal, or human tissues. The most common is direct scraping of mucus from the wall of intestines. Scraped mucus has been used to demonstrate that large nanoparticles, if properly coated, can rapidly penetrate mucus compared to smaller nanoparticles[86]. It has also been shown that the interaction of mucus with food associated stimuli such as lipids, calcium and pH significantly reduce the transport of microspheres[76]. An important limitation of this scraping technique is that contamination of unprocessed mucus with cellular debris can cause unwanted immunological responses or cytotoxicity in vitro[34]. Alternatively, several studies have purified the mucin proteins from intestinal mucus[87-88]. Purified mucins retain the rheological properties of mucus[89-90] and have been used to show that mucin chain entanglement is dominant at neutral pH and high concentration[91]. At low pH the gel formation is accompanied by formation of large-scale heterogeneities within the mucin solutions[92]. This purification method has limited yield, is time intensive and requires costly specialized equipment, which limits its widespread use for effective recapitulation of

mucus barriers with physiological thickness and concentration in vitro. In recent years, little progress has been made in advancing mucus extraction protocols at large scale[90, 93-94].

The goal of our study was to develop a method for extracting intestinal mucus and to quantify the effect of environmental factors on its barrier properties. We hypothesized that the permeability and barrier function of intestinal mucus is reversible and changes in response to calcium ions in the local environment. To quantify these properties, the extraction method needed to produce sufficient quantities of mucus that retained its pH-responsive rheology and contained minimal cellular contaminants. A systematic process was used to determine the extraction conditions that would result in a high yield, cause minimal cellular damage, and isolate mucus that would form a gel. Spectrometric and rheometric measurements were used to quantify the absorbance and physical properties in response to acidic and high calcium environments. The physical structure of mucus proteins in these environments was determined by microscopy. The ability of mucus to limit molecular diffusion and bacterial penetration was determined in an in vitro mucus barrier model. This development of a high throughput extraction method will enhance mucus research. Understanding the mechanisms that control the barrier function of mucus will ultimately lead to better treatments of mucus-related diseases of the intestines.

2.2 Results

2.2.1. Extraction of Natural Mucus

We have developed a new method to extract mucus from the porcine small intestines (Figure 2.1B). The goal of the design process was to develop a method that isolates mucus while retaining its pH-responsive rheology and minimizing the inclusion of cellular contaminants. This method was based on the observation that after mucus is scraped from the intestine, it dissolves in an alkaline solution. To determine the optimal solution to dissolve mucus from the intestine *in situ*, washed intestinal tubules were filled with 1M HCl, PBS or 1 M NaOH for 24 hours (Figure 2.1C). Before treatment, the intestinal lining was undamaged, and mucus was tightly bound to the lining (Figure 2.1C, *left*). The pH of the solvating solution affected the appearance of the intestine and the mucus layer (Figure 2.1C&D) and extent of solvation (Figure 2.1E). Filling the intestinal tubules with an acidic solution (1 M HCl) for 24 hours turned the mucus layer into a whitish gel and the tissue became rigid (Figure 2.1D, *middle left*). A neutral solution (saline) only partially solubilized the mucus layer (Figure 2.1D, *middle right*). An alkaline solution (1 M NaOH) dissolved most of the mucus layer and turned the viscera semi-solid (Figure 2.1D, *right*). The total amount of protein in the alkaline solution was significantly higher ($P<0.05$) than in the HCl and PBS solutions (Figure 2.1E).

The concentration of the alkaline solution affected the amount of protein recovery and the extent of tissue damage (Figure 2.1F-H). Treatment with HCl (Figure 2.1F, *middle left*) caused some tissue damage compared to untreated controls (Figure 2.1F, *left*). Treatment with PBS did not significantly affect the epithelial tissue, which retained much of the

villous architecture of untreated tissue (Figure 2.1F, *middle right* and *inset*). At a strength of 1 M NaOH, the underlying epithelial tissue showed some damage and individual villi were difficult to identify (Figure 2.1F, *right*). Treatment with a lower concentration of NaOH (0.01 M), compared to 1M NaOH, reduced epithelial damage and retained villous architecture (Figure 2.1G). Treatment with 0.1 M NaOH, produced comparable amounts of recovered protein to treatment with 1 M NaOH (Figure 2.1H). The amount of recovered protein significantly decreased after treatment with NaOH solutions of lower concentration (0.01 M and below; $P < 0.05$; Figure 2.1H).

The amount of cellular contaminant proteins in the extracted mucus was reduced by exploiting the reversible, pH-dependent sol-gel transition of mucin (Figure 2.1I). After intestinal mucus was solubilized in 0.01 M NaOH, it was purified by a pH adjustment step. The acidity of the solution was reduced to a pH of 4.0 and then increased to a value of 8.0. When the pH was reduced, a gel formed (Figure 2.1B) enabling the supernatant to be removed. One cycle of this pH-adjustment process reduced the total protein in the extract by 40% ($P < 0.05$), but repeated sol-gel cycles did not significantly change the protein content (Figure 2.1I). It took 4 sol-gel cycles to reduce the DNA content by 30% ($P < 0.05$; Figure 2.1J). DNA contamination was reduced significantly by DNase treatment ($P < 0.05$; Figure 2.S1). The removed supernatant did not gel at pH 4.0. After dialysis and lyophilization, the entire process generated 1,274 ± 49 mg of dry protein per meter of intestine. The theoretical amount of mucus in the intestine was calculated to be 1,775 mg/m, accounting for the increase in cross-sectional surface area due to plicae circularis and villi structure (Figure 2.S2) ([95-96]). Compared to this theoretical value, PSIM extraction

had a yield of 71.75 %. The final product reconstituted in a buffer medium was termed porcine small intestinal mucus (PSIM).

2.2.2 Reconstituted PSIM Preserves Reversible pH Dependence.

The pH of PSIM affected its appearance, absorbance, rheological properties, and aggregation. At pH 7, reconstituted PSIM (20 mg/ml) was optically clear and became turbid at lower pH (Figure 2.2A, *left* and *middle*). High concentration PSIM (80 mg/ml) was a viscous fluid that flowed in an inverted tube (Figure 2.2B *left tube*). At pH 4, high concentration PSIM formed a gel that retains its shape in an inverted tube (Figure 2B *right tube*). The turbidity of reconstituted PSIM increased with decreasing pH until a maximum at pH 4 (Figure 2.2C *top*). This change in physical appearance matched the absorbance at 410 nm over this range (Figure 2.2C *bottom*). Reconstituted PSIM exhibited an absorbance peak at 410 nm in the range from 290 to 790 nm (Figure 2.S3). The absorbance at pH 4 was significantly greater than at pH 7 ($P < 0.05$) and pH 2 ($P < 0.05$; Figure 2.2D) and the greatest difference in absorbance was between pH 7 and pH 6 ($P < 0.05$).

The rheological properties of reconstituted PSIM matched the physical appearance and absorbance. The viscous (G″) and elastic (G′) moduli were greater at pH 4 than at pH 7 ($P < 0.05$; Figure 2.2D), matching the gel-like behavior at low pH (Figure 2.2B). Further acidification to pH 2, reduced both moduli from that of pH 4 ($P < 0.05$; Figure 2.2D) similar to the reduction in absorbance (Figure 2.2C). For all pH levels (2, 4, and 7), G′ was greater than G″ ($P < 0.05$), and the greatest difference (more than 4 times) was at pH 4 (Figure 2D). The elastic modulus was greater than the viscous modulus over the entire frequency

range from 1 to 68.3 rad/s (Figure 2.S4). At a microscopic level, pH affected the aggregation of PSIM (Figure 2.2E). At pH 7 no aggregation was observed. At pH 6 and below, microscopic aggregates were present (Figure 2.2E). The overall size and branching of PSIM aggregates gradually increased with decreasing pH until a pH value of 4. At pH values of 3 and lower, the size of the aggregates decreased. Area coverage increased with decreasing pH until a value of 4 and then decreased as pH was reduced to a value of 2 (Figure 2.2F). The pH affected the physical properties of PSIM similarly. Each had its highest value at pH 4. Absorbance correlated positively with the viscous modulus (R^2 = 0.95), the elastic modulus (R^2 = 0.90) and the area coverage (R^2 = 0.9998).

The pH-dependent change in absorbance was reversible. As the pH of a PSIM solution was rapidly changed from 8 to 4 and back to 8 (Figure 2.2G) the solution went from clear to turbid and back to clear (Figure 2.2A). When this reversibility was quantified using absorbance measurements and smaller pH intervals, the results matched the observed changes in turbidity. Decreasing the pH of the PSIM solution from 8 to 4 increased absorbance and it returned to a similar value as the pH was increased back to 8 (Figure 2.2G).

2.2.3 Barrier Function of PSIM is pH Dependent

The mucus barrier function changed with the pH and aggregation of PSIM. When a bacterial solution was applied to a transwell membrane covered in PSIM, transmigration of the bacteria resulted in an increase in bacterial density in the bottom well as a function of time (Figure 2.3A-B). Two species of bacteria, *Escherichia coli* (Figure 2.3A) and

Salmonella enterica serovar Typhimurium (Figure 2.3B), both transmigrated through mucus. PSIM at pH 7, which had not formed a gel, significantly slowed *E. coli* transmigration compared to a PSIM-free control ($P < 0.05$; Figure 2.3C). *Salmonella* transmigration was not affected by the presence of PSIM at pH 7 (Figure 2.3B). At pH 4, the aggregated PSIM significantly decreased transmigration of both bacteria ($P < 0.05$). At pH 2, bacterial transmigration was significantly reduced compared to pH 7, while more bacteria migrated across the mucus barrier compared to pH 4 ($P < 0.05$). These effects on bacterial transmigration were significant at all time points (Figure 3A-B) and were inversely correlated with PSIM aggregation ($R^2 = -0.97$ for *E. coli* and $R^2 = -0.99$ for *Salmonella*; compare Figure 2.3C-D to 2F).

PSIM affected the motility of both *Salmonella* and *E. coli* at low pH (Figure 2.3E-H). In PSIM at pH 7, the average speeds of *E. coli* and *Salmonella* were not different from PSIM-free controls (Figure 2.3F). At pH 4, aggregated PSIM significantly decreased the motility of both species; the speeds of *E. coli* and *Salmonella* were slowed by 370% and 40% compared to controls ($P < 0.05$, Figure 2.3F). In PSIM at pH 7, both bacterial species were in a free-swimming state. In both aqueous controls and neutral pH PSIM, more than 80% of the bacteria were motile with speeds of at least 2 μm/s (Figure 2.3G-H). In aggregated PSIM at pH 4, the bacteria were immobilized. At pH 4, the presence of PSIM increased the percentage of non-motile *Salmonella* and *E. coli* with speeds less than 2 μm/s from 35% to 54% and 12% to 87%, respectively ($P < 0.05$). *Salmonella* were more motile than *E. coli* in PSIM at pH 4; there were fewer immobilized bacteria (speed < 2 μm/s; $P < 0.05$) and more moderately motile bacteria (speed = 2 to 4 μm/s; $P<0.05$). The effect of pH on

motility indicates how pH affected bacterial migration through layers of PSIM (Figure 2.3A-D).

2.2.4 Calcium Regulates PSIM at Neutral pH.

Calcium affected the microscopic and macroscopic properties of PSIM. The addition of calcium at neutral pH increased the visible turbidity and absorbance of PSIM in a similar manner to reducing pH (Figure 2.4). At pH 7, PSIM was optically clear. Increasing the Ca^{2+} concentration proportionally increased the turbidity (Figure 2.4A). At pH 4, increasing the Ca^{2+} concentration had no effect on the turbidity of PSIM. Similar to pH, absorbance at 410 nm matched turbidity. At pH 7, increasing the Ca^{2+} concentration significantly increased PSIM absorbance ($P < 0.05$), whereas, at pH 4, increasing the Ca^{2+} concentration did not affect the absorbance (Figure 2.4B). The effect of calcium on absorbance was reversible. Addition of calcium chelating EDTA reduced the absorbance that increased in response to the addition of calcium ($P < 0.05$; Figure 2.4C).

Calcium caused similar microscopic changes to PSIM as acidic pH. Small aggregates formed at pH 7 with 1 mM Ca^{2+} (Figure 2.4D), whereas no aggregates formed without Ca^{2+} (Figure 2.2E). With 1 mM Ca^{2+}, area coverage increased with pH until a value of 4 and then decreased (Figure 2.4E) with a similar pattern to PSIM without calcium (Figure 2.2F). The effect of calcium was greatest at neutral pH. The addition of 1 mM Ca^{2+} significantly increased ($P < 0.05$) the area coverage (Figure 2.4E) compared to PSIM without calcium (Figure 2.4E *inset* and 2F).

2.2.5. Calcium Controls the Thickness and Porosity of the Mucus Barrier.

At neutral pH, the Ca^{2+} concentration affected the thickness and permeability of PSIM. When the Ca^{2+} concentration was 5 mM and above, PSIM formed visible layers after overnight incubation as aggregated mucins precipitated (*arrows* in Figure 2.5A). No layers formed when the Ca^{2+} concentration was 1 mM. The thicknesses of the mucus layers increased linearly with Ca^{2+} concentration ($P < 0.05$; Figure 2.5B). The mucus layers formed at different Ca^{2+} concentrations affected the transport of fluorescent FITC-dextran in an unexpected manner (Figure 2.5C-D); the lowest transport was not observed in the thickest layer. The FITC-dextran concentration, which resulted from diffusion through PSIM layers, increased with time (Figure 2.5C). FITC-dextran transport was highest at 1 mM Ca^{2+}, where there was no visible PSIM barrier ($P < 0.05$; Figure 2.5D). Transport was lowest at 5 mM Ca^{2+} ($P < 0.05$). At Ca^{2+} concentrations of 10 and 20 mM, the transport of FITC-dextran was greater than at 5 mM, even though the barriers were thicker ($P < 0.05$; Figure 2.5D). This pattern was consistent for all time points (Figure 2.5C).

The differences in diffusion for the PSIM layers formed with different levels of Ca^{2+} was caused by its microscopic structure. Calcium affected the size of PSIM aggregates, the spacing between them and the total area of aggregated material. In the presence of 1 mM Ca^{2+}, PSIM formed microscopic, 2-5 μm diameter aggregates (Figure 2.6A). In 5 mM Ca^{2+} there were more aggregates of about the same size. At 10 and 20 mM Ca^{2+} PSIM formed larger, branched aggregates (*arrows* in Figure 2.6A). At 5 mM Ca^{2+}, the aggregates were closest (Figure 2.6B). Most of spaces (> 95%) between the aggregates were less than 5 μm, which was significantly greater than the aggregate spacing for 1 mM ($P < 0.05$). At 1 mM

Ca^{2+}, about half (49.8%) of the spaces were 5 - 10 μm, which was significantly greater than the percentage of spaces at 5 mM (~ 5%; $P < 0.05$). At 10 and 20 mM Ca^{2+}, there were more large spaces (15 - 20 and 20 – 25 μm) between aggregates than at 1 and 5 mM ($P < 0.05$). At these higher Ca^{2+} concentrations, PSIM aggregates formed islands with low inter-particle distances (< 5 μm) and higher distances (> 5 μm) between islands (Figure 2.6A). These large spaces between islands created pores through the PSIM layers. At 1 mM Ca^{2+}, about 3% of the surface area was covered by PSIM aggregates (Figure 2.6C). Increasing the Ca^{2+} concentration to 5 mM increased area covered 15-fold ($P < 0.05$). Further increase in the Ca^{2+} concentration to 10 mM reduced the area coverage to 18%. Similar to the aggregate distribution, no significant difference in the area coverage was observed if Ca^{2+} concentration was increased from 10 to 20 mM Ca^{2+}.

Molecular retention within PSIM layers was dependent on Ca^{2+} concentration (Figure 2.6D-G). As with the transmitted light measurements (Figure 2.6A), the size of PSIM aggregates increased with increasing Ca^{2+} concentration (Figure 2.6D). Green fluorescence from FITC-dextran, which indicates the location of molecules retained in the PSIM layers, became patchy with increasing Ca^{2+} concentration (Figure 2.6D). With an increase in calcium concentration from 1 to 5 mM, the average GFP fluorescence decreased ($P < 0.05$; Figure 2.6E), indicating a decrease in the number of molecules retained in the PSIM layer. A further increase in calcium concentration to 10 mM, reversed this direction and increased the average GFP fluorescence ($P < 0.05$; Figure 2.6E). The local structure of the PSIM aggregates explains this behavior (Figure 2.6F). Regions of high PSIM aggregation (*stars* in Figure 2.6F) had low GFP intensities. Pores in the PSIM layer, identified as regions with

low red fluorescence (*dashed circles* in Figure 2.6F), had high GFP fluorescence. The GFP intensity in the pores was greater than in the aggregated material ($P < 0.05$; Figure 2.6G), indicating exclusion from PSIM aggregates.

2.3 Discussion

We have developed a new method for isolating mucus from the porcine intestine (Figure 2.1). This method dissolves the mucus layer from intact intestines using NaOH. A dilute (0.01 M) solution was used because it dissolved most of the mucus layer (Figure 2.1E and 1G) and caused minimal damage to the epithelial cell layer (Figure 2.1F). Minimizing the damage reduced the amount of contaminating proteins in the purified mucus (Figure 2.1G). A sol-to-gel transition in the extraction method (Figure 2.1H) eliminated pH-unresponsive macromolecules and cellular proteins without the use of high-cost instrumentation. Solubilized mucus proteins were recovered with a yield of 1274 mg per meter length of small intestine. The biophysical and biochemical properties of the produced mucus are in line with those reported previously[58, 66, 70, 81]. At acidic pH values, PSIM becomes more gel-like, with increasing viscous and elastic moduli (Figure 2.2D). With increasing concentrations of calcium, the extent of PSIM aggregation at neutral pH increases (Figure 2.4B). The thickness of the PSIM layer formed in the in vitro mucus model has a thickness comparable to the mucus layer in the small intestine[58] (Figure 2.5B).

This new process has several advantages over other methods. Compared to direct scraping of mucus from the epithelial lining, solubilization of mucus greatly simplifies the extraction process. Dissolving mucus in dilute NaOH and purifying with a sol-gel transition

significantly decreases contamination with cellular debris (Figure 2.1G). In immunogenic experiments, contamination with cellular or bacterial component could cause unwanted responses. In addition, the process is scalable and can be applied to entire lengths of PSI tubes simultaneously. Compared to commercial mucin, PSIM retains the rheological properties of natural mucus. Commercial mucins do not form a gel (Figure 2.S5), which limits their use as a barrier in experiments *in vitro*[33]. Compared to mucin extraction protocols, this process does not require extensive downstream equipment[87-88]. Most of these methods are limited by the quantity and yield of mucus that can be produced, which prevents the widespread use of mucus in research.

The extraction of large volumes of mucus enabled many of its properties to be quantified. An important property that was observed was the reversibility of pH and calcium-induced aggregation and gelation (Figure 2.2G and 2.4C). Reversibility suggests that the properties of mucus respond to conditions in the local environment. This dynamic change was easily monitored because the absorbance at 410 nm was directly correlated to the degree of aggregation (Figure 2.2C and 2.2F) and the viscous and elastic moduli (Figure 2.2D). Reconstituted PSIM retained the ability to be a barrier to bacterial penetration (Figure 2.3) and this property was dependent on pH. At neutral pH, mucus only minimally prevented penetration, but when the mucus aggregated at lower pH, penetration was considerably reduced (Figure 2.3A-D). The aggregation of the mucus at pH 4 appeared to slow penetration because the bacteria became immobilized in aggregated mucus. A gel layer of PSIM can act like a natural barrier by controlling molecular diffusion and bacterial transmigration.

Another observation was that calcium plays a critical role in the intestinal milieu. Similar to pH, the availability of calcium ions affected the thickness of the mucus layer (Figure 2.5B). Increasing the calcium concentration increased PSIM aggregation, suggesting that calcium affected PSIM by similar mechanisms as changes in pH. In addition, there was an interplay between the responses of mucus to pH and calcium. Overall, acidic pH had a greater effect on mucus aggregation than calcium concentration within the physiological range (Figure 2.4B). At neutral pH and in the absence of calcium, mucus was not aggregated. Increasing the calcium concentration increased mucus aggregation but did not reach the same extent as that observed at pH 4 (Figure 2.4B). Calcium-driven aggregation also affected the barrier function. From low (5 mM) to high (20 mM) physiological levels of calcium [76, 78], the molecular permeability of mucus increased (Fig 2.5C).

The microscopic structure of mucus explains how calcium controls the barrier function of mucus. The primary microscopic features that affects the physical properties of mucus are the arrangement and density of aggregates. At very low calcium levels (1 mM), mucus aggregation is minimal (Figure 2.6A). At low physiological calcium concentrations (5 mM), small and uniform aggregates begin to appear. At higher calcium concentrations (10 - 20 mM), larger, more branched aggregates form. The branching of mucin aggregates did not increase once Ca^{2+} concentration was higher than 10 mM. Although the density of aggregates increases, this condensation decreases the surface area coverage (Figure 2.6C). The branched nature of the aggregates formed void spaces in the mucus layer (Figure 2.6D) that increase molecular diffusion while also increasing the thickness of the layer (Figure

2.5A). The structure and extent of these aggregates explains how calcium increased both mucus layer thickness and molecular transport.

These effects suggest how the local calcium concentration controls the properties of the mucus barrier (Figure 2.7). The increased concentration of ionic molecules after ingesting food (predominantly calcium) induce mucin aggregation and increases the thickness of the mucus barrier. The increased aggregation increases molecular permeability (Figure 2.6), while simultaneously increasing resistance to microbial penetration from the lumen. If the behavior of PSIM in high calcium is similar to pH 4, where both had considerable aggregation (Figure 2.4B), then PSIM aggregation at high calcium would also have high resistance to microbial penetration from the lumen (Figure 2.3 and Figure 2.5). Therefore, dense branched aggregates increase the open channels for molecular diffusion while also creating a network to ensnare invasive microbes. As the mucus flows along the epithelium its viscoelastic and barrier properties change in response to the lumen content. Because the properties of the mucus are reversible, it is instantaneously responsive and serves different functions in different intestinal environments, e.g. an empty lumen and one directly after eating.

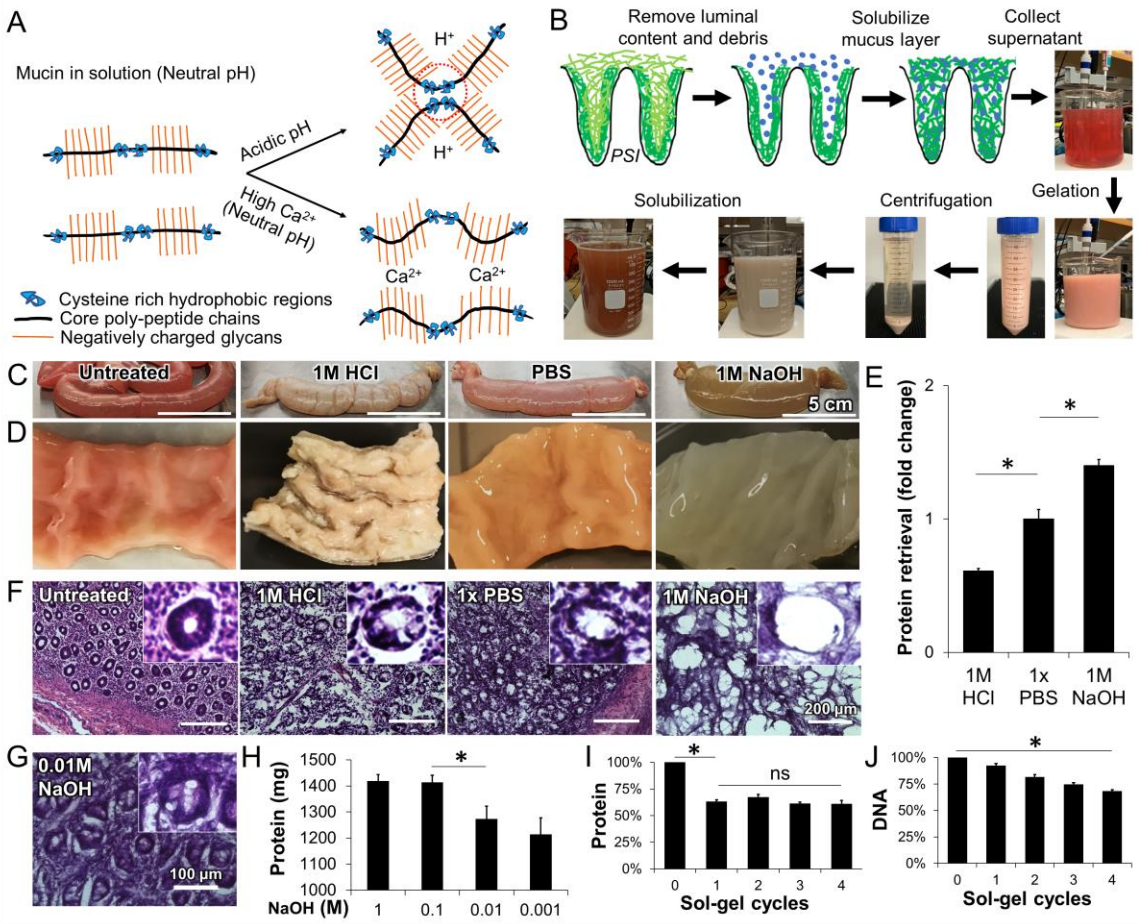

Figure 2.1 Extraction of porcine small intestine mucus (PSIM). (A) Schematic of mucin microstructure, stable polymeric chains at neutral pH, hydrophobic interactions of cysteine rich regions at acidic pH (dashed circles), and ionic interactions between calcium ions (Ca^{2+}) and negatively charged glycans at neutral pH. (B) Mucus extraction procedure starting with direct solubilization of the mucus layer with NaOH, and separation of pH responsive mucus via reversible sol-gel transition. (C) PSI tubules after 24 hours exposure to 1 M HCl, PBS, and 1 M NaOH. (D) The luminal surface of PSI tissue sections after 24 hours exposure to HCl, PBS, and NaOH. (E) Recovered protein with solutions of different pH, relative to PBS. (*, $P < 0.05$; $n = 3$). (F) Hematoxylin and Eosin (H&E) stained histological sections of PSI tissues treated with different pH solutions. Inner panels show individual villi. (G) H&E stained PSI section after 0.01 M NaOH treatment. (H) Total protein extracted when PSI tubules were filled with NaOH solutions ranging from 0.001 M to 1 M ($n = 3$). (I) Total protein content with repeated sol-gel cycles relative to initial total protein extracted. (J) Total DNA content with repeated sol-gel cycles relative to the total DNA initially present in the PSIM extract. (*, $P < 0.05$)

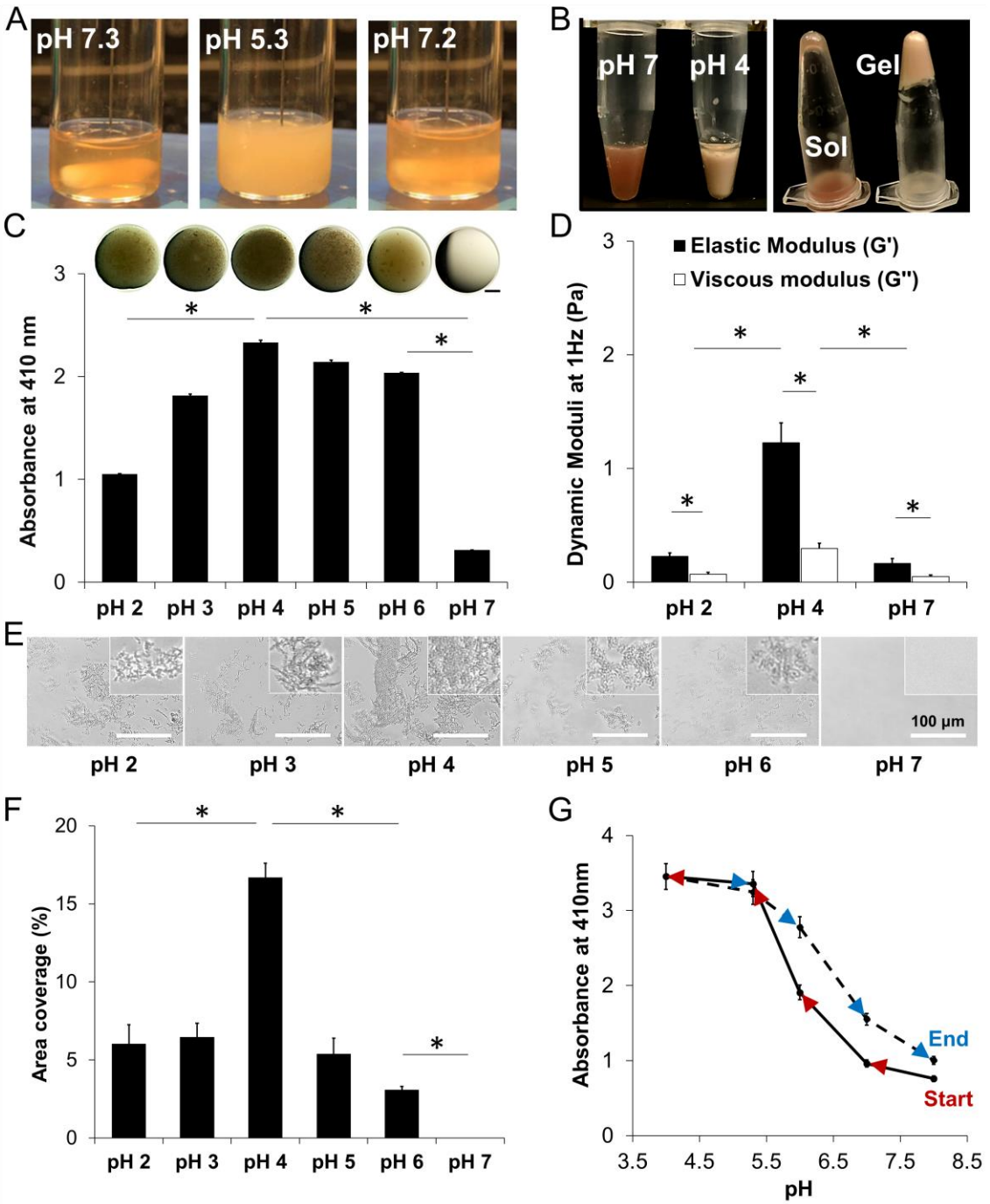

Figure 2.2 Response of PSIM to pH. (A) PSIM (20 mg/ml) in 20 mM HEPES at pH 7.3 was clear. At a pH of 5.3 the PSIM solution was turbid. Returning the pH to 7.2, after decreasing it to 5.3, restored optical clarity. All solutions were at 20 mg/ml concentration unless otherwise noted. (B) PSIM (80 mg/ml) in 20 mM HEPES at pH 7 was a viscous solution (*left tube, left image*) that flowed after inversion (*left tube, right image*). At pH 4, PSIM was a gel (*right tube, left image*) that did not flow after inversion (*right tube, right image*). (C, *top*) Droplets of PSIM (20 mg/ml) on a glass slide imaged using a stereoscope. Darkness was due to the turbidity of the droplets. (C, *bottom*) Absorbance of PSIM solutions (20 mg/ml) at different pH values at a wavelength of 410 nm. (D) Dynamic

rheological moduli (G′ and G″) of PSIM at pH 2, 4, and 7 and at 1 Hz and 37°C (n = 3, mucus from individual pigs). (E) Microscopic images of PSIM between two glass coverslips in the pH range 2-7. Insets show close-up images of aggregates. (F) Surface area covered by PSIM aggregates per image (as in panel E) in the pH range 2-7 (n = 10). (G) Real-time sampling and characterization of the reversible aggregation of PSIM in the pH range 4-8. The solid line represents an increase in the absorbance as the pH was reduced from 8 to 4 (*red arrows*). The dotted line represents the decrease in absorbance (*blue arrow*s) as the pH was increased from 4 to 8 (n = 3; *, $P < 0.05$).

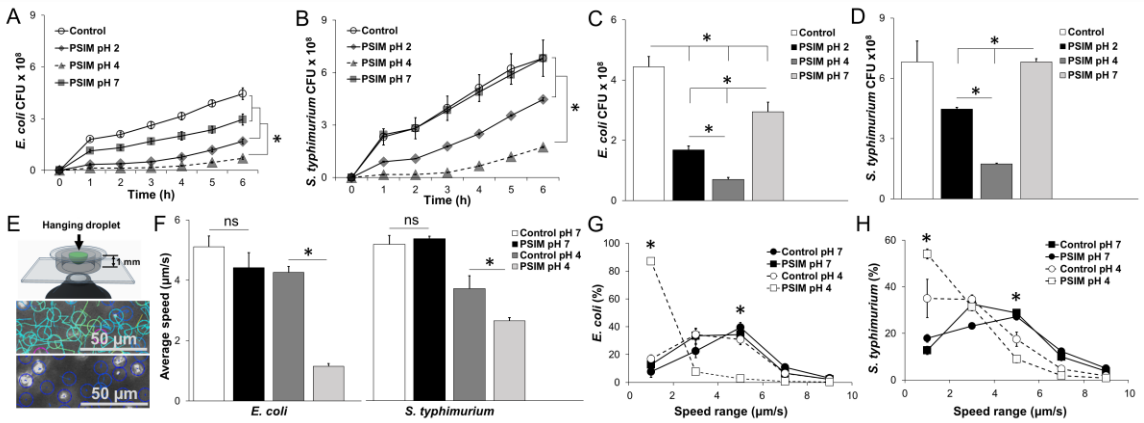

Figure 2.3. Barrier function of PSIM. (A) Time-resolved transmigration of *E. coli* through 3 µm pore transwell membranes layered with PSIM at pH 7, 4, and 2. Controls were HEPES buffer at pH 7 without PSIM *(n* = 3). (B) Transmigration of *Salmonella*. (C) Number of *E. coli* that migrated across the PSIM layers at 6 h time point. (D) Number of *Salmonella* that migrated across the PSIM layers at 6 h. (E) The speeds of individual bacteria were measured in hanging drops of PSIM mixed with bacteria and suspended above the objective of an inverted microscope. At pH 7 (*top*), velocities (indicated by line lengths) were greater than at pH 4 (*bottom*), where all bacteria were visibly non-motile. (F) The average speeds of *E. coli* and *Salmonella* in PSIM at pH 4 were significantly lower than PSIM-free controls at pH 4 (*, $P < 0.05$; $n = 3$). At pH 7, PSIM had no effect on bacterial motility compared to control. (G) Distribution of speeds of *E. coli* in PSIM at pH 4 and 7 compared to controls (HEPES buffer without PSIM; $n = 3$). The percentage of bacteria with speeds less than 2 µm/s was greater in PSIM at pH 4 compared to pH 7 and controls (*, $P < 0.05$). The percentage of bacteria swimming at 5 µm/s was lower in PSIM at pH 4 compared to pH 7 and controls (*, $P < 0.05$). (H) The distribution of speeds of *Salmonella* in PSIM at pH 4 and 7 compared to controls was functionally similar to *E. coli*.

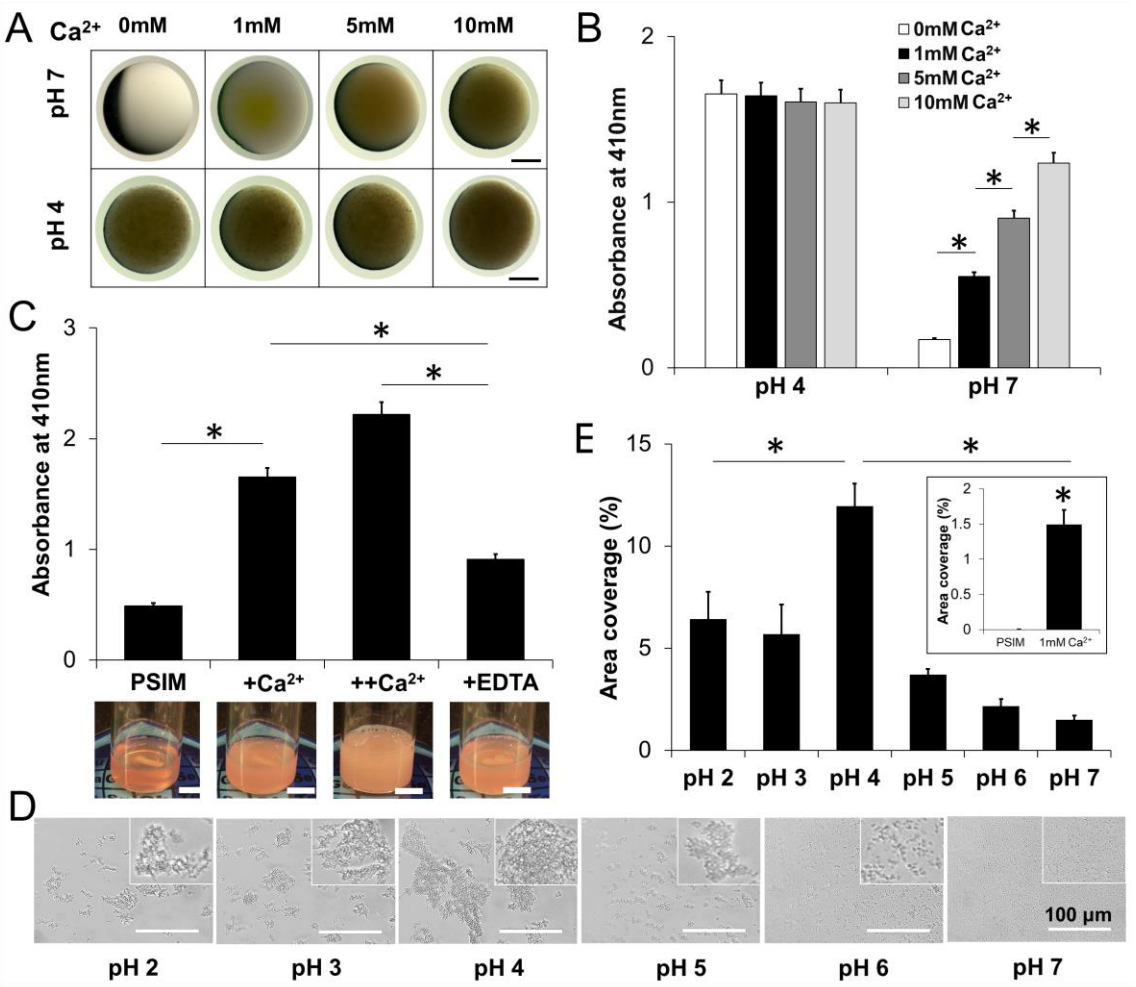

Figure 2.4. Calcium regulates the physical properties of PSIM. (A) Stereoscope images of PSIM at pH 4 and 7 with Ca^{2+} ranges from 0 to 10 mM. Scale bar is 1 mm. (B) The absorbance of PSIM at 410 nm and pH 7 increased with increasing Ca^{2+} concentrations of 0, 1, 5 and 10 mM (*, P<0.05; *n* = 3). Absorbance did not change at pH 4. (C) The absorbance of PSIM at 410 nm and pH 7 with 100 µl Ca^{2+} ($+Ca^{2+}$) was greater than control PSIM without Ca^{2+} (*, P < 0.05; *n* = 3). A second addition of 100 µl Ca^{2+} ($++Ca^{2+}$) further increased absorbance. The absorbance was reduced by adding 100 µl EDTA (+EDTA), a Ca^{2+} chelator, compared to $+Ca^{2+}$ and $++Ca^{2+}$ (*, P < 0.05). Inset images are snapshots of PSIM solutions at the different Ca^{2+} conditions. Scale bar is 10 mm. (D) Microscopic images of reconstituted PSIM (2% w/v) between two glass coverslips in pH range 2-7 with 1 mM Ca^{2+}. Insets show close-up images of the aggregates. (E) The surface area covered by PSIM aggregates with 1 mM Ca^{2+} was greatest at pH 4 compared to pH 2- 3 and pH 5-6 (*, P < 0.05; *n* = 10). At pH 7 (*inset*), The surface area covered by PSIM aggregates with 1 mM Ca^{2+} was greater than the area covered by PSIM aggregates without Ca^{2+} (*, P < 0.05).

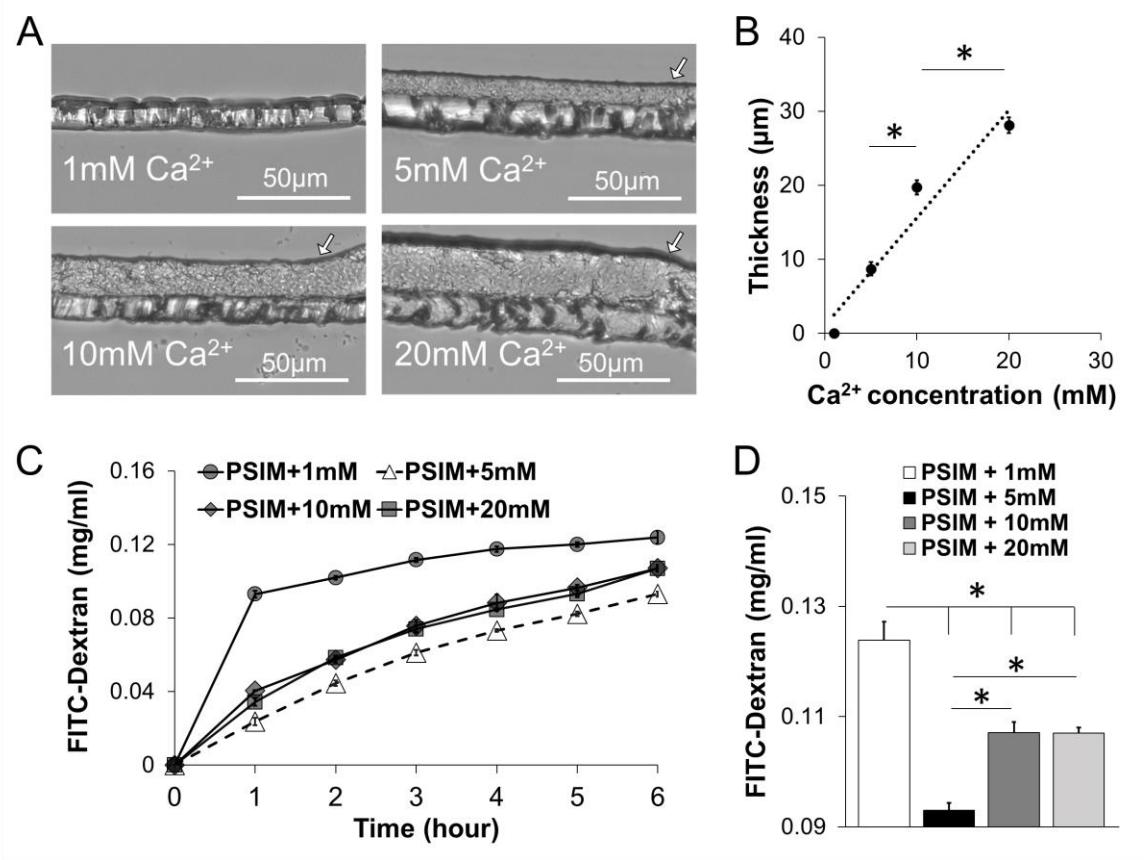

Figure 2.5. Calcium controls the thickness of the mucus barrier. (A) Cross-section images of PSIM gel layers formed on transwell membranes at 1, 5, 10, and 20 mM Ca^{2+} and pH 7. (B) PSIM layer thickness increased linearly with Ca^{2+} concentration. The thicknesses at 10 and 20 mM were greater than at 5 and 10 mM, respectively (*, $P < 0.05$; $n = 3$). (C) Concentration of FITC-dextran after transport through a PSIM layer formed on a transwell membrane in the presence of 1, 5, 10, and 20 mM Ca^{2+} at pH 7. (D) Concentration of FITC-dextran at 6 hrs after transport through the PSIM layers in (C). The concentration was greatest with 1 mM Ca^{2+} compared to all other concentrations (*, $P < 0.05$; $n = 5$). The concentration of FITC-dextran was less at 5 mM compared to 10 and 20 mM Ca^{2+} (*, $P < 0.05$).

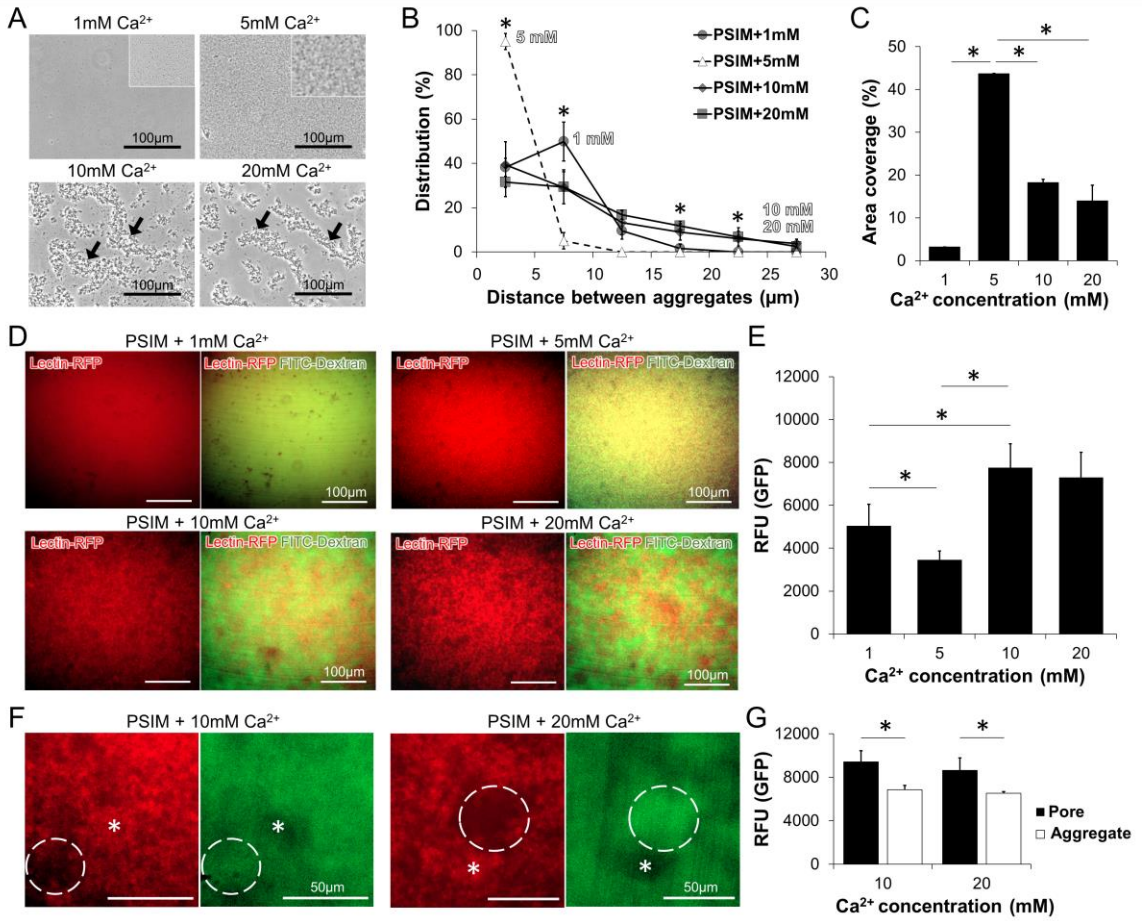

Figure 2.6. Calcium controls the porosity of the mucus barrier. (A) Microscopic images of PSIM aggregates at 1, 5, 10, and 20 mM Ca^{2+} and pH 7. Higher resolution images show homogeneous, dense, and small PSIM aggregates at 5 mM Ca^{2+}. (B) Distribution of distances between PSIM aggregates as a function of Ca^{2+} concentration. The percentage of distances less than 5 μm was greater at 5 mM compared to 1, 10 and 20 mM (*, $P < 0.05$; $n = 5$). The percentage of distances between 5 and 10 μm was greater at 1 mM compared to 5 mM (*, $P < 0.05$). The percentage of distances between 15 and 25 μm was greater at 10 and 20 mM compared to 1 and 5 mM (*, $P < 0.05$). (C) The surface area covered by the PSIM-aggregates at 5 mM was greater than at both 1 and 10 mM Ca^{2+} (*, $P < 0.05$; $n = 10$). (D) Fluorescent microscopic images of Cy5-lectin-tagged PSIM layers (red, *left*) and overlaid with FITC-dextran (green, *right*) at 1, 5, 10, and 20 mM Ca^{2+}. (E) The average GFP fluorescence (in relative fluorescence units, RFU) was less at 5 mM compared to 1, 10 and 20 mM (*, $P < 0.05$; $n = 5$). (F) Expanded images of pores (*dashed lines*) and aggregates (*stars*) formed in PSIM layers at 10 and 20 mM Ca^{2+}. (G) The fluorescence intensity of FITC-dextran in pores was greater than in aggregates at both 10 and 20 mM Ca^{2+} (*, $P < 0.05$; n = 5).

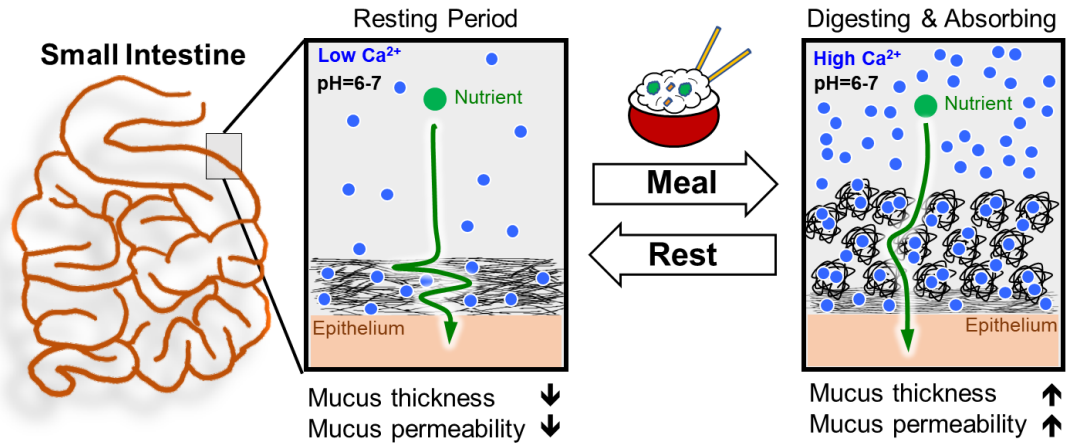

Figure 2.7. Role of calcium as a regulator of molecular transport. Proposed dynamic regulation of the thickness and permeability of the small intestine mucus barrier in response to available luminal calcium ions that fluctuate between meals.

2.4 Materials and Methods

All chemicals and supplies were purchased from Fisher Scientific and Sigma Aldrich unless otherwise specified.

2.4.1 Natural mucin extraction from a porcine small intestine

Small intestines from freshly slaughtered pigs were obtained from a local slaughterhouse and transported to the laboratory on ice within 2 hours. Porcine small intestines (PSIs) were cut into 6-inch long segments and washed with running DI water. The tissues were filled with 50 ml of 1M HCl, 1x PBS, and 1M NaOH. After both ends are tied, PSI tubules were incubated at 4 ºC for 24 hours. The solutions were collected and aliquoted into 1 ml Eppendorf tubes and centrifuged in a microcentrifuge at 10,000 x g for 30 minutes. The supernatant was collected, and total protein was quantified using a Bradford assay. Bovine serum albumin was used as a standard for known protein concentration. For optimization of NaOH concentration, cleaned PSIs (6-inch, n=3) were filled with 10 ml of serially diluted NaOH solutions (1, 0.1, 0.01, and 0.001 M) and incubated at 4 ºC for 24 hours. The solutions were collected and stored at -80 ºC. To quantify total soluble protein, the frozen solutions from all four conditions were thawed at 4 ºC, vortexed thoroughly, and divided into 1 ml aliquots. The aliquots were centrifuged in a microcentrifuge at 10,000 x g for 30 min. Supernatant from 3 aliquots were dialyzed against DI water in a cellulose membrane (molecular size cut-off = 14 kDa) for 72 hours at 4 ºC with a water change every 12 hours. The dialyzed solution was lyophilized to quantify the dry mucus weight and reconstituted at an equal concentration in DI water to quantify total protein content using a Bradford assay.

For the scale-up, PSIs (2 meter) were flushed with running tap water to remove the luminal content and the loosely bound mucus layer. The luminal space was then filled with 350 ml 0.01 M NaOH with both ends tied and incubated at 4 ℃ for 24 hours. The solubilized mucus extract was collected and centrifuged at 20,000 x g for 2 hours at 4 ºC to precipitate debris in 50 ml tubes. After collecting the clear supernatant, the pH was adjusted to 4 to induce PSIM aggregation. Aggregated PSIM was separated by centrifugation at 200 x g for 15 minutes and resuspended to get a clear solution in sterile DI water by adjusting pH to 8.0-8.5. The solubilized PSI was filtered through a 40 μm strainer and dialyzed (molecular size cut-off = 14 kDa). The dialyzed mucus extract was sterilized by adding 1% (v/v) chloroform under constant stirring at 4 ºC for 72 hours. The sterile solution at a pH of approximately 7, was frozen at -80 ºC, lyophilized, and stored as a powder at -20 ºC until used. All the experiments were conducted using the lyophilized powder reconstituted in an appropriate buffer or cell culture medium and the term PSIM is used to denote the reconstituted form at a known concentration. The theoretical density of mucin protein in the intestine was calculated by considering the surface area increased due to the intestinal folds and the villous architecture.

2.4.2 Histological sectioning of the intestinal tissues

Tissues were cut into 2 cm sections and excess water was removed. Tissues were embedded in optimum cutting temperature (OCT) cryomatrix and snap frozen in liquid nitrogen. Using a cryostat (Thermo Scientific, CRYOSTAR NX70), frozen tissues were sectioned at a 20 μm thickness. Sections were fixed with 10 % formalin and stained with hematoxylin and eosin (H&E).

2.4.3 Biophysical characterizations of the reconstituted mucus

1. Rheological characterization. Bulk rheology on reconstituted PSIM samples from 3 different pig intestines was conducted. Small amplitude oscillatory shear measurements were performed in a Kinexus Pro rheometer (Malvern Instruments, U.K.) using a cuvette cell geometry. PSIM samples were loaded into the cup at pH values of 2, 4, and 7 and held at a constant temperature of 37 °C. Oscillatory frequency sweeps were conducted between 1 and 100 Hz at a constant 0.25 % strain.

2. Absorbance characterization. PSIM aggregation was quantified using UV-vis spectroscopy. The absorbance value at 410 nm was used as a measure of PSIM aggregation. Lyophilized PSIM powder was reconstituted in 20 mM HEPES at pH 7. The pH value of the reconstituted PSIM was adjusted using 2 M HCl and 2 M NaOH. 100 µl of PSIM samples were added to a 96-well plate and the absorbance was measured using a microplate reader (Synergy H1, BioTek).

3. Microscopic characterization of PSIM aggregates. Twenty microliter droplets of PSIM solution were placed between glass coverslips and clear glass slides and were imaged using a brightfield microscope (EVOS). The images were binarized using a built-in scheme in the image analysis software ImageJ. The area covered by aggregates per image was quantified and plotted as percentage area covered normalized by the total area of the image.

4. Dynamic viscoelastic characterization. PSIM 2 % (w/v) at pH 7.3 was added to a glass vial and subjected to constant stirring. The pH was monitored in real time using a needle-

type pH probe (PreSens) and was adjusted using 2N HCl and 2N NaOH solutions. Samples were collected at specific pH values for UV absorbance measurements.

2.4.4 Bacterial cell culture

Two bacterial strains *S. typhimurium* (SL1344) and *E. coli* (MG1655) were used for live bacterial experiments. Frozen stocks of the bacterial strains were inoculated in Luria Broth (LB) and grown overnight. Optical density at 600 nm (OD600) of the overnight cultures was measured and the bacteria were seeded at a density of $1x10^7$ in fresh LB medium and allowed to grow to an OD600 of 0.6-0.8 and used for further experiments.

2.4.5 Two-dimensional bacterial motility assay in PSIM on a glass slide

Live bacterial imaging was performed in a hanging drop assembly for bacterial motility quantification. Bacteria cultured in LB were diluted 1:10 in PSIM (2 % w/v) or control (20 mM HEPES solution), and a 2 μl droplet was added on top of a circular cover glass. The cover glass with the droplet was inverted and rested on top of a 1mm thick PDMS ring bound to a glass slide. The glass slide with the hanging drop was imaged using an inverted fluorescent microscope (Zeiss). Bacterial movement was tracked in a single 2D plane and the average speed was quantified using the in-built particle tracker plug-in 'Trackmate' in ImageJ software.

2.4.6 Three-dimensional bacterial diffusion assay through PSIM in transwell inserts

HEPES solution (20 mM) was added to transwell inserts (50 μl/transwell) and used as the no barrier condition and compared to 50 μl of PSIM 2 % (w/v) at pH values of 2, 4, and 7.

Transwell inserts were placed into the wells of a 24-well plate containing 600 µl of LB. A 100 µl of live bacterial culture (10^{11} cells/ml) was gently added to the inserts and the plates were incubated at 37 ºC and 5 % CO_2. Fluorescence intensity was measured at 1-hour intervals for 6 hours in the bottom well and converted to colony forming units (CFUs) using a previously established standard curve.

2.4.7 Fixation and cryo-sectioning of PSIM layers on transwell membranes

Transwell inserts with different PSIM gel layers formed in response to added Ca^{2+} were held vertical. A small cut was created on the edge of the membrane from the bottom side. The inserts were kept on tissue paper to absorb all liquid from the membrane and mucin gel. Transwell inserts were transferred into wells of 24 well plate containing 600 µl of 10% formalin solution in PBS. Formalin (10% in phosphate buffered saline) solution was gently added on the apical side of the transwell and kept at room temperature for 10 minutes. Inserts were moved to a different well and the formalin solution was carefully replaced by PBS 3 times on apical and basal sides. The membranes were dehydrated again using tissue paper and carefully cut out from the inserts using a scalpel. The membranes were embedded in OCT and snap frozen in liquid nitrogen. Frozen membranes were cross sectioned at a 10 µm thickness using a cryostat and collected on glass slides. The sections were imaged using a bright field microscope (EVOS) and the thickness of the gel layers was calculated using ImageJ.

2.4.8 Lectin staining for visualization of PSIM aggregates

Far-red-fluorescence (Cy5)-conjugated Sambucus Nigra (SNA) lectins (Vector Labs) were added to PSIM 2 % (w/v) at a final concentration of 10 µg/ml and incubated at room temperature for 30 minutes. The solution was dialyzed against DI water for 24 hours constant stirring in a dark room at 4 ºC. The fluorescent lectin tagged PSIM was used to visualize PSIM aggregates using fluorescence microscopy.

2.4.9 Pore size distribution

Aggregates were imaged microscopically in PSIM (2 % w/v) containing 1, 5, 10, and 20 mM Ca^{2+}. Inter-aggregate distance was measured at 100 random locations per image using ImageJ. An average number distribution (%) of at least 5 independent images from each condition was plotted in a range of 0 - 30 µm. FITC-dextran diffusion was measured at different calcium concentrations. HEPES solution (20 mM) was added to the wells of a 24 well plate (600 µl/well). PSIM solution 2 % (w/v) in 20 mM HEPES at a pH of 7 and containing 1, 5, 10, and 20 mM Ca^{2+} was added to transwell inserts (100 µl/transwell). Transwell inserts were placed into the wells of 24 well plates containing 600 µl of HEPES solution and the well plate was incubated for 12 hours at 37 ºC and 5 % CO_2 to allow for mucus layer formation. A 10 µl droplet of 10 mg/ml solution of FITC dextran (MW= 20 kDa) in DI water was gently added to the inserts and the plate was incubated at 37 ºC and 5 % CO_2. Fluorescence intensity was measured at 1-hour intervals for 6 hours in the bottom well and converted to concentration of FITC dextran.

2.4.10 Fluorescent imaging and area overlap analysis

PSIM 2% (w/v) at pH 7 and containing 1, 5, 10, and 20 mM Ca^{2+} was added to a 96-well plate (100 µl/well). The well plate was incubated overnight at 37 ºC and 5 % CO_2 to allow for mucus layer formation. FITC-dextran (MW = 20 kDa) at a concentration of 10 mg/ml in 20 mM HEPES was gently added to the transwells (10 µl/transwell) and the plate was incubated at 37 ºC and 5% CO_2. Fluorescent images using were captured using a Zeiss Axiovert 4-laser spinning disc confocal microscope (20x magnification) after 1 hour. Image analysis for GFP intensity (FITC-dextran) and RFP intensity (Cy5 lectin tagged PSIM) was performed using ImageJ and normalized for the total area of the images. Areas with bright RFP intensity were considered as 'aggregate' and low RFP intensity areas as 'pore'. The average intensity of FITC was determined in the entire image and in the pore and aggregate regions.

2.4.11 Statistical analysis

A two-tailed Student's t-test assuming unequal variances was used for statistical analysis of different conditions. One-way ANOVA with Bonferroni post-hoc test was used for multiple comparisons. Differences were considered significant at $p < 0.05$. All data are presented as a mean ± standard deviation.

CHAPTER 3

MODEL OF INTESTINAL MUCOSA TO QUANTIFY THE ROLE OF MUCUS AND EPITHELIAL BARRIER IN REGULATING THE HOST INNATE IMMUNE RESPONSES TO PROBIOTIC AND PATHOGENIC BACTERIA

3.1 Introduction

In the intestines, three major components mediate the host-response to pathogens and the gut microbiota: the mucosal barrier, the epithelial layer and tissue-resident immune cells [97]. The interactions of these components in pathophysiological conditions are poorly understood. Two major disease states result from disruption of these protective mechanisms, acute enteropathogenic infections, and chronic inflammatory bowel diseases (IBD) [98-99]. The mucus layer is the first line of defense, which plays a critical role in the prevention of enteropathogenic infections. In the healthy colon, the secreted mucus layer that covers the entire epithelium minimizes interactions of commensal bacteria with host cells [63, 100]. Dysfunction of the mucus layer and bacterial infiltration are linked to tissue inflammation and disease [47, 49, 101-102]. During enteropathogenic infections, bacteria can penetrate intestinal regions of disrupted mucus [103-105], but there is recent evidence that bacteria can also penetrate regions with intact mucus [106]. A better understanding of the interaction between microbes and the protective host mechanisms could lead to improved treatment for intestinal diseases.

The responses of epithelial and immune cells to bacterial infiltration are difficult to decouple from in vivo measurements and are poorly understood. The epithelial barrier and cells of the innate immune system collectively function as the subsequent layers of

protection after the mucus layer [107]. In the colon, tight junctions between epithelial cells prevents transmigration of pathogens into underlying tissue [108]. Colonic epithelial cells produce chemokines, such as interleukin-8 (IL-8), that attract neutrophils and other effector cells of the innate and adaptive immune system [109]. Monocytes, which are innate immune cells, detect pathogens directly as well as respond to epithelial derived signals. One response to these stimulants is differentiation into macrophages and dendritic cells [110-111]. LPS and flagellin are common pathogen associated molecular patterns (PAMPs) that bind to toll-like receptors (TLR4 and TLR5) and activate the downstream pathways that cause pro-inflammatory cytokine secretion [112-114]. Immune-cell-derived tumor necrosis factor (TNF-α) is a cause of systemic inflammation. Both TNF-α and IL-8 levels are significantly upregulated in the intestines of patients with IBD [115-116].

A common enteropathogenic infection is Salmonellosis [117-118]. Salmonella enterica subsp. enterica serovar Typhimurium is a foodborne pathogen that causes diarrhea and can often be fatal [118]. In humans, infection with Salmonella or other enteropathogenic bacteria is linked to higher incidence of IBD [119-121]. Studies have shown that attachment of Salmonella to mucus is a critical step for infection [122-125]. In mouse models, Furter et al. showed that Salmonella infects the colonic epithelium even when covered with a thick layer of mucus [106]. This recent observation contradicts the common notion that the mucus barrier serves as a sticky net to trap the invading luminal microbes [126]. How Salmonella penetrate the mucus barrier and the effects of this penetration on epithelial and immune cells is not fully understood.

Murine models are the most common method to study the gastrointestinal biology. However, studying the complex interactions between luminal microbes, tissue immune cells and the mucosal barrier in living animals is challenging. Alternately, in vitro platforms are well suited to studying these complex interactions. For example, three-dimensional biomaterial platforms have been developed to mimic the morphology of the epithelial layer [12, 127]. Epithelial and immune cell interactions are commonly measured in transwell-based platforms [128-129]. Flow based microfluidic platforms have enabled long-term co-culture of gut-representative microbial communities [16-17, 130]. Incorporation of mechanical forces within microfluidic platforms induced three-dimensional villus differentiation and allowed quantification of communication between bacteria-epithelial-immune cell compartments [11, 15, 130].

The inclusion of a mucus layer is critical because of its role in mediating bacteria-epithelial cell interactions. Some cultured epithelial cells secrete mucus and form mucus layers that enable the quantification of drug and molecular interactions with mucus [131-132]. Two recent studies demonstrated thick mucus layer secretion from primary human colonic epithelial cells using air-liquid interface in transwell culture or colon-on-a-chip microfluidic culture [133-134]. Most cultured cell lines, however, do not generate a layer matching physiological thickness of colonic mucus. Due to insufficient mucus secretion from cultured human epithelial cells, porcine gastric mucin (PGM) has been used as human mucin substitute [34-35]. PGM has been used to recreate the intestinal mucus layer by mixing with agar and forming a solid interface with luminal solution that supported bacterial attachment and growth [16-17]. However, stomach mucus has different physicochemical properties than

intestinal mucus and commercially available PGM does not undergo sol-gel transitions [135]. An alternative to PGM is purified intestinal mucus. It has been shown that MUC2, which is purified from intestinal mucus, has antiviral activity and attenuates the virulence of pathogenic bacteria [136-137]. We have developed a method to extract porcine small intestinal mucus (PSIM). Reconstituted PSIM undergoes sol-gel transitions with changes in pH and ion concentrations, similar to native intestinal mucus [138]. Low pH caused mucus aggregation and reduced bacterial transport, and moderate calcium concentrations formed microscopic aggregates that impeded molecular diffusion.

Here, we demonstrate a model of intestinal mucosa to quantify the role of mucus and epithelial barrier in regulating the host innate immune responses to probiotic and pathogenic bacteria. We hypothesize that mucus prevents the penetration of bacteria through the intestinal lining and that the motility of pathogenic bacteria affects their penetration and immune response. To decouple the host-microbe interactions, mucus and epithelial layers were developed in a physiological form on transwell membranes. The porous transwell membrane enabled molecular communication between human epithelial (HT-29) cells and human monocytic (THP-1) cells. The hypotheses were tested with commensal VSL#3 bacteria, wild-type SL1344 Salmonella, and a non-motile *flhDC* knockout strain of Salmonella. Bacterial penetration, immune cell differentiation, and cytokine release were quantified using fluorescent immunostaining, microscopic imaging, and ELISA. The effects of a mucus layer on bacterial transmigration and molecular diffusion were quantified using fluorescent spectroscopy. This intestinal mucosa model enabled the quantification of the differences in the integrity of mucosal barrier compared

to epithelial barrier alone when challenged with live bacteria. This mucosal barrier model enabled the measurement of bacterial penetration, immune cell differentiation and cytokine release. Understanding the mechanisms of action of probiotics or pathogens when in contact with the mucosal barrier will lead to development of therapies for bacterial infections and immunological diseases of the intestine.

3.2 Results

3.2.1 PSIM formed a gel layer on top of epithelial cells without affecting cell viability.

We have developed a method to mechanistically study the host-microbe interactions at the mucosal interface of the intestines. A mucus gel layer was reconstituted on top of epithelial cells growing on transwell membranes (Figure 3.1). Human colonic epithelial cells (HT-29) genetically labeled to express red fluorescent protein (RFP) covered the entire surface of the transwell membrane and coverage was not affected by the presence of PSIM (Figure 3.1A). PSIM (20 mg/ml) was added to the epithelial cells and after 12 hours it formed an opaque gel layer in situ that was structurally porous (Figure 3.1B). This 12-hour incubation at 37 °C reduced the thickness of the PSIM layer (Figure 3.1C). Initially, the total height of solubilized PSIM (100 µl/well) layered on top of epithelial cells was approximately 2.7 mm. Final thickness of the gel layer formed was 880 ± 230 µm (Figure 3.1B). The PSIM gel layer formation was robust and the structure was maintained after cryo-freezing and histological sectioning. PSIM formed a tightly bound gel layer and did not affect the viability of HT-29 cells (Figure 3.1D). No significant difference was observed in the live (green) and dead (red) cell area coverage between the presence and absence of a PSIM

layer (Figure 1E). DAPI (4′,6-diamidino-2-phenylindole) staining of PSIM (red) showed that the PSIM gel layer has a fibrous structure (Figure 1F). When added, fluorescent wild type Salmonella (green) were suspended in the three-dimensional mucus matrix (Figure 3.1F).

3.2.2 PSIM is not immunogenic to epithelial or immune cells.

To test its immunogenicity with human-derived cell lines, reconstituted PSIM was directly added to the monocultured HT-29 and THP-1 cells. PSIM mostly did not induce a pro-inflammatory cytokine and chemokine response from HT-29 and THP-1 cells. HT-29 cells were cultured on the apical side of 24-well transwell inserts (Figure 3.2A) and IL-8 and TNF-α were quantified in the basolateral medium. HT-29 cells secreted a small but significantly higher amount of IL-8 in response to PSIM when compared to HT-29 cells alone ($P < 0.05$, Figure 3.2B). There was no difference in the amount of TNF-α secreted from HT-29 with and without PSIM application (Figure 3.2C). THP-1 cells were cultured in suspension in 24 well plates and IL-8 and TNF-α quantified in the culture medium (Figure 3.2D). PSIM did not induce IL-8 or TNF-α secretion from THP-1 cells compared to cells without PSIM (Figure 3.2E, F).

3.2.3 Immunological responses from epithelial and immune cells are stimulant dependent.

When cultured independently, HT-29 and THP-1 cells respond differentially after direct contact with bacterial antigen LPS, a set of 8 live probiotic bacteria (VSL#3), and pathogenic bacteria Salmonella. Intestinal epithelial cells have regular incidence of

bacterial contact, but immune cells only come in direct contact with live bacteria during bacterial infection events. The amounts of pro-inflammatory chemokine (IL-8) and cytokine (TNF-α) secreted from epithelial and immune cells were stimulant dependent. Salmonella induced a robust chemokine response in HT-29 cells, causing approximately 24-fold higher IL-8 secretion compared to unstimulated cells ($P < 0.01$, Figure 3.3A). Direct contact of HT-29 cells with LPS or VSL#3 did not increase IL-8 secretion (Figure 3.3A). LPS-stimulated THP-1 cells secreted 61-fold more IL-8 compared to unstimulated cells ($P < 0.01$, Figure 3.3B). Direct contact with VSL#3 and Salmonella each caused an approximately 30-fold increase in IL-8 secretion from THP-1 cells compared to bacteria-free controls ($P < 0.01$, Figure 3.3B).

There was no increase in the level of TNF-α secreted by HT-29 cells after direct contact with LPS or live bacteria compared to unstimulated cells (Figure 3.3C). TNF-α secretion from THP-1 cells was significantly increased when cultured with LPS or live bacteria (Figure 3.3D). LPS induced the highest TNF-α secretion and the level of TNF-α was 342-fold higher compared to unstimulated THP-1 cells ($P < 0.01$, Figure 3.3D). Direct contact of THP-1 cells with VSL#3 ($P < 0.01$) and Salmonella ($P < 0.05$) caused 77 and 20-fold increases in TNF-α, respectively (Figure 3.3D).

The morphology of THP-1 cells changed significantly when cultured in direct with VSL#3 (Figure 3.3E). Change in morphology indicates the differentiation into macrophage and dendritic-like cells. THP-1 cells stimulated with VSL#3 induced approximately 6-fold increase in the number of differentiated cells per millimeter squared area ($P < 0.01$, Figure 3.3F). Stimulation with LPS or Salmonella did not induce a change in morphology and

cells were mostly round (Figure 3.3E). Collectively, the results show that epithelial and immune cell activation and immunological responses are stimulant dependent.

3.2.4 A PSIM gel layer prevents LPS induced immunogenic responses.

In the co-culture platform, we hypothesized that the mucus layer would act as a physical barrier for molecular diffusion. Mucus layers prevented pro-inflammatory chemokine and cytokine secretion by human epithelial and immune cell co-culture in response to bacterial products. To test this hypothesis, epithelial-immune cell co-culture was used with and without mucus (Figure 3.4A). Co-culture of the HT-29 and THP-1 cells did not affect the basolateral levels of IL-8 and TNF-α when compared to monocultures (compare without mucus and without LPS in Figure 3.4B, C to Figure 3.2B, C, E, F). The addition of PSIM on the apical side of the epithelial layer caused no change in the levels of IL-8 and TNF-α (Figure 3.4B, C). LPS increased the concentrations of both IL-8 ($P < 0.05$, Figure 3.4B) and TNF-α ($P < 0.05$, Figure 3.4C) 4-fold in the absence of a PSIM layer. The presence of a mucus layer significantly reduced the levels of IL-8 ($P < 0.05$, Figure 3.4B) and TNF α ($P < 0.05$, Figure 3.4C) after LPS stimulation. The total amounts of IL-8 and TNF-α from the co-cultures were significantly lower compared to direct stimulation of THP-1 cells by LPS ($P < 0.05$, compare Figure 3.4B, C to Figure 3.3B, D). Collectively, the results show that the epithelial barrier attenuates immune cell stimulation by preventing direct contact of immune cells with bacteria derived molecules, and the mucus layer further increases this barrier function.

3.2.5 A PSIM gel layer is a barrier to migration of live probiotic bacteria.

To investigate the barrier function of the mucus layer in presence of commensal bacteria, we added a commercial probiotic mix VSL#3 to the HT-29 and THP-1 co-culture and measured the bacterial transmigration across the epithelial layer and the corresponding cytokine and chemokine responses. Without mucus, bacteria transmigrate across the epithelial layer to the bottom well (Figure 3.5A). The mucus layer reduced bacterial transmigration by 7-fold ($P < 0.05$, Figure 3.5B). Bacterial transmigration in the absence of a mucus layer induced THP-1 cell differentiation characterized by changes in morphology from round to elongated (Figure 3.5A). A 11-fold higher number of differentiated cells per millimeter squared surface area were present without the mucus layer when compared to the conditions containing a mucus layer ($P < 0.01$, Figure 3.5C). Due to increased bacterial loads, significantly higher concentrations of both IL-8 and TNF-α were measured in the bottom well ($P < 0.01$, Figure 3.5D and $P < 0.05$, Figure 3.5E). The mucus layer reduced the IL-8 concentration by 16-fold (Figure 3.5D) and TNF-α concentration by 7-fold (Figure 3.5E). Immunohistostaining showed the spatial arrangement of the epithelial cell layer expressing epithelial cell adhesion molecule (EpCAM) at the base and the mucus layered on top of the epithelial surface. VSL#3 bacteria that stained positive for nuclear stain DAPI were mostly seen on the outer surface of the mucus layer and few or no bacteria were present deeper in the mucus layer (Figure 3.5F). Collectively, the results show that a reconstituted mucus layer reduced bacterial transmigration, thereby preventing direct contact between commensal bacteria and epithelial cells. The barrier effect leads to reduced epithelial damage by bacteria and

reduced proinflammatory cytokine and chemokine responses from the underlying immune cells.

3.2.6 A PSIM gel layer enhances the transmigration of Salmonella.

To test if active motility enables bacteria to transmigrate across the mucus layer, we used motile Salmonella. Surprisingly, the presence of mucus significantly increased the transmigration of wild type Salmonella and 3-fold more Salmonella transmigrated across the epithelial cell layers in presence of mucus ($P < 0.05$, Figure 3.6A). In the HT-29 and THP-1 co-culture, wild type Salmonella significantly increased the amounts of IL-8 and TNF-α in the presence of mucus and an epithelial layer compared to an epithelial layer alone ($P < 0.05$, Figure 3.6B, C). To test if these effects are controlled by flagella, a flagellar knockout (ΔflhDC) strain of Salmonella was created. The knockout caused a loss in Salmonella motility and the mean velocity was similar to VSL#3. Mean velocity of wild type Salmonella was significantly higher compared to the knockout strain and VSL#3 ($P < 0.05$, Figure 3.6D). The presence of a mucus layer reduced the transmigration of knockout Salmonella across the epithelial cell layer ($P < 0.05$, Figure 3.6A). The amount of IL-8 was significantly lower in presence of a mucus layer compared to epithelial cells alone for knockout Salmonella (Figure 3.6B). The concentration of TNF-α in the medium with knockout Salmonella with or without a mucus layer (Figure 3.6C) was equivalent to basal levels from an unstimulated co-culture of cells (Figure 3.4C). Immunostaining showed the flagella of wild type Salmonella and the lack of flagella of knockout Salmonella (Figure 3.6E). Histological sections of the mucosal layers on transwell membranes showed wild type Salmonella embedded deeper into the mucus layer (Figure 3.6F) than VSL#3 (Figure

3.5F). Within the gel layer, a significantly higher number of bacteria were found at the top and center of the mucus layer compared to the area proximal to the epithelial surface (Figure 3.6G). Collectively, these results show that motile Salmonella, in presence of mucus, utilize flagellar motility for higher transmigration across the mucus and epithelial layers. Higher transmigration caused significantly higher immune responses from the epithelial-immune cell co-culture.

3.3 Discussion

To gain a deeper understanding of how commensal and pathogenic bacteria interact with the mucosal lining of the intestine, we created an in vitro model of this barrier which consisted of a mucus layer, an epithelial cell layer and cells of immune system. These components represent essential complexities of the mucosal barrier. With this model we showed that the mucosal layer decreased the penetration of LPS and non-motile bacteria (Figure. 3.4&3.5). All bacteria tested in this study induced the production of cytokines and chemokines by THP-1 monocytes (Figure 3.3B, D). Additionally, Salmonella induced the production of IL-8 by HT-29 epithelial cells. In contrast, VSL#3 did not induce epithelial IL-8 production (Figure 3.3A, C). These results indicate that epithelial cells tolerate contact with commensal bacteria but respond to pathogens, whereas innate immune cells respond to all bacterial contact.

This intestinal mucosa model was built upon the commonly used transwell platform, which enabled creation of epithelial and mucus gel layers, and co-culture with bacteria and immune cells (Figure 3.1). The mucus was not cytotoxic (Figure 3.1) and was

biocompatible to human epithelial and immune cells (Figure 3.2). The thickness of the mucus gel layer can be adjusted to match the thickness of mucus in different compartments of the gastro-intestinal tract (Figure 3.S1). The mucus layer caused spatial segregation of live commensal bacteria away from the epithelial layer and enabled co-culture studies up to 24 hours. The mucosa model demonstrated key mucus-layer-associated processes that have been reported in animal models but are difficult to reproduce in vitro.

In this model, both mucus and epithelial cells formed a physical barrier to molecular diffusion and bacterial penetration. The amounts of IL-8 and TNF-α produced in the co-culture system without mucus (Figure 3.4B, C) were lower than THP-1 cells directly stimulated with same amount of LPS (Figure 3.3B, D). When mucus was present, these amounts were further reduced (Figure 3.4). In the absence of the mucus layer, more bacteria crossed the epithelial cell layer (Figure 3.5D) and more monocytes differentiated (Figure 3.5E). This dependence indicates that the mucus layer helps maintain the integrity of epithelial barrier in presence of commensal bacteria. The lack of production of TNF-α by epithelial cells indicates that inflammation is only induced after a breach in epithelial barrier and direct contact of live bacteria with immune cells.

As a barrier, the mucus layer was more effective at preventing penetration of commensal bacteria (Figure 3.5) than immunogenic molecules (Figure 3.4). The transmigration of non-motile commensal bacteria (*VSL#3*) across the epithelial layer was significantly lower in presence of mucus (Figure 3.5). With mucus, the amounts of IL-8 and TNF-α induced by VSL#3 were very low (Figure 3.5), similar to the amounts produced by unstimulated

epithelial and immune cells (-LPS in Figure 3.4). The difference in penetration between bacteria and molecules was most likely because of the structure of intestinal mucus. The mucus gel layer was porous as shown by histological sectioning and fluorescent confocal microscopy (Figure 3.1B, F). After gelation, intestinal mucus forms islands of aggregated protein that permit easier transmigration of small molecules than microbes and particulates [138].

An unexpected result was that the presence of mucus *increased* the penetration of Salmonella through the intestinal barrier (Figure 3.6). In comparison, mucus reduced the penetration of LPS (Figure 3. 3), and non-motile commensal bacteria (Figure 3.5). Salmonella transmigration followed complete penetration of the mucus layer and the epithelial barrier (Figure 3.6A). This effect was surprising because the penetration of Salmonella through mucus and an epithelial layer was greater than through an epithelial layer alone (Figure 3.6A-E), which was considerably thinner (Figure 3.1B). Flagella were required for this increase in transmigration through mucus (Figure 3.6A-E), showing that this phenomenon is dependent on bacterial motility. Two explanations for this observation are that mucus increases the motility of Salmonella by (a) attracting flagellated Salmonella or (b) inducing the production of flagella.

The intestinal barrier responded in distinct ways to immunogenic molecules. The primary immunogenic molecules in Salmonella are LPS and flagellin, which are detected by toll-like receptors (TLR) 4 and 5, respectively [113, 139]. When LPS was applied to THP-1 monocytes, they did not differentiate (Figure 3.3F). The LPS successfully crossed both the

mucus and epithelial barriers as indicated by the secretion of IL-8 and TNF-α (Figure 3.4). This result show that monocyte differentiation after contact with bacteria (Figure 3.3E) is controlled by a mechanism that is independent of LPS and TLR4. When knockout (Δ*flhDC*) Salmonella were applied to the intestinal barrier model, the THP-1 monocytes did not produce TNF-α (Figure 3.6C). This result suggests that the production of TNF-α is mediated by TLR5, the primary toll-like receptor to detect the flagella of Salmonella.

Combined, these results paint a picture of how the intestinal barrier could react to contact with bacteria (Figure 3.7). In the healthy condition of an intact mucus layer and a lumen filled primarily with commensal bacteria (condition 1, Figure 3.7A), no bacteria penetrate the barrier layer and no cytokines are produced. When there is physical damage to the mucus layer (condition 2, Figure 3. 7B), commensal bacteria penetrate the epithelial layer and trigger the production of cytokines and chemokines by monocytes (Figure 3.5F, G). After this contact, the monocytes differentiate into macrophages and dendritic cells (Figure 3.5C, E). Chemokines, e.g. IL-8, recruit neutrophils to contain the infection. When motile Salmonella are present in the lumen in significant amounts (condition 3), the mucus layer does not prevent penetration (Figure 3.7C). In this condition, the epithelial layer produces chemokines (Figure 3.3A) to recruit neutrophils before the pathogens cross the epithelial barrier. Once this barrier is breached, monocytes are activated, producing a similar immune response to an infection of commensal bacteria (Figure 3.3B, D and 6C, D).

The intestinal mucosa model presented here provided insights into the role of mucus and epithelial barrier against bacteria and bacteria-derived molecular factors in presence of

innate immune cells. We envision that this platform will be useful for screening host response against pathogenic, opportunistic, and probiotic strains of bacteria. Many of the obtained results could only have been obtained with an in vitro system that includes the three essential components of the mucosal barrier: mucus, epithelial cells and immune cells. For example, it was found that the epithelial barrier is a key component of the innate immune response to bacterial infection, especially in the detection of pathogens. A better understanding of the relation between microbial pathogens, the intestinal barrier and the immune system has the potential to improve treatment of infections and immunological diseases.

3.4 Materials and Methods

All chemicals and supplies were purchased from Fisher Scientific and Sigma Aldrich unless otherwise specified.

3.4.1 Human cell culture

HT-29 (ATCC, HTB-38) adherent cells were cultured in McCoy's 5A medium (Sigma Aldrich) supplemented with 2.2 g/L sodium bicarbonate. THP-1 (ATCC, TIB-202) suspension cells were cultured in RPMI-1640 medium (containing 0.05 mM β-Mercaptoethanol). HEK293T/17 (ATCC, CRL-11268) cells were cultured in Dulbecco's Modified Eagle Medium (DMEM). All media were supplemented with 10% fetal bovine serum (FBS) and 1% penicillin/streptomycin and referred to as complete medium in the methods. Cells were maintained in a 37 ^{o}C humidified incubator with 5% CO_2.

RFP-expressing HT-29 cells were made by lentivirus transfection. For lentivirus production, HEK293T/17 cells grown in a 10 cm dish were transfected with four plasmids acquired from addgene: (4 μg pLV-mcherry (Cat #36084), 2 μg pMDLg/pRRE (Cat #12251), 2 μg pRSV-Rev (Cat #12253) and 2 μg pMD2.G (Cat #12259), using the standard calcium-phosphate co-precipitation method. Virus was harvested 24 h post transfection and filtered through 0.45 μm filter. For transduction, HT-29 cells cultured in six well plates were cultured in equal volumes of the virus containing medium and complete McCoy's 5A medium. Cells were monitored for RFP expression and sub-cultured after most cells expressed RFP when checked for fluorescence qualitatively.

3.4.2 PSIM extraction and purification

PSIM was extracted as described before [138] with changes in sterilization procedure. Briefly, intact small intestine tubules were cut into 2-meter lengths and rinsed with water to eliminate food particles from the lumen. The tubules were drained gently, and the lumen was filled with 350 ml of 0.01 M NaOH. The ends of the tubules were tied and incubated for 24 hours at 4 ^{o}C. After incubation the solubilized material was drained by squeezing and collected. The extract was subjected to centrifugation at 20,000 x g (Thermo Scientific) at 4 ^{o}C for 2 hours to remove insoluble debris. The supernatant was collected without disturbing the precipitate. The clear supernatant was subjected to sol-gel transition by adjusting the pH to 4 using 2 M HCl. The aggregates formed at pH 4 were subjected to centrifugation at 200 x g for 15 minutes and resolubilized in sterile DI water by adjusting the pH value to 8. The solution was passed through a 40 μm strainer and subjected to dialysis using a membrane with molecular size cut-off equal to 14 kDa. The dialyzed

mucus extract was sterilized by adding 1% (v/v) chloroform under constant stirring at 4 ºC for 72 hours. The solution (30 ml aliquots) was transferred to 50 ml conical polypropylene tubes, frozen to -80 ºC, and freeze dried (Labconco Freezone 2.5L freeze dry system). The freeze-dried mucus was reconstituted aseptically in serum- and antibiotic-free McCoy's 5A medium. The solutions were sterilized in 15 ml polypropylene tubes by adding 10% chloroform and allowing to sit at 4 ºC for 24 hours without shaking. The chloroform solution formed a distinct layer at the bottom and mucus solutions were collected without disturbing the interface under aseptic conditions. The solutions were aliquoted in 1.5 ml polypropylene tubes and stored at -80 ºC until use.

3.4.3 Bacteria culture

Probiotic VSL#3 bacteria were acquired from a commercial source (VSL Pharmaceuticals, Inc.) and stored at 4 ºC until use. For co-culture experiments, the freeze-dried bacteria were aseptically reconstituted in serum- and antibiotic- free McCoy's 5A medium at a cell density of 10^{10} CFU/ml. Bacterial cells were incubated at 37 ºC for 1 hour to recover. After 1 hour, the cell density was diluted to required cell density by serial dilution.

Wild type Salmonella strain SL1344 was used for live motile bacterial experiments. The Δ*flhDC* SL1344 strain was created using a modified lambda red recombination procedure [140]. SL1344 was transformed with plasmid pkd46 by electroporation. Single colonies were inoculated into 50 ml of LB supplemented with 100 μg/ml of carbenicillin and grown at 30 ºC. Once the absorbance at 600 nm (OD600) of the culture reached 0.1, arabinose was added to the culture to a final concentration of 20 mM and grown until the OD600 was

equal to 0.8. Bacteria were centrifuged at 3000xg for 10 minutes and washed twice with nanopure water (Millipore). Bacterial pellet was resuspended in 400 µl of nanopure water. In a polypropylene tube, 1 µg of DNA (PCR amplification of pkd4 using the primers, 5'-FOFZCACGGGGTGCGGCTACGTCGCACAAAAATAAAGTTGGTTATTCTGGgtctt gagcgattgtgtaggc-3' and 5'-ZZFFACAGCCTGTTCGATCTGTTCATCCAGCAGTTGTGGAATAATATCGGaattag ccatggtccatatgaatatc-3') was mixed with 50 µl of resuspended Salmonella. Bacteria were electroporated in a 1 mm cuvette (Fisher Scientific catalog # FB101) with the following settings on the electroporation system (BIORAD, GenePulser Xcell): Voltage = 1.8 kV, Capacitance = 25 µF, Resistance = 200 Ω, and 5 ms time constant. Primers were purchased from Invitrogen, where FOFZ are phosphorothioated nucleotides corresponding to ATAC and ZZFF correspond to TTAA. After electroporation, bacteria were recovered in 1 ml of LB for 2 hours at 37 ^{o}C. The recovery solution was plated on agar plates supplemented with kanamycin (50 µg/ml) and incubated at 37 ^{o}C overnight. Positive colonies were regrown on kanamycin plates overnight at 43 ^{o}C in order to eliminate pkd46 from the bacteria. Salmonella were transformed with a plasmid encoding for GFP under the control of constitutive Plac promoter using electroporation as discussed above. The cultures were stored at -80 ^{o}C in 25% glycerol solution.

For experiments, frozen stocks of the Salmonella strains were inoculated in LB medium and grown overnight at 37 ^{o}C. Small amount of overnight culture was inoculated in fresh LB medium and allowed to grow to a density of 4 x 10^{8} CFU/ml and used for further experiments. To prepare bacteria for transwell co-culture experiments, bacteria culture was

subjected to centrifugation at 2500 x g for 10 minutes. The bacterial cell pellet was washed three times with PBS by gentle pipetting multiple times and repeating the centrifugation step in between. Final pellet was reconstituted in serum- and antibiotic-free McCoy's 5A medium and the required cell density was adjusted by serial dilution.

3.4.4 Epithelial cell seeding in transwell inserts

For transwell assays, HT-29 cells were detached from culture flasks using trypsin and seeded at a density of 10^5 cells per insert in 3 μm pore size polycarbonate membrane transwell inserts (CLS3415, Corning). Inserts were cultured for 7 days in 24 well plates in complete McCoy's medium. The culture medium was changed 24 hours after cell seeding and every 48 hours after that. After day 7, the culture medium was aspirated from the transwell inserts. The inserts were washed three times with PBS on both the apical and basolateral sides. To check for incomplete cell coverage, inserts were filled with 250 μl of PBS and the change in liquid level was checked for 5 minutes. The inserts with no change in liquid level were used for further experiments. To check for coverage microscopically, inserts were seeded with RFP-expressing HT-29 cells. After 7 days of culture, the inserts were imaged using EVOS FL Auto imaging system (Life technologies). Images captured using a 10x objective were tiled using in-built EVOS software.

3.4.5 Mucus layer formation and cytotoxicity of PSIM on epithelial cells

To form mucus layers, HT-29 cells were cultured for 7 days in the transwell inserts and layered with 100 μl of sterile PSIM (20 mg/ml). Inserts were incubated in a 37 ^{o}C humidified incubator with 5% CO_2 for 12 hours.

For testing cytotoxicity of PSIM, HT-29 cells were cultured for 7 days in the transwell inserts and washed three times with phosphate buffer saline (PBS). The inserts were transferred to a new 24 well plate and 600 µl of serum- and antibiotic-free McCoy's 5A medium was added to the basolateral side. To form the mucus layers, 100 µl of thawed PSIM was added to the apical side. For controls, 100 µl of serum- and antibiotic-free McCoy's 5A medium was added to the apical side. The plates were incubated for 24 hours at 37 ^{o}C. The viability of HT-29 cells after application of the PSIM layer was performed using a viability/cytotoxicity assay kit (Cat # L3224, Invitrogen). The transwell inserts were transferred to a fresh 24-well plate containing 600 µl of phosphate buffer saline (PBS) and rocked gently. The PBS was replaced three times to wash the bottom surface of the transwell membrane. Finally, the wash solution was replaced with PBS containing 2 µm Calcein AM and 4 µm Ethidium homodimer-1 and incubated for 30 minutes at room temperature. Fluorescent images were acquired using Zeiss Spinning Disk Axio Observer Z1 microscope (Carl Zeiss) with a C-Apochromat 63x oil immersion objective and Zen software. To quantify area coverage, fluorescent images of the stained cells were background subtracted and segmented to isolate green (Live) and red (Dead) signal. The percent area covered by positive signal from green and red channels was quantified relative to the total image area.

To visualize bacteria embedded in the mucus gel, 10^3 CFU/ml wild type GFP Salmonella were mixed in the PSIM solution prior to adding it to transwell inserts covered with HT-29 cells (as above). After incubation at 37^{o}C for 12 h, the cells and mucus in the inserts were fixed using 10% formalin solution in phosphate buffer saline for 20 minutes. The

membranes were cut from the inserts and washed in PBS three times. The mucus gel layer was separated from the membrane and the cells, transferred onto a coverslip and stained with DAPI, which identified the mucus gel under UV light. GFP-expressing Salmonella embedded in PSIM gel were imaged using Zeiss Spinning Disk Axio Observer Z1 microscope (Carl Zeiss). Z-stack images were captured with a 63x oil immersion objective at 1 μm height intervals using Zen software. Three-dimensional rendering and image processing were performed using Imaris (Bitplane, Belfast, UK).

3.4.6 Immunological response of epithelial and immune cells to PSIM

For testing immunogenicity of PSIM, HT-29 cells cultured for 7 days in the transwell inserts were washed three times with phosphate buffer saline (PBS). The inserts were transferred to a new 24 well plate and 600 μl of serum- and antibiotic-free McCoy's 5A medium was added to the basolateral side. Mucus layers were formed by adding 100 μl of thawed PSIM (20 mg/ml) to the apical side. For controls, 100 μl of serum- and antibiotic-free McCoy's 5A medium was added to the apical side. The plates were incubated for 24 hours at 37 ^{o}C. The media from the basolateral side was collected. Manufacturers protocol was followed to quantify human IL-8 (Cat # DY 208) and human TNF-α (Cat # DY 210) concentrations using DuoSet ELISA assay kit (R&D Systems). Assays were calibrated to the standard curve created for serially diluted IL-8 and TNF-α standard solutions on each plate per assay.

Cultured THP-1 cells were washed three times with PBS. After centrifugation, 10^5 THP-1 cells were suspended in serum- and antibiotic-free medium (600 μl); seeded into 24 well

plates; and 100 µl of thawed PSIM (20 mg/ml) was directly added to the medium. After 24 hours of incubation at 37 ºC, the media were collected and the concentrations of human IL-8 and TNF-α were quantified using ELISA assays.

3.4.7 Direct stimulation of HT-29 and THP-1 monocultures

Twenty-four well tissue culture treated plates were seeded with 10^5 HT-29 cells per well and cultured for 4 days with a media change every day. After 4 days, the cells were washed with PBS three times and replaced with 450 µl serum- and antibiotic-free McCoy's medium. To each well, 50 µl of medium was added that contained bacterial endotoxin lipopolysaccharide (LPS, 10 µg/ml) from Escherichia coli O55:B5 (Cat # L6529), VSL#3 (2 x 10^9 CFU/ml), or Salmonella (2 x 10^5 CFU/ml). Media alone (50 µl) was added to control wells. After 12 hours of incubation at 37 ºC, the media were collected. Human IL-8 and TNF-α concentrations were quantified using ELISA assays.

Using a similar procedure as above, 10^5 THP-1 cells were suspended in serum- and antibiotic-free medium (600 µl); seeded into 24 well plates; and stimulated with 50 µl LPS (10 µg/ml), VSL#3 (2 x 10^9 CFU/ml), and Salmonella (2 x 10^5 CFU/ml). After 12 hours of incubation at 37 ºC, the medium was collected and the concentrations of human IL-8 and TNF-α were quantified using ELISA assays.

3.4.8 Construction of in vitro mucosal lining model

Epithelial cells were grown on transwell inserts and checked for coverage and leakage using PBS as described above. Mucus layers was formed by adding 100 µl of sterile PSIM

(20 mg/ml) and incubating at 37 ^{o}C for 12 hours. For controls without mucus, 100 µl serum- and antibiotic-free McCoy's 5A medium was added to the apical side of the inserts. In cultures of THP-1 cells, the medium was removed by centrifugation and the cells were washed with PBS three times. The cell pellet was suspended in serum- and antibiotic-free McCoy's 5A medium. The medium in the basolateral side of the transwell inserts was replaced with 600 µl of THP-1 cell suspension at a density of 10^5 cells/well.

3.4.9 LPS interaction with in vitro mucosal lining model

The in vitro mucosal lining model was challenged by adding 50 µl per well LPS (10 µg/ml) from Escherichia coli O55:B5 (Cat # L6529) to the apical side of the transwell inserts in the presence and absence of a pre-formed PSIM layer. After 24 hours of incubation with LPS, the medium from the bottom well was collected for quantification of human IL-8 and TNF-α using ELISA.

3.4.10 VSL#3 interaction with in vitro mucosal lining model

The in vitro mucosal lining model was challenged by adding 50 µl per well of VSL#3 culture (2 x 10^9 CFU/ml) to the apical side of the transwell inserts. After 24 hours of incubation at 37 ^{o}C, the transwell inserts were removed and brightfield images of the bottom well containing THP-1 cells were captured using EVOS FL Auto imaging system (Life technologies). The contrast of the images was uniformly enhanced. Post-imaging, the medium was collected from the bottom well. Half of the medium was used for quantification of human IL-8 and human TNF-α with ELISA. The other half was used for bacterial quantification by serial dilution, plating on solid agar plates and incubated at 37

^{o}C for 24 hours. The colonies were manually counted and converted to CFU based on the dilution factor. The THP-1 cell morphology change was manually quantified using ImageJ (NIH). Differentiated immune cell were identified as cells having stretched or dendrite-like morphology. The number of cells was normalized by the total area of the images.

3.4.11 Salmonella interaction with in vitro mucosal lining model

The in vitro mucosal lining model was challenged by adding 50 µl per well of GFP-labeled Salmonella (2 x 10^5 CFU/ml) to the apical side of the transwell inserts. After 12 hours of incubation at 37 ^{o}C, the transwell inserts were removed. Using a plate reader (Synergy H1, BioTek Instruments, Inc.), the GFP intensity was quantified in the bottom well plate to measure of bacterial cell density. The medium was collected and used for quantification of human IL-8 and human TNF-α with ELISA.

3.4.12 Bacterial motility analysis

Aqueous motility of wild type Salmonella, flagella knockout Salmonella and VSL#3 was quantified using fluorescent microscopy. Salmonella strains expressing GFP were grown in LB until OD600 was in the range 0.6 – 0.8. A 20 µl droplet containing 10^7 CFU/ml was added onto a glass slide and covered with a coverslip. Fluorescent microscope images were captured every 0.141 s for 60 s. Bacterial velocity was analyzed using an automated particle tracking program, Trackmate in ImageJ (NIH). The average velocity of all the tracks was calculated per sample. To measure the velocity of VSL#3, the bacteria were inoculated in serum- and antibiotic-free McCoy's 5A medium and allowed to recover at 37^{o}C for 1 hour. The cells were nuclei stained using Hoechst 33342 (NucBlue, Thermo Fisher, Cat #

R37605). A 20 μl droplet containing 10^7 CFU/ml was added onto a glass slide and covered with a coverslip. Fluorescent microscope images were captured every 0.5 s for 60 s. The average velocity was calculated as described above.

3.4.13 Cryopreservation, histological sectioning, and immunofluorescence staining

To image wild type and flagella knockout Salmonella, bacteria were grown to an OD600 of 0.8. Twenty μl droplets were applied to glass slides and allowed to dry in a biosafety cabinet approximately six hours.

For histological sectioning, the transwell membranes with intact epithelial and mucus layers were cut from the inserts and fixed using 10% formalin solution in phosphate buffer saline for 20 minutes. Fixed membranes were embedded in optimum cutting temperature (OCT) medium and flash frozen in liquid nitrogen. Using a cryostat (CRYOSTAR NX70, Thermo Scientific), 30 μm thick cross-sections were cut and collected on ColorMark Plus glass slides for imaging. Brightfield images were acquired using an EVOS FL Auto imaging system (Life technologies) and the thickness of the mucus layers were measured manually using ImageJ (NIH).

For immunofluorescent staining of slides with dried Salmonella, FITC-conjugated anti-Salmonella antibody (1:200, ab69253, Abcam) was used. Fluorescent images were acquired using Zeiss Spinning Disk Axio Observer Z1 microscope (Carl Zeiss) with a C-Apochromat 63x oil immersion objective and Zen software (Carl Zeiss). For immunofluorescent staining of histological cross-sections two antibodies were used: FITC-

conjugated anti-Salmonella antibody and Alexa Fluor 594 conjugated anti-human CD326 (EpCAM) antibody (1:200, Cat # 324228, BioLegend). Both samples on glass slides were blocked in the blocking solution (1% BSA, 22.52 mg/ml in PBST (PBS + 0.1% Tween20)) for 1 hour at room temperature. Slides were incubated with antibodies diluted in 1% BSA in PBST for 1 hour at room temperature and washed three times with PBS. Histological slices were counter-stained with DAPI (1:10,000, D9542, Sigma Aldrich) to identify cell nuclei. Fluorescent images were acquired using Zeiss Spinning Disk Axio Observer Z1 microscope (Carl Zeiss) with a LD C-Apochromat 40x oil immersion objective and Zen software (Carl Zeiss).

The stained histological images were analyzed using ImageJ. To quantify Salmonella density in the mucus gel layer, images were tiled to capture from the top of the mucus to the bottom of the epithelial layer. Tiled images from three planes deep into the mucus layer on the glass slides were captured with 10 μm intervals. These three tiled images were projected on to a single plane. Projected images were uniformly segmented to isolate bacteria morphologically. The mucus layer height was divided into three regions of equal height (T: top; C: center; B: bottom). The amount of Salmonella in each region was measured as the percent area with FITC over the total area using ImageJ.

3.4.14 Statistical analysis

A two-tailed Student's t-test assuming unequal variances was used for statistical analysis of pairwise comparison. One-way ANOVA with Bonferroni post hoc test was used for multiple comparisons. All data are presented as a mean ± standard deviation. Differences

were considered significant at $P < 0.05$, with * denoting $P < 0.05$, and ** denoting $P < 0.01$.

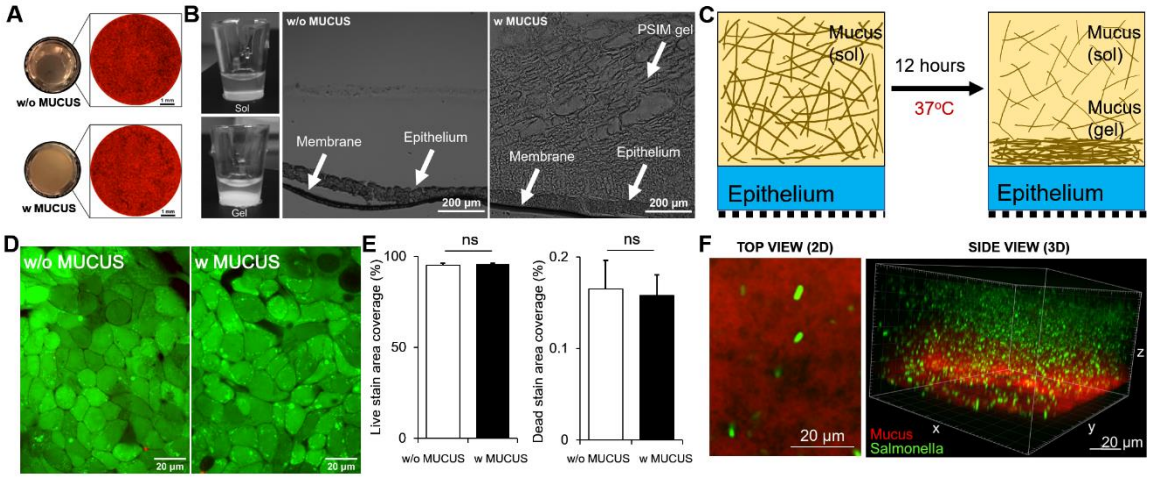

Figure 3.1. Biocompatibility of epithelial and mucus gel layers formed on a transwell membrane. (A) Macroscopic, bottom-view images of the translucent membrane without mucus (*top left*) and the opaque mucus layer after gel formation (*bottom left*). Tiled microscopic image of the transwell membrane with RFP-expressing HT-29 cells covering the entire membrane without (*top right*) and with a mucus layer (*bottom right*). (B) Side view of transwell inserts demonstrating sol (*left, top*) to gel (*left, bottom*) transition of PSIM at 0 and 12 hours. Microscopic image of a 20 µm thick histological cross-section of the transwell membrane covered with HT-29 cell layer (*middle*) and PSIM gel layer formed on top (right). (C) A mucus gel layer formed 12 hours after addition of solubilized PSIM (20 mg/ml) and incubation at 37 °C. (D) Live (Green) and Dead (Red) cell staining of the epithelial cell layer on a transwell membrane. (E) Quantified area covered by GFP positive and RFP positive signals showed no significant difference with or without mucus (n = 3). (F) Confocal microscope image of a DAPI-stained PSIM gel layer (red) with embedded GFP-expressing Salmonella (green).

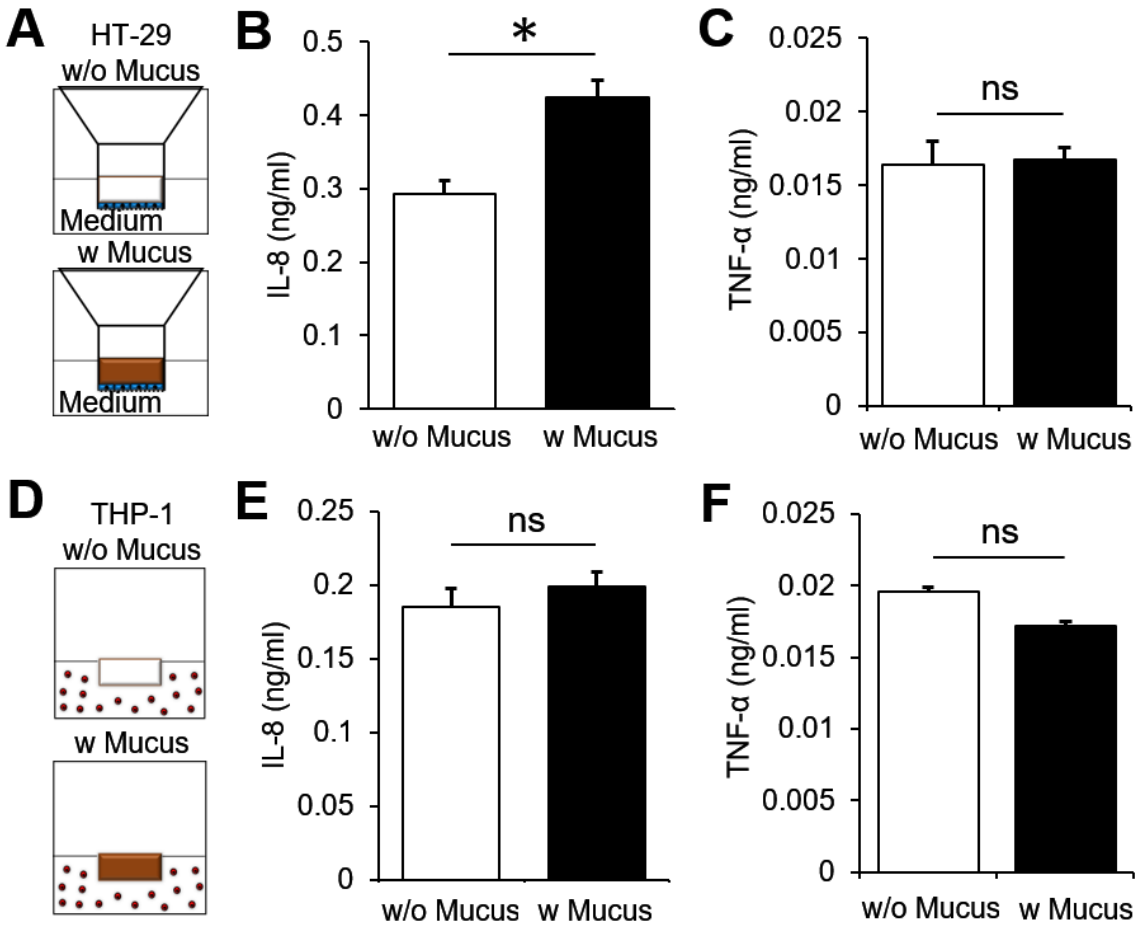

Figure 3.2. Immunological response of epithelial and immune cells to PSIM. (A) Schematic depiction of the transwell insert placed in 24 multi well plates. HT-29 cells (*blue*) were cultured on the apical side of the transwell membrane and cell culture medium was added to the apical (*100 μl*) and basolateral (*600 μl*) side of the cells (*w/o mucus*). Reconstituted mucus at 20 mg/ml concentration (*brown, 100 μl*) layered on top of the epithelial cells (*w mucus*). (B) THP-1 cells cultured in 24 multi well plates and cell culture media (*w/o mucus, 100 μl*) or reconstituted mucus (*w/ mucus, 100 μl*) added directly to the culture medium (*600 μl*). (C) Mucus increased chemokine (IL-8) secretion from HT-29 cells (*, $P < 0.05$; $n = 3$) and (D) no change in cytokine (TNF-α) secretion. Mucus did not cause a significant change in (E) IL-8 or (F) TNF-α concentration in THP-1 culture medium (n=3).

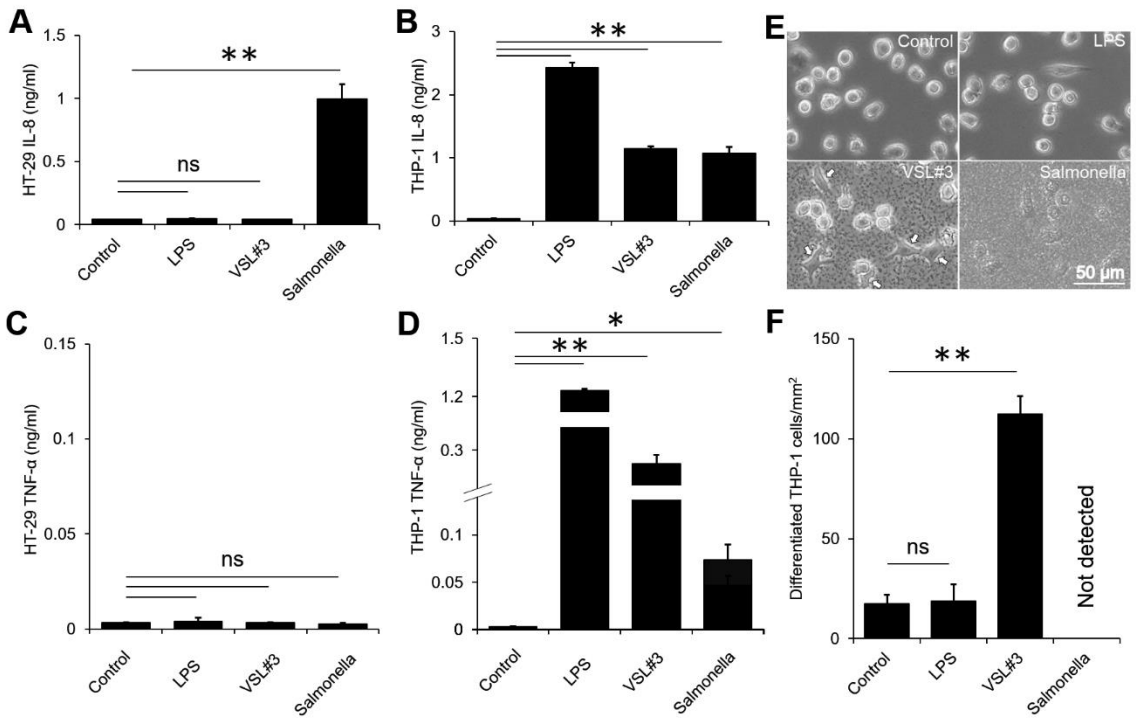

Figure 3.3. Stimulation of HT-29 and THP-1 monocultures by LPS and live bacteria. (A) IL-8 secretion from HT-29 cells was significantly increased by direct contact with Salmonella (**, $P < 0.01$; $n = 3$). LPS (10 µg/ml) and VSL#3 caused no significant change in IL-8 secretion. (B) LPS and direct contact with VSL#3 and Salmonella caused IL-8 secretion from THP-1 cells (**, $P < 0.01$; $n = 3$). (C) LPS, VSL#3 or Salmonella did not cause any TNF-α secretion from HT-29 cells. (D) LPS and direct contact with VSL#3 and Salmonella caused TNF-α secretion from THP-1 cells (*, $P < 0.05$; **, $P < 0.01$; $n = 3$). (E) Direct contact with VSL#3 caused a change in THP 1 cell morphology (arrows). LPS and Salmonella did not change THP-1 morphology. Images were taken 12 hours after adding a stimulant. (F) The number of differentiated THP-1 cells per squared millimeter was significantly higher with VSl#3 compared to controls (**, $P < 0.01$; $n = 3$).

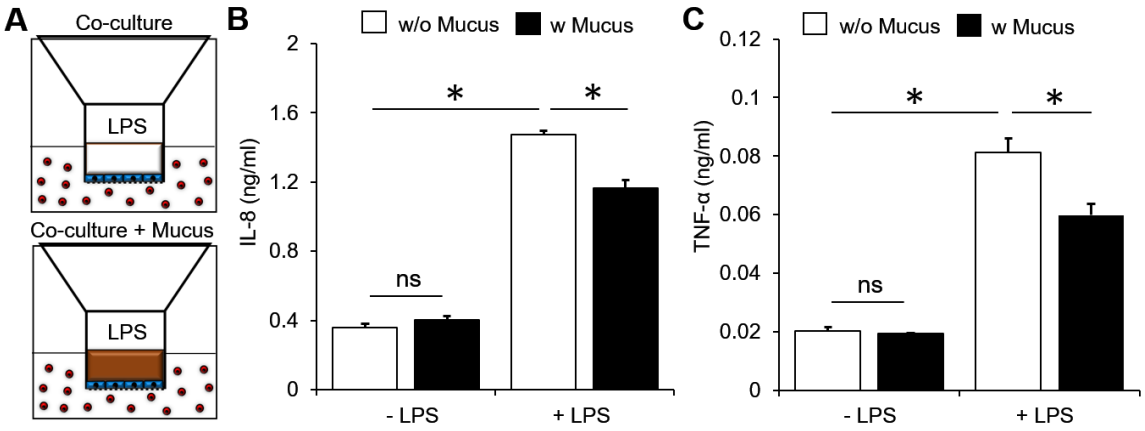

Figure 3.4. **Barrier function of PSIM layer to molecular diffusion.** (A) HT-29 cells (blue) on the apical side of the membrane co-cultured with THP-1 cells (red) in 24 multi-well plates in the absence (top) and presence (bottom) of a PSIM layer (brown). (B,C) The concentrations of IL-8 (B) and TNF-α (C) from the co-cultures did not change by adding a PSIM layer, significantly increased by adding LPS to the apical side without mucus, and was significantly attenuated by adding PSIM layer prior to LPS stimulation (*, $P < 0.05$; $n = 3$).

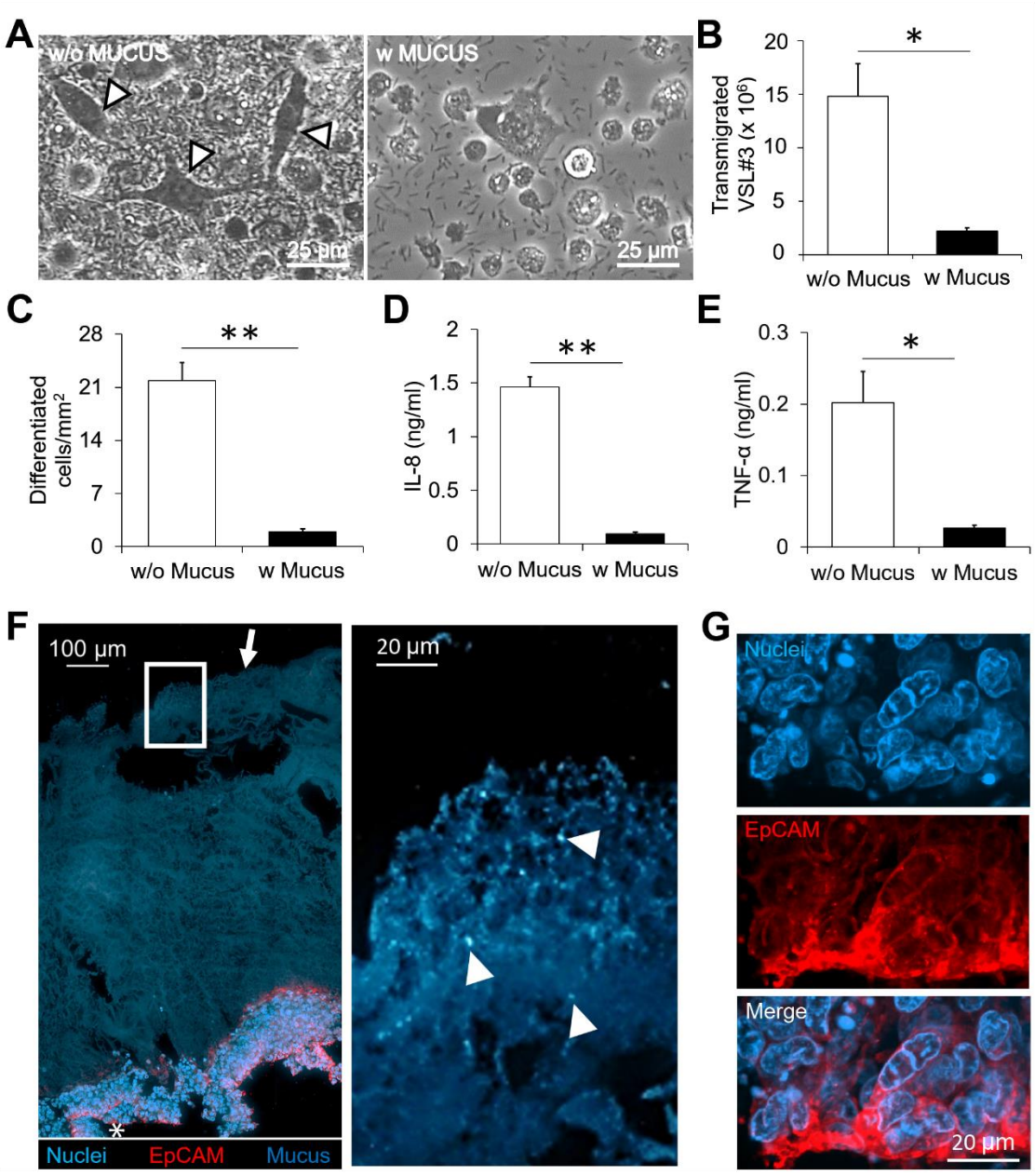

Figure 3.5. Barrier function and immune modulation by a PSIM gel layer in response to VSL#3. (A) VSL#3 transmigrated across the epithelial layer and caused THP-1 cell differentiation identified by elongated morphologies (arrows). Images were taken 24 hours after addition of bacteria. (B) The mucus layer significantly reduced the number of transmigrated VSL#3 bacteria (*, $P < 0.05$; $n = 3$). (C-E) The mucus layer significantly reduced the number of differentiated cells per mm^2 (C; **, $P < 0.01$; $n = 3$), the concentration of IL-8 (D; (**, $P < 0.01$), and the concentration of TNF- α (E; *, $P < 0.05$) in the co-culture. (F) A 20 µm thick histological section (Left) stained with EpCAM (Red) and DAPI (Blue). The PSIM gel layer is auto fluorescent (Blue, arrow). Expanded image (Right) shows DAPI-stained VSL#3 bacteria embedded at the outer surface of the PSIM

gel layer (Arrows). (G) Expanded images of the epithelial layer (white star) showing nuclei and EpCAM staining.

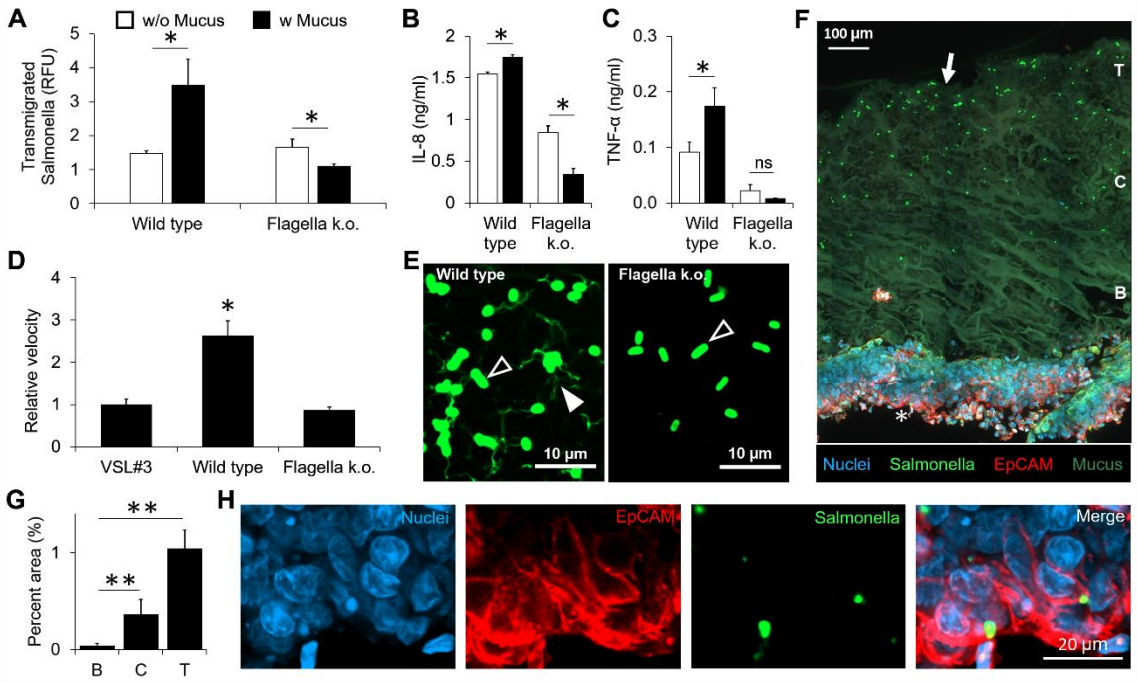

Figure 3.6. Mucus gel layer is not protective against motile Salmonella. (A) In the presence of a mucus layer, the number of transmigrated wild type Salmonella increased (*, $P < 0.05$; n = 3). Mucus decreased the number of transmigrated flagella knockout (k.o.) Salmonella (*, $P < 0.05$). (B) The mean velocity of wild type Salmonella was greater than VSL#3 and knockout (Δ*flhDC*) Salmonella (*, $P < 0.05$; n=5). (C, D) The concentrations of IL-8 (C) and TNF-α (D) in the co-culture in response to wild type and knockout Salmonella with and without mucus (*, $P < 0.05$; n = 3). (E) Fluorescent microscope images showing the cell bodies (black arrows) and flagella (white arrow) of the wild type (left) and the knockout (right). Only cell bodies are present for the knockout. (F) A histological section stained for EPCAM-1 (Red), nuclei (Blue), Salmonella (Green), and the auto fluorescent PSIM gel layer (Green, arrow). Depth into the mucus layer is indicated as T: top surface, C: center, B: bottom. (G) Bacterial density in the mucus layer as a function of depth quantified as the area covered by positive signal from Salmonella stain (**, $P < 0.01$; n = 3). Expanded images of the epithelial layer (white star) showing nuclei and EpCAM staining.

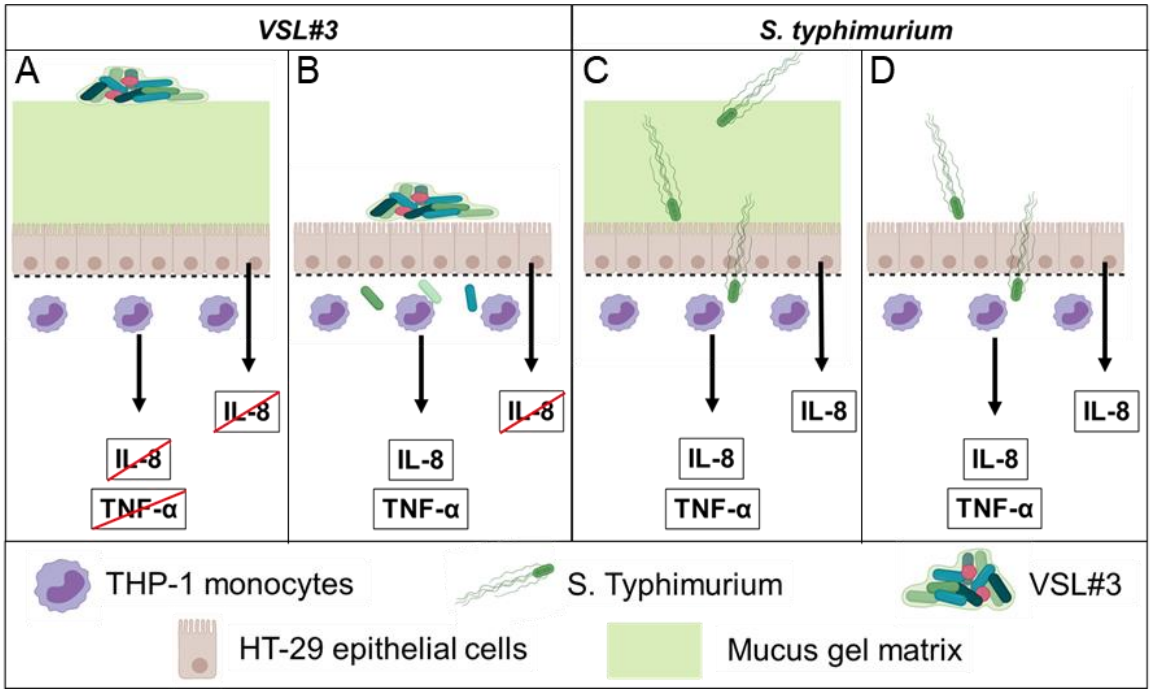

Figure 3.7. The mucus layer regulates the extent of host-bacterial interactions and the resultant immune responses. (A) The mucus layer acts as a barrier to VSL#3 and prevents any immune response. (B) In the absence of a mucus barrier, VSL#3 breach the epithelial barrier and induce immune responses (TNF-α and IL-8). (C) Despite the presence of a mucus layer, Salmonella breach the epithelial barrier and induce chemokine (IL-8) responses from epithelial cells and cytokine (TNF-α) and chemokine (IL-8) responses from immune cells. (D) In the absence of a mucus layer, Salmonella breach the epithelial barrier and induce immune responses, similar to in the presence of mucus.

CHAPTER 4

APPLICATION OF INTESTINAL MUCOSA MODEL TO INVESTIGATE THE EFFECT OF PROBIOTICS ON PATHOGENIC SALMONELLA INFECTION

4.1 Introduction

Intestinal health is highly dependent on the balance between the microbial species present in the intestinal tract and the host immune system. Intestinal microbiota plays an important role in the development of mucosal immunity, maintenance of homeostasis, and mucosal barrier function. An imbalance in the intestinal microbiota also known as dysbiosis is linked to several intestinal disorders including inflammatory bowel diseases (IBD) [98-99]. Dysbiosis can be caused by external factors including abrupt dietary changes, use of antibiotics, exposure to pathogens, and medical interventions like chemotherapy. The role of dysbiosis in the initiation and severity of enteropathogenic infection is not completely understood. The barrier function to pathogens in the intestines is provided by colonization resistance from commensal microbiota, the biochemical barrier of mucus, tight junctions in the epithelial cell layer, and inflammation induced immunological response from resident immune cells [97]. The individual, pairwise, and combined interplay of luminal bacteria, mucosal barrier, and immune system during enteropathogenic infections are not well understood.

Salmonella enterica subsp. enterica serovar Typhimurium (*S. typhimurium*) is a common enteropathogenic strain causing diarrhea, fever, stomach aches, and can often be fatal [117-118]. According to CDC estimates, *Salmonella* bacteria account for over 1.35 million infections, 26,500 hospitalizations, and 420 deaths every year in The United States alone

(CDC). The severity of *S. typhimurium* infections is higher in patients with weakened immunity (WHO). A prior exposure to *S. typhimurium* also correlates positively with incidence of chronic conditions in the intestines such as Inflammatory Bowel Diseases (IBD) [119-121]. Because of the strong link between *S. typhimurium* infection and host immunological response, understanding exact mechanisms involved in these interactions will help prevent long-term effects of *S. typhimurium* infections. The role of commensal microbiota and the protective mucus layer in *S. typhimurium* infection is not fully understood.

At the luminal interface, the first point of contact between the ingested pathogens and the intestines is the secreted mucus layer. The colonic epithelial cell surface is uniformly covered with a mucus layer approximately 800 um thick and minimizes bacterial contact with the epithelial cells and tissue resident immune cells [63, 100]. Depletion or the improper barrier function of the colonic mucus layer is linked to bacterial infiltration [103-105], intestinal inflammation and pathology [47, 49, 101-102]. In healthy condition, the commensal gut microbiota resides in the outer mucus layer closer to the lumen and mucus close to the epithelium is devoid of bacteria [63, 100]. The microbiota provides competition against colonization of ingested pathogens. Dysbiosis of the intestinal microbiota lowers the host resistance to pathogenic infections and can lead to chronic conditions like IBD [141]. For example, dysbiosis associated changes in host metabolism and inflammatory environment in the intestines provided a growth advantage to S. typhimurium over the commensal microbiota [142]. Treatment with antibiotics caused depletion of commensal microbiota leading to reduced host resistance to *S. typhimurium* infection [143]. The near surface

swimming of *S. typhimurium* and the attachment to the mucus layer play a role in its infection ability [106, 122-125]. *S. typhimurium* can use flagella-driven motility and taxis to access nutrients at the mucosal surface [144-145]. How *S. typhimurium* navigate the colonic mucosal interface in presence of dense microbiota residing in the outer mucus layer is unknown. A better understanding of the interaction between commensal microbes and *S. typhimurium* at the mucosal interface could help uncover mechanisms of enteric salmonellosis.

After crossing the mucus barrier, pathogens encounter the physical barrier created by the tight junctions that prevent most bacteria from crossing the epithelial barrier [107-108]. Most bacteria are detected by binding of common pathogen associated molecular patterns (PAMPs) to receptors present on the epithelial cell surface called the toll-like receptors (TLRs) [112-114]. Binding of PAMP with TLRs cause activation of downstream pathways like NF-κB that regulate secretion of signaling and effector molecules called chemokines and cytokines. In the intestines, epithelial cell derived chemokine interleukin-8 (IL-8) after detection of bacteria help recruit effector cells like neutrophils to clear the infection [109]. In case of epithelial barrier breakdown, tissue resident dendritic cells and macrophages detect the bacterial PAMPs using TLRs and secrete IL-8 and pro-inflammatory cytokines including tumor necrosis factor (TNF-α). TNF-α and IL-8 are pro-inflammatory and commonly upregulated in IBD patients [115-116]. Identifying the source of these pro-inflammatory molecules during infection or inflammation can be useful for targeted therapy in chronic inflammatory disorders including IBD [146-147].

Recently, probiotics have been considered as potential mainstream therapeutics for chronic intestinal disorders [148-149]. This transition has shown significant success in clinical trials and research performed in animals as well as experimental models [150-152]. Apart from chronic conditions, probiotics have been tested in the treatment of acute pathogenic infections both as a treatment as well as a prophylactic. Introducing a defined set of microbes into mice provided a strong resistance against S. typhimurium infection and reduced pathogenic load in feces [153]. For conditions such as recurrent pouchitits, *VSL#3* is being used as a recommended therapy and is shown effective as a primary prevention measure [154]. *VSL#3* is a commercial probiotic mix containing eight bacterial strains (namely Streptococcus thermophilus, Bifidobacterium breve, B. longum, B. infantis, Lactobacillus acidophilus, L. plantarum, L. paracasei, and L. delbrueckii subsp. Bulgaricus). VSL#3 was shown effective in mitigating pathogenic burden and pro-inflammatory effects caused by Campylobacter jejuni infections in mice [155]. *VSL#3* showed a protective effect when administered before inducing inflammation (prophylactic) [156] but had no healing effect when administered after inducing inflammation (treatment) [157].

Probiotic bacteria induce these protective effects in the host by several mechanisms. These mechanisms may include competitive growth inhibition of pathogenic bacteria by nutrient sequestration or production of compounds such as bacteriocins that inhibit the growth of specific bacteria. It is critical that the probiotics once ingested, effectively colonize the gastro-intestinal tract, and accumulate there in significant numbers to provide a tangible probiotic effect. There is a direct correlation between longer colonization times and high effectiveness of probiotic bacteria [158]. Therefore, continual ingestion of probiotics may be

required for sustained impact on the host. An understanding of the optimum cell number required to impart the probiotic effect would improve the dosage strategies.

Post colonization probiotic bacteria impart several health benefits to the diseased host. For example, enhancing epithelial barrier function (ref), modulating epithelial cytokine secretion into an anti-inflammatory dominant profile (ref), altering mucus production (ref), and modifying the innate and systemic immune responses [159]. However, it is not well understood if the direct contact of the probiotic bacteria with the epithelial cells is essential or they can impart some probiotic effect via secretory mechanisms. Since mucus layer coats the epithelium, it is critical to evaluate the role of mucus barrier in mediating the effects of probiotics on the host. The complexity of the intestinal microenvironment with continuously evolving luminal environment, diverse microbiota and high prevalence of immune cells make it difficult to parse out bacteria-mucus-host cell interactions in vivo.

In vitro investigations into the bacteria-epithelial interactions are limited due to the poor mucus secretion and non-uniform coverage in the cellular models commonly used as intestinal epithelium. Recent advances using primary colonic cells combined with air-liquid interface and gut-on-a-chip microfluidic culture methods achieved significantly thicker mucus layer compared to cell lines [133-134]. For non-mucus secreting cell line based models, porcine mucus is a good alternative for rarely available human mucus [16-17, 34-35]. We have developed a method to extract porcine small intestinal mucus (PSIM) that retained the functions of native intestinal mucus [138]. Subsequently, we developed an intestinal mucosa model including a mucus gel matrix on top of the epithelium that enabled co-culture with live bacteria and immune cells [160]. The intestinal mucosa model consists of all

three components (structural mucus gel matrix, epithelial layer, and innate immune cells) that captures the essential complexities of the mucosal layer in the intestine.

Here, we use the intestinal mucosa model [160] to quantify the role of mucus and epithelial barrier in regulating the host innate immune responses to probiotic and pathogenic bacteria. In case of a pathogenic infection, investigating a range of an effective ratio of probiotic to pathogen that could prevent the growth of the pathogen can help dictate the dosage and the duration of probiotic intake. To investigate if probiotic mixture *VSL#3* can prevent pathogenic *S. typhimurium* growth, different mixing ratios were co-cultured and *S. typhimurium* growth was quantified using fluorescent spectroscopy. The co-cultures were added to independently cultured epithelial and innate immune cells to quantify the amount of pro-inflammatory chemokine and cytokine by enzyme-linked immunosorbent assay (ELISA). The intestinal mucosa model was used to test the hypothesis that *S. typhimurium* could escape any inhibitory or anti-inflammatory effects exerted by *VSL#3* in the presence of mucus. In the mucosa model, a selectively permeable mucus gel matrix formed closely attached to the epithelium that enabled the investigation into the role of mucus barrier on the interactions of cocultured bacteria with epithelial cells. Additionally, the mucosa model provided easy access to the culture medium for quantification of immunological responses from human epithelial and immune cell cocultures. Bacterial penetration across the epithelial barrier was quantified using fluorescent confocal microscopy of the transwell membranes that support the epithelial layers. Mechanistic understanding of the interactions of pathogenic and probiotic bacteria with mucus, epithelial cell layer and immune cells

independently as well as in co-culture will help improve the probiotic formulations and dosage strategies for intestinal diseases.

4.2 Results

4.2.1 *VSL#3* suppresses the growth of *S. typhimurium* in co-culture.

In co-culture, the growth of *S. typhimurium* was affected by the initial density of VSL#3 (Figure 1). When *S. typhimurium* were cultured alone, the time to maximum density increased with decreasing initial density (Figure 1B, top left). At initial densities of 10^3,10^2 and 10, the time to maximum density was 6.8, 9.2 and 11.1 h, respectively. These times to maximum density did not change with the addition of VSL#3 (Figure 4.1B).

At an equal seeding density, *VSL#3* had almost no effect on *S. typhimurium* growth (Figure 1B, top right, circles) compared to *S. typhimurium* alone (Figure 4.1B, top left). When the initial density of VSL#3 was 10^2 times that of *S. typhimurium*, the maximum density reduced (Figure 4.1B, bottom left, circles). The greatest effect on growth was when the initial density of VSL#3 was 10^4 times the density of *S. typhimurium* (Figure 4.1B, bottom right). This condition almost completely blocked the growth of *S. typhimurium*. At the point of maximum density (8 h for an initial *S. typhimurium* density of 10^3), the Salmonella density was reduced to almost zero (**, $P < 0.01$; Figure 4.1C). The density at the endpoint (12 h) was also significantly reduced (**; $P < 0.01$, Figure 4.1D).

The growth of *S. typhimurium* was dependent on both the initial density ratio and the absolute initial density. At a density ratio of 10^4 and low densities (10 and 10^5 CFU/well of *S. typhimurium* and VSL#3, respectively), there was considerable growth (Figure 4.1B, bottom left, squares). At the same density ratio but higher overall densities (10^3 and 10^7 CFU/well), growth was almost completely suppressed (Figure 4.1B, bottom right, circles).

The different growth responses at these conditions represent four physiological conditions in the intestinal lumen. (1) All VSL#3 (10^7 CFU/well; termed V7) represents healthy commensal microbiota with no pathogens. (2) All *S. typhimurium* (10^3 CFU/well; termed S3) represents a high pathogen load with depleted commensal microbiota. (3) Equal density (10^3 VSL#3 and *S. typhimurium* CFU/well; termed V3S3) represents a high pathogen load with commensal dysbiosis. (4) Mostly VSL#3 (10^7 CFU/well VSL#3 and 10^3 CFU/well *S. typhimurium*; termed V7S3) represents a low pathogen load with healthy commensal microbiota. These four conditions were used for most of the subsequent experiments.

4.2.2 Mucus gel matrix using PSIM match the colonic mucus layer in vivo.

The native mucus barrier is impenetrable to bacteria-sized beads. The mucus gel matrix formed at different concentration of PSIM (Figure 4.2A) and prevented the bacteria-sized polystyrene beads are from coming in contact with the epithelial cells (Figure 4.2B). The mucus gel matrix is impenetrable to bacteria sized beads. At a PSIM concentration of 0.5 mg/ml, fluorescent bacteria-sized beads were in direct contact with the epithelial cell layer. Increasing the PSIM concentration to 1 mg/ml caused a separation of 40.85 ± 0.7 μm. Further increase in the PSIM concentration to 2.5 mg/ml caused a separation greater than 100 μm, since the beads were not present in the field of view. A PSIM concentration of 20

mg/ml matches the overall thickness of the colonic mucus layer in vivo (Figure 4.2C). The mucus gel matrix formed using solubilized PSIM is structurally stable, closely attached to the epithelium, and qualitatively resembles the mucus layer structure in vivo (Figure 4.2D).

4.2.3 Presence of *VSL#3* alters the host immune responses to *S. typhimurium*.

VSL#3 affects the *S. typhimurium* induced pro-inflammatory chemokine and cytokine secretion from human epithelial and immune cell co-culture. Bacteria were co-cultured in the mucosal barrier platform to quantify the effect of *VSL#3*, *S. typhimurium* and the mixed bacterial cocultures on the epithelial and immune cell responses (Figure 4.3A). The co-cultures were performed with or without mucus barrier added on top of epithelial cell layer. *VSL#3* alone did not induce a chemokine (IL-8) response. Also, IL-8 response was significantly higher in presence of *S. typhimurium* alone compared to *VSL#3* (**; $P < 0.01$, Figure 4.3B). Addition of mucus caused a small increase in IL-8 in presence of *S. typhimurium*. When *VSL#3* and *S. typhimurium* mixed at equal proportion were added, IL-8 response further increased significantly in the absence of mucus (**; $P < 0.01$, Figure 4.3B). Similar addition of the bacteria mixed in equal proportions and in presence of mucus caused a 2-fold increase in IL-8 compared to the absence of mucus. Compared to *S. typhimurium* alone, equal density mixture of *VSL#3* and *S. typhimurium* caused an increase of 2.6-fold in IL-8 when mucus is present. In the absence of mucus this increase is significantly lower (1.8-fold). Increasing the ratio of *VSL#3*:*S. typhimurium* to 10^4:1 reduced the IL-8 amount 10-fold in the absence of mucus but only 3-fold reduction was seen in the presence of mucus. In the absence of mucus, the IL-8 amount under this condition was equal to the amount of IL-8 induced by *VSL#3* alone. These results suggest

that *VSL#3* at high density ratio of 10^4:1 significantly suppress the IL-8 response and this anti-inflammatory effect is stronger in the absence of mucus barrier. Similar to IL-8, co-culture of *VSL#3* alone did not cause TNF-α production in the mucosal barrier platform. Addition of *S. typhimurium* alone caused a 6-fold increase in TNF-α in the absence of mucus and a 10-fold increase in the presence of mucus (**; $P < 0.01$, Figure 4.3C) when compared to *VSL#3* alone. Presence of mucus caused a 2-fold increase in TNF-α caused by *S. typhimurium* alone. Adding *VSL#3* and *S. typhimurium* in equal ratio caused a significant increase in TNF-α without mucus but did not have any effect in presence of mucus. Increasing the ratio of *VSL#3*:*S. typhimurium* to 10^4:1 caused a significant reduction in TNF-α. As seen with IL-8 response, *VSL#3* completely suppressed the TNF-α production in the absence of mucus. The presence of mucus caused a 2-fold increase in the TNF-α secretion suggesting that presence of mucus promotes a pro-inflammatory response in presence of *S. typhimurium*.

4.2.4 More *S. typhimurium* cross the epithelial layer in presence of the mucus gel matrix.

Higher number of *S. typhimurium* crossed the epithelial layer in presence mucus gel matrix. Fluorescent confocal microscopy was used to quantify the number of *S. typhimurium* that have crossed the epithelial layer (Figure 4.4A). In presence of mucus gel matrix, addition of *S. typhimurium* alone increased the number of bacteria by 2.5-fold compared to epithelial layer only (*; $P < 0.05$, Figure 4.4B). Compared to *S. typhimurium* alone, equal density mixture of *VSL#3* and *S. typhimurium* caused an increase of 4-fold in IL-8 when mucus is present (**; $P < 0.01$, Figure 4B). In the absence of mucus this increase in the number of

S. typhimurium is significantly lower (1.9-fold). Increasing the ratio of VSL#3:*S. typhimurium* to 10^4:1 prevented *S. typhimurium* completely and no bacteria were found on the membrane in the absence of mucus. On the other hand, presence of mucus significantly increased the number of *S. typhimurium* present on the transwell membrane compared to without mucus (*; $P < 0.05$, Figure 4.4B). The results show that increase in the cytokine and chemokine response is linked to higher migration of *S. typhimurium* across the mucosal barrier.

4.2.5 Epithelial and immune cell responses vary depending on the bacterial stimuli.

To parse out the individual contributions of epithelial and immune cells to the responses discussed above, bacteria were co-cultured with individual cultures of HT-29 and THP-1 cells (Figure 4.5A). Bacteria were introduced to the cultures in the same schemes as discussed with the mucosal barrier model. *VSL#3* alone did not cause IL-8 secretion from the HT-29 cells. *S. typhimurium* alone caused a 17-fold increase in IL-8 secretion from HT-29 cells (**; $P < 0.01$, Figure 4.5B). Adding *VSL#3* and *S. typhimurium* in equal ratio increased the IL-8 secretion 43-fold compared to *VSL#3* alone. Further increasing the ratio of *VSL#3*:*S. typhimurium* to 10^4:1 caused a significant reduction as the level of IL-8 was similar to the level observed with *VSL#3* alone. HT-29 cells did not secrete TNF-α in response to any configuration of bacteria (Figure 4.5C). Compared to HT-29 cells, a reverse trend in IL-8 secretion from THP-1 cells was observed. *VSL#3* alone caused a significantly higher IL-8 secretion from THP-1 cells compared to *S. typhimurium* or any combination of *VSL#3* and *S. typhimurium* mixtures. *S. typhimurium* alone caused a 3-fold reduction in IL-8 secretion from THP-1 cells compared to *VSL#3* alone. Equal ratio of

VSL#3 and *S. typhimurium* had a similar effect, and there was no difference compared to *S. typhimurium* alone. Increasing the ratio of *VSL#3*:*S. typhimurium* to 10^4:1 caused a significant increase in IL-8 secretion from THP-1 cells compared to *VSL#3* alone (*; $P < 0.05$, Figure 4.5D). Similarly, the TNF-α production from THP-1 cells was highest in response to *VSL#3* alone. Presence of *S. typhimurium* significantly suppressed the TNF-α response from THP-1 cells (**; $P < 0.01$, Figure 4.5E).

4.3 Discussion

In this study, we investigated the role of dysbiosis in pathogenic infection by coculturing pathogenic *S. typhimurium* SL1344 with a mixture of eight bacteria (*VSL#3*). We found that relative ratios of *VSL#3* and *S. typhimurium* in the lumen dictate the effectiveness of *VSL#3* in suppressing pathogenic infection and host inflammatory response. *VSL#3* was most effective in suppressing *S. typhimurium* growth when the number of *VSL#3* exceeded that of *S. typhimurium* by a factor of 10^4 or more. The bacteria present in *VSL#3* represent the members of commensal microbiota in healthy humans. The competitive growth inhibition of *S. typhimurium* by *VSL#3* present at high numbers effectively demonstrates how the species of commensal microbiota provide resistance to pathogens in vivo.

Dysbiosis of the intestinal microbiota lowers the host resistance to pathogenic colonization and infections. Indeed, when the number of *VSL#3* and *S. typhimurium* in the coculture were equal, no significant reduction in *S. typhimurium* growth was seen. Another factor that affected *S. typhimurium* growth was the initial number of *S. typhimurium* irrespective of the *VSL#3* to *S. typhimurium* ratio. The results suggest that if a sufficient number of *S.*

typhimurium are present at the site of infection, the commensal microbiota may not be effective in preventing infection. Therefore, the factors including ingestion in large numbers through food or an imbalance in the commensal microbiota provide a growth advantage to *S. typhimurium* and may promote its infection ability. For example, such imbalance in the commensal microbiota may be induced by broad-spectrum antibiotic treatment which leaves the host susceptible to virulent pathogens like *S. typhimurium* [143].

The relative ratios of *VSL#3* and *S. typhimurium* also dictated the pro-inflammatory chemokine (IL-8) response from human epithelial cells. The reduction in IL-8 was most effective at the ratio of 10^4:1, when the growth of *S. typhimurium* was completely suppressed suggesting that inhibition of *S. typhimurium* growth is key for reducing inflammation. A coculture of *S. typhimurium* and *VSL#3* at equal numbers significantly increased IL-8 secretion from epithelial cells compared to *S. typhimurium* alone. Since *VSL#3* alone did not induce any inflammatory response in epithelial cells, this result indicates some communication between the bacterial species that leads to a strong pro-inflammatory response induced by *S. typhimurium*. A possible explanation is that with equal numbers, VSL#3 does not inhibit *S. typhimurium* growth effectively but contributes to nutrient deprivation. Nutrient deprived conditions can induce a switch to a hypervirulent phenotype in *S. typhimurium* [161]. Overall, these results show that *VSL#3* is protective only when the ratio of *VSL#3* to *S. typhimurium* is in the order of 10^4 or higher but can contribute to depletion of nutrients and therefore a more robust S. typhimurium infection when the ratio is close to one. Clinically, this could mean that an insufficient dosage of *VSL#3* can lead to side effects and worsen the pathogenic infection causing higher inflammation.

We have developed an intestinal mucosa model that consists of all three components (structural mucus gel matrix, epithelial layer, and innate immune cells) required to capture the essential complexities of the mucosal layer in the intestine. The mucus gel matrix not only matched the thickness and structure of colonic mucus layer but is also impenetrable to bacteria sized beads (Figure. 4.2) and non-motile bacteria [160]. The intestinal mucosa model was used to confirm the hypothesis that mucus gel matrix helps *S. typhimurium* escape the competitive growth inhibition and anti-inflammatory effects exerted by *VSL#3*. In the absence of mucus, *S. typhimurium* induced a strong IL-8 and TNF-α secretion which was significantly suppressed by addition of 10^4 times higher number of *VSL#3*. However, in the presence of mucus, *VSL#3* failed to suppress *S. typhimurium* induced IL-8 and TNF-α secretion. Combined, these results show that the protective effect of *VSL#3* in limiting *S. typhimurium* growth and suppressing inflammation is limited to the luminal interface of mucus. We have shown that the non-motile bacteria in *VSL#3* does not penetrate the mucus gel matrix and accumulate at the mucus interface [160]. On the contrary, the presence of mucus increased the penetration of motile *S. typhimurium* across the intestinal barrier. The increase in transmigration of *S. typhimurium* in the presence of mucus is flagella dependent since the strain of *S. typhimurium* with a flagella-knockout gene did not penetrate the intestinal barrier. Therefore, the limited migration of *VSL#3* and preferential taxis of *S. typhimurium* across the mucus layer enables *S. typhimurium* to cause intestinal infection and inflammation.

A similar scenario happens in vivo where most of the commensal microbiota in the colon reside in the outer mucus layer closer to the lumen and the mucus close to the epithelium is devoid of bacteria. The mucus layer and commensal microbiota combined must therefore provide protection from pathogens. Despite the presence of commensal microbiota in the outer mucus layer and the strong barrier effect of the inner mucus layer, *S. typhimurium* is highly successful at infecting the underlying epithelium. This suggests that in the intestinal mucosa of a host, motile *S. typhimurium* use the mucus layer to its advantage and escape competition from the microbiota. In this regard, the use of 'motile probiotics' that can effectively navigate the mucus layer and compete with motile pathogens can be explored. An example of a motile probiotic is Escherichia coli strain Nissle 1917 (EcN) that possess flagella[162], is antagonistic against pathogens[163], has been safely administered in humans [164-165], and can be genetically engineered to develop safe and effective therapy against motile enteric pathogens [166]. These motile probiotics would not only cause growth inhibition at the luminal mucus interface but also compete for nutrients and antagonize the pathogens throughout the mucus gel matrix. Using the intestinal mucosa model, future coculture studies can be performed to systematically investigate the utility of motile probiotics in preventing infections caused by pathogens that overcome the mucus barrier.

Clinical use of probiotics targeted towards protection against pathogen invasion and intestinal inflammation is on the rise [167]. In vivo studies have shown mixed results for protective effects of *VSL#3* on mucosal barrier healing. VSL#3 showed a protective effect when administered before inducing inflammation (prophylactic) [156] but had no healing effect when administered after inducing inflammation (treatment) [157]. The results presented

here show that the prophylactic effect of VSL#3 against *S. typhimurium* infection can be negated in the presence of mucus. Additionally, clinical benefit can be achieved by a high dosage routine of *VSL#3* enabling robust colonization and growth in the intestines to outnumber the pathogens and prevent pathogenic growth. This strategy can be most effective in patients with pre-existing intestinal conditions like Ulcerative colitis since the mucus layer is either very thin or absent in the lesion areas.

With the rise in antibiotic resistant pathogens due to rampant use of antibiotics, the use of probiotics can be a successful alternative in preventing food poisoning from common pathogens. This study provides preliminary proof of the use of *VSL#3* as a prophylactic and could guide the dosing strategies for its use in preventing conditions like traveler's diarrhea. About 55% of people traveling from developed countries to developing countries develop acute diarrhea [168-169]. Therefore, development of general prophylactic treatments against diarrhea causing pathogens in the form of probiotics are required. In this regard, the intestinal mucosa model presented here served as an effective tool to test probiotic efficacy against *S. typhimurium* infection. The modular nature of this model allowed us to parse out individual and synergistic interactions of bacteria amongst themselves and with the host mucosal interface. The platform is amenable to most common characterization methods including histology, immunostaining, confocal microscopy, and immunological assays like ELSIA. Most results presented here are only feasible by combining the barrier components of the mucosal layer including mucus gel matrix, epithelial layer, and innate immune cells. A mechanistic understanding of how all these components interact in the

intestinal milieu will help advance therapeutic discovery and treatment for common intestinal infections and chronic diseases like IBD.

4.4 Materials and Methods

All chemicals and supplies were purchased from Fisher Scientific and Sigma Aldrich unless otherwise specified.

4.4.1 Mammalian cell culture

HT-29 (ATCC, HTB-38) adherent cells were cultured in McCoy's 5A medium (Sigma Aldrich) supplemented with 2.2 g/L sodium bicarbonate. THP-1 (ATCC, TIB-202) suspension cells were cultured in RPMI-1640 medium (containing 0.05 mM β-Mercaptoethanol). All media were supplemented with 10% fetal bovine serum (FBS) and 1% penicillin/streptomycin and referred to as complete medium in the methods. Cells were maintained in a 37 ^{o}C humidified incubator with 5% CO_2.

4.4.2 Solubilized PSIM preparation

PSIM was extracted, sterilized, and prepared for cell culture as described before [138, 160]. Briefly, intact small intestine tubules were cut into 2-meter lengths and rinsed with water to eliminate food particles from the lumen. The tubules were drained gently, and the lumen was filled with 350 ml of 0.01 M NaOH. The ends of the tubules were tied and incubated for 24 hours at 4 ^{o}C. After incubation, the solubilized material was drained by squeezing and collected. The extract was subjected to centrifugation at 20,000 x g (Thermo Scientific) at 4 ^{o}C for 2 hours to remove insoluble debris. The supernatant was collected without

disturbing the precipitate. The clear supernatant was subjected to sol-gel transition by adjusting the pH to 4 using 2 M HCl. The aggregates formed at pH 4 were subjected to centrifugation at 200 x g for 15 minutes and resolubilized in sterile DI water by adjusting the pH value to 8. The solution was passed through a 40 μm strainer and subjected to dialysis using a membrane with molecular size cut-off equal to 14 kDa. The dialyzed mucus extract was sterilized by adding 1% (v/v) chloroform under constant stirring at 4 ºC for 72 hours. The solution (30 ml aliquots) was transferred to 50 ml conical polypropylene tubes, frozen to -80 ºC, and freeze dried (Labconco Freezone 2.5 L freeze dry system). The freeze-dried mucus was reconstituted aseptically in serum- and antibiotic-free McCoy's 5A medium. The solutions were sterilized in 15 ml polypropylene tubes by adding 10% chloroform and allowing to sit at 4 ºC for 24 hours without shaking. The chloroform solution formed a distinct layer at the bottom and mucus solutions were collected without disturbing the interface under aseptic conditions. The solutions were aliquoted in 1.5 ml polypropylene tubes and stored at -80 ºC until use.

4.4.3 *VSL#3* and *S. typhimurium* bacteria culture

Probiotic VSL#3 bacteria were acquired from a commercial source (VSL Pharmaceuticals, Inc.) and stored at 4 ºC until use. For co-culture experiments, the freeze-dried bacteria were aseptically reconstituted in serum- and antibiotic- free McCoy's 5A medium at a cell density of 10^{10} CFU/ml. Bacterial cells were incubated at 37 ºC for 1 hour to recover. After 1 hour, the cell density was diluted to required cell density by serial dilution.

Wild type *S. typhimurium* strain SL1344 was used for live motile bacterial experiments. For experiments, frozen stocks of the *S. typhimurium* strains were inoculated in LB medium and grown overnight at 37 ^{o}C. Small amount of overnight culture was inoculated in fresh LB medium and allowed to grow to a density of 4 x 10^8 CFU/ml and used for further experiments. To prepare bacteria for transwell co-culture experiments, bacteria culture was subjected to centrifugation at 2500 x g for 10 minutes. The bacterial cell pellet was washed three times with PBS by gentle pipetting multiple times and repeating the centrifugation step in between. Final pellet was reconstituted in serum- and antibiotic-free McCoy's 5A medium and the required cell density was adjusted by serial dilution.

4.4.4 HT-29 cell seeding and culture in transwells

For transwell assays, HT-29 cells were detached from culture flasks using trypsin and seeded at a density of 10^5 cells per insert in 3 μm pore size polycarbonate membrane transwell inserts (CLS3415, Corning). Inserts were cultured for 7 days in 24 well plates in complete McCoy's medium. The culture medium was changed 24 hours after cell seeding and every 48 hours after that. After day 7, the culture medium was aspirated from the transwell inserts. The inserts were washed three times with PBS on both the apical and basolateral sides. To check for incomplete cell coverage, inserts were filled with 250 μl of PBS and the change in liquid level was checked for 5 minutes. The inserts with no change in liquid level were used for further experiments. To check for coverage microscopically, inserts were seeded with RFP-expressing HT-29 cells. After 7 days of culture, the inserts were imaged using EVOS FL Auto imaging system (Life technologies). Images captured using a 10x objective were tiled using in-built EVOS software.

4.4.5 Mucus gel matrix formation on HT-29 cell surface and mucosal barrier platform setup

Epithelial cells were grown on transwell inserts and checked for coverage and leakage using PBS as described above. Mucus layers was formed by adding 100 µl of sterile PSIM (20 mg/ml) and incubating at 37 ^{o}C for 12 hours. For controls without mucus, 100 µl serum- and antibiotic-free McCoy's 5A medium was added to the apical side of the inserts. In cultures of THP-1 cells, the medium was removed by centrifugation and the cells were washed with PBS three times. The cell pellet was suspended in serum- and antibiotic-free McCoy's 5A medium. The medium in the basolateral side of the transwell inserts was replaced with 600 µl of THP-1 cell suspension at a density of 10^5 cells/well. Manufacturers protocol was followed to quantify human IL-8 (Cat # DY 208) and human TNF-α (Cat # DY 210) concentrations using DuoSet ELISA assay kit (R&D Systems). Assays were calibrated to the standard curve created for serially diluted IL-8 and TNF-α standard solutions on each plate per assay.

4.4.6 Stimulation of HT-29 and THP-1 monocultures with *VSL#3* and *S. typhimurium*

Twenty-four well tissue culture treated plates were seeded with 10^5 HT-29 cells per well and cultured for 4 days with a media change every day. After 4 days, the cells were washed with PBS three times and replaced with 450 µl serum- and antibiotic-free McCoy's medium. To each well, 50 µl of medium was added that contained bacterial endotoxin lipopolysaccharide (LPS, 10 µg/ml) from Escherichia coli O55:B5 (Cat # L6529), VSL#3 (2 x 10^9 CFU/ml), or *S. typhimurium* (2 x 10^5 CFU/ml). Media alone (50 µl) was added to control wells. After 12 hours of incubation at 37 ^{o}C, the media were collected from three

independent experimental conditions. Human IL-8 and TNF-α concentrations were quantified using ELISA assays.

Using a similar procedure as above, 10^5 THP-1 cells were suspended in serum- and antibiotic-free medium (600 µl); seeded into 24 well plates; and stimulated with 50 µl LPS (10 µg/ml), VSL#3 (2 x 10^9 CFU/ml), and *S. typhimurium* (2 x 10^5 CFU/ml). After 12 hours of incubation at 37 ^oC, the medium was collected and the concentrations of human IL-8 and TNF-α were quantified using ELISA assays. Results from three independent experiments were used analysis.

4.4.7 *VSL#3* interaction with in vitro mucosal lining model

The in vitro mucosal lining model was challenged by adding 50 µl per well of *VSL#3* culture (2 x 10^9 CFU/ml) to the apical side of the transwell inserts. After 12 hours of incubation at 37 ^oC, the transwell inserts were removed and brightfield images of the bottom well containing THP-1 cells were captured using EVOS FL Auto imaging system (Life technologies). The contrast of the images was uniformly enhanced. Post-imaging, the medium was collected from the bottom well. Half of the medium was used for quantification of human IL-8 and human TNF-α with ELISA. Data was analyzed for three independent experiments.

4.4.8 *S. typhimurium* interaction with mucosal barrier model

The in vitro mucosal lining model was challenged by adding 50 µl per well of GFP-labeled *S. typhimurium* (2 x 10^5 CFU/ml) to the apical side of the transwell inserts. After 12 hours

of incubation at 37 ^{o}C, the transwell inserts were removed. The medium was collected and used for quantification of human IL-8 and human TNF-α with ELISA. Measurements and analysis were performed for three independently conducted experiments.

4.4.9 *VSL#3* and *S. typhimurium* coculture interaction with mucosal barrier model

The in vitro mucosal lining model was challenged by adding 50 µl per well of GFP-labeled *S. typhimurium* and untagged *VSL#3* at specified density ratios to the apical side of the transwell inserts. After 12 hours of incubation at 37 ^{o}C, the transwell inserts were removed. The medium was collected and used for quantification of human IL-8 and human TNF-α with ELISA. Measurements and analysis were performed for three independently conducted experiments.

4.4.10 Cryopreservation, sectioning, and immunohistochemistry

To image and wild type and flagella knockout *S. typhimurium*, bacteria were grown to an OD600 of 0.8. Twenty µl droplets were applied to glass slides and allowed to dry in a biosafety cabinet for approximately six hours.

For histological sectioning, the transwell membranes with intact epithelial and mucus layers were cut from the inserts and fixed using 10% formalin solution in phosphate buffer saline for 20 minutes. Fixed membranes were embedded in optimum cutting temperature (OCT) medium and flash frozen in liquid nitrogen. Using a cryostat (CRYOSTAR NX70, Thermo Scientific), 30 µm thick cross-sections were cut and collected on Color Mark Plus glass slides for imaging. Brightfield images were acquired using an EVOS FL Auto

imaging system (Life technologies) and the thickness of the mucus layers were measured manually using ImageJ (NIH). Images from three independent samples were used for measuring the thickness.

For immunofluorescent staining of histological cross-sections two antibodies were used: FITC-conjugated anti-*S. typhimurium* antibody and Alexa Fluor 594 conjugated anti-human CD326 (EpCAM) antibody (1:200, Cat # 324228, Bio Legend). Sections on the glass slides were blocked in the blocking solution (1% BSA, 22.52 mg/ml in PBST (PBS + 0.1% Tween20)) for 1 hour at room temperature. Slides were incubated with antibodies diluted in 1% BSA in PBST for 1 hour at room temperature and washed three times with PBS. Histological slices were counter-stained with DAPI (1:10,000, D9542, Sigma Aldrich) to identify cell nuclei. Fluorescent images were acquired using Zeiss Spinning Disk Axio Observer Z1 microscope (Carl Zeiss) with a LD C-Apochromat 40x oil immersion objective and Zen software (Carl Zeiss).

The stained histological images were analyzed using ImageJ. To quantify *S. typhimurium* density in the mucus gel layer, images were tiled to capture from the top of the mucus to the bottom of the epithelial layer. Tiled images from three planes deep into the mucus layer on the glass slides were captured with 10 μm intervals. These three tiled images were projected on to a single plane. Projected images were uniformly segmented to isolate bacteria morphologically. The mucus layer height was divided into three regions of equal height (T: top; C: center; B: bottom). Images were collected from three independent

samples. The amount of *S. typhimurium* in each region was measured as the percent area with FITC over the total area using ImageJ.

4.4.11 Statistical analysis

A two-tailed Student's t-test assuming unequal variances was used for statistical analysis of pairwise comparison. One-way ANOVA with Tukey post hoc test was used for multiple comparisons. All data are presented as a mean ± standard deviation for three or more independent experimental conditions. Differences were considered significant at $P < 0.05$, with * denoting $P < 0.05$, and ** denoting $P < 0.01$.

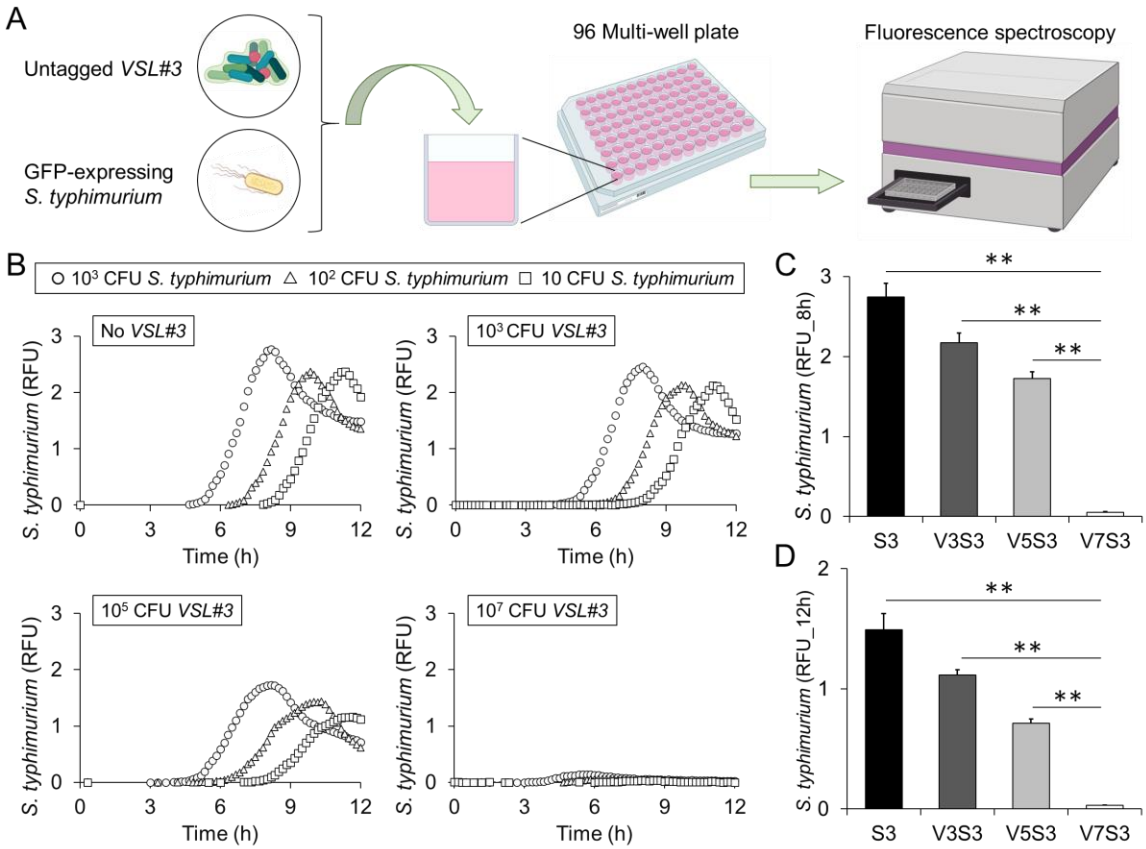

Figure 4.1. *S. typhimurium* growth in co-culture with *VSL#3*. (A) Schematic of the co-culture of untagged *VSL#3* and GFP-expressing *S. typhimurium* in 96 multi-well plates and quantification of growth by fluorescence spectroscopy in a multi-well plate reader. (B) Growth curves of *S. typhimurium* with changing initial seeding density. (C) Cell density (RFU) at 8 hours where the peak was observed for all growth curves (**, $P < 0.01$; $n = 3$). (D) Cell density (RFU) at the end point of 12 hours used for all the co-culture studies with human epithelial and immune cells (**, $P < 0.01$; $n = 3$). (S, V denotes and *S. typhimurium*, *VSL#3*, and Numerals 3, 5, 7 denotes 10^3, 10^5, 10^7 CFU/well of the 96 multi-well plate).

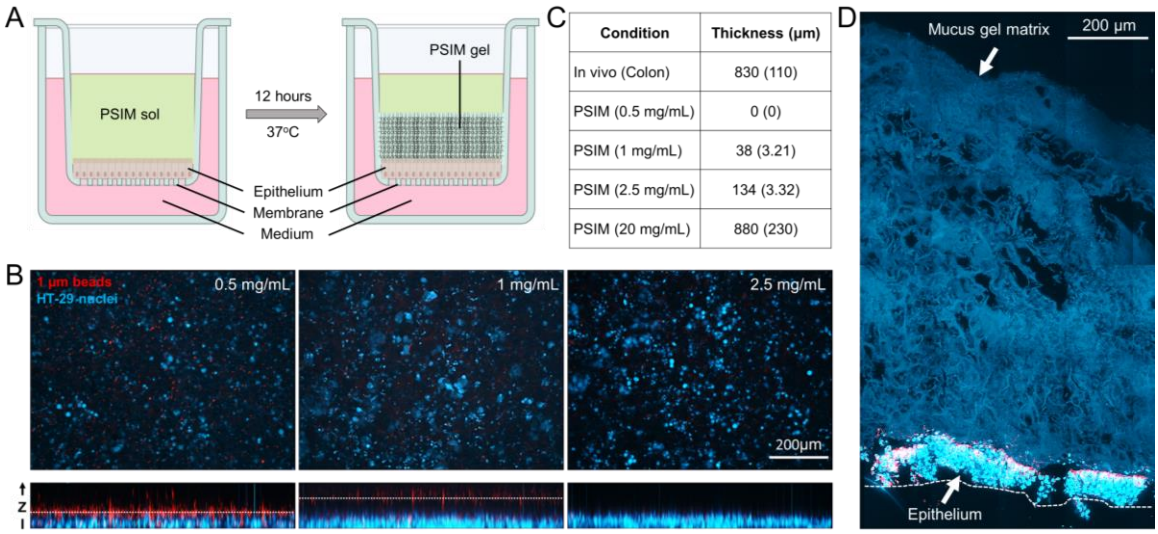

Condition	Thickness (µm)
In vivo (Colon)	830 (110)
PSIM (0.5 mg/mL)	0 (0)
PSIM (1 mg/mL)	38 (3.21)
PSIM (2.5 mg/mL)	134 (3.32)
PSIM (20 mg/mL)	880 (230)

Figure 4.2. Mucus gel layer formation matching the thickness of colonic mucus. (A) Schematic of the mucus gel layer formation on top of HT-29 epithelial cells growing on transwell membrane. A 100 µl of PSIM at known concentrations were added on the apical side of the transwell inserts containing the HT-29 cell layers and cultured for 12 hours at 37ºC to form the mucus gel matrix. (B) Confocal images of red fluorescent polystyrene beads added after mucus gel layer formation on HT-29 cells (Blue) at different PSIM concentration 0.5, 1, and 2 mg/ml. Top row shows the x-y projection and the bottom row shows the z-projection. Dotted line represents the plane of highest intensity of the fluorescent beads. (C) Table containing the average thicknesses of the mucus gel layer using PSIM[160] at different concentrations compared with the average mucus layer thickness of colonic mucus layer in vivo[58]. (D) Mucus gel layer formed at PSIM concentration of 20 mg/ml matched the thickness and structure of the colonic mucus layer in vivo. Dotted line represents the porous transwell membrane location.

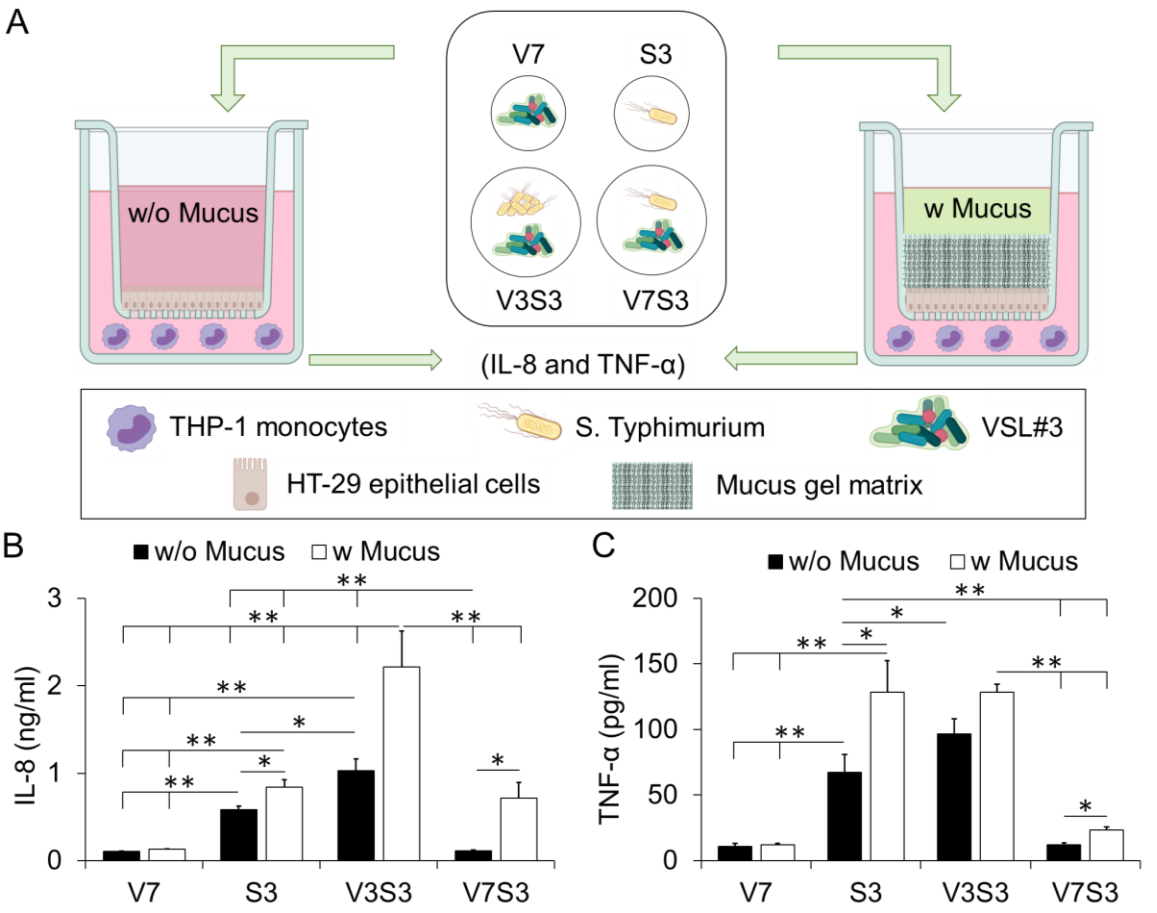

Figure 4.3. Chemokine (IL-8) and cytokine (TNF-α) levels in the mucosal barrier model. (A) The infection scheme for introducing *VSL#3* and *S. typhimurium* individually and cocultured into the mucosal barrier model with or without mucus gel matrix. IL-8 and TNF-α were quantified in the media collected from the basolateral compartment after 12 hours of culture. Notations denote V7 = 10^7 CFU/insert of *VSL#3*, S3 = 10^3 CFU/insert, V3S3 = 10^3 CFU/insert of *VSL#3* + 10^3 CFU/insert of *S. typhimurium*, and V7S3 = 10^7 CFU/insert of *VSL#3* + 10^3 CFU/insert of *S. typhimurium* added apically (100 µl) and cultured for 12 hours. Concentration of (B) IL-8 and (C) TNF-α from the mucosal barrier platform in response to stimulation with different bacterial cell densities after 12 hours of culture (*, $P < 0.05$; **, $P < 0.01$; n = 3).

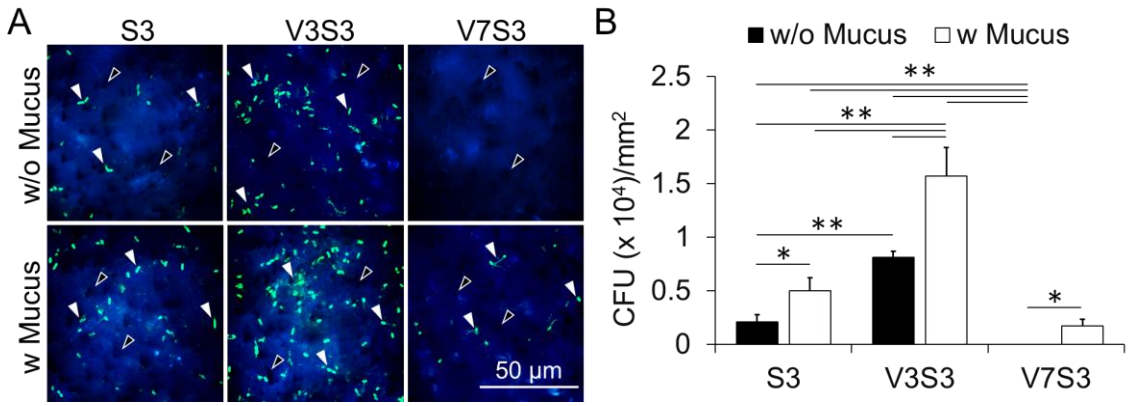

Figure 4.4. Quantification of *S. typhimurium* crossing the epithelial barrier. (A) *S. typhimurium* (Green) that have crossed the epithelial (Blue) barrier visualized using confocal microscopy. Black arrows indicate the pores in the transwell membrane and white arrows indicate *S. typhimurium*. (B) The number of *S. typhimurium* quantified by manual counting individual bacteria (*, $P < 0.05$; **, $P < 0.01$; $n = 3$).

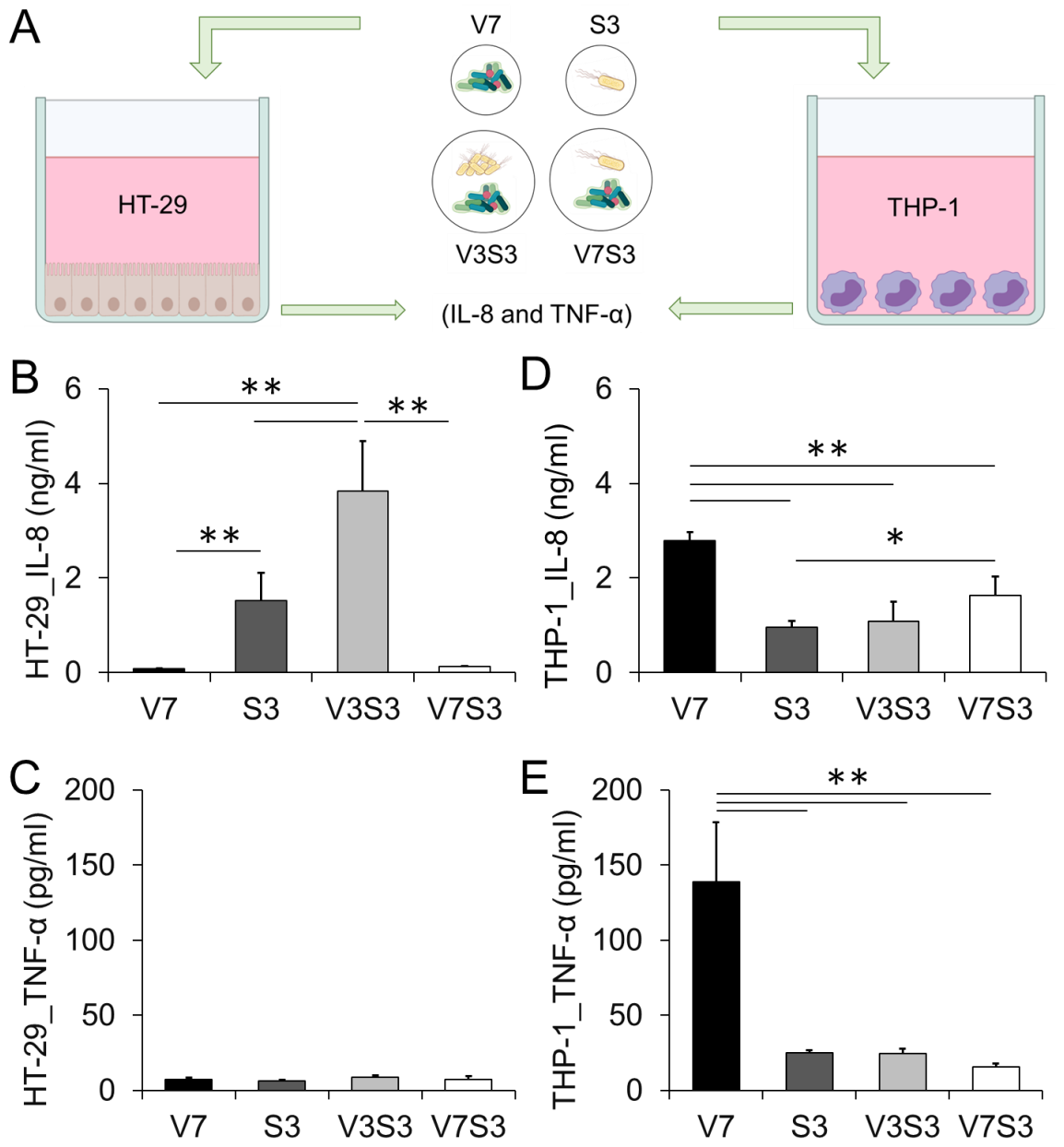

Figure 4.5. Chemokine (IL-8) and cytokine (TNF-α) levels from stimulated epithelial (HT-29) and immune (THP-1) cells. (A) The infection scheme for introducing *VSL#3* and *S. typhimurium* individually and cocultured into 24 well plates with adherent HT-29 cells and suspended THP-1 cells. IL-8 and TNF-α were quantified in the media collected after 12 hours of culture. Concentration of (B) IL-8 and (C) TNF-α from the HT-29 cells in response to stimulation with different bacterial cell densities (*, $P < 0.05$; **, $P < 0.01$; n = 3). Concentration of (D) IL-8 and (E) TNF-α from the THP-1 cells in response to stimulation with different bacterial cell densities (*, $P < 0.05$; **, $P < 0.01$; n = 3).

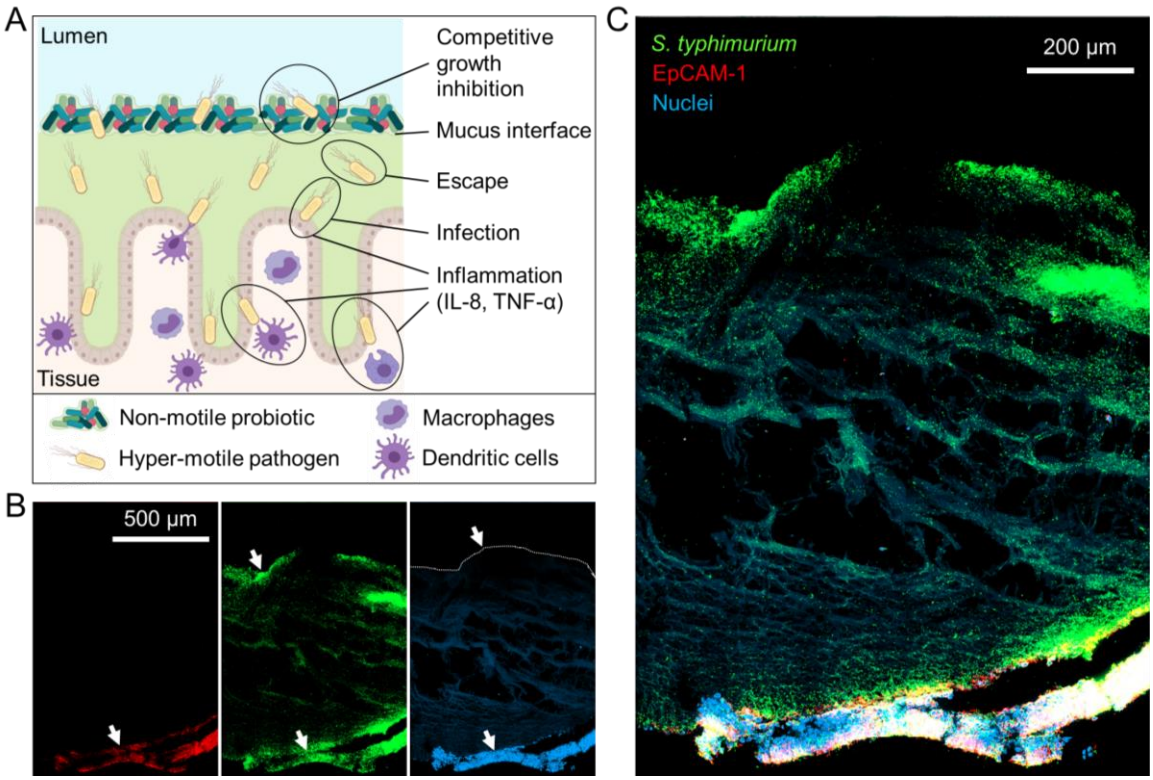

Figure 4.6. *S. typhimurium* utilize the mucus barrier to escape competitive growth inhibition from commensal bacteria and cause intestinal infection. (A) Non-motile probiotic bacteria (*VSL#3*) present at higher cell density compared to pathogen (*S. typhimurium*) effectively prevent *S. typhimurium* growth. The mucus interface is impenetrable to non-motile *VSL#3*, but hyper-motile *S. typhimurium* preferentially colonize the mucus layer. The escape mechanism is flagella dependent and enhance the infection ability of *S. typhimurium*. The epithelial barrier and innate immune cells (Macrophages and Dendritic cells) are the first responders in the inflammatory responses to pathogenic infection. (B) Fluorescent confocal microscope images showing epithelial cell adhesion molecule-1 localization (Red, arrow), *S. typhimurium* distribution (Green, arrows), and Epithelial cell nuclei with mucus gel matrix (Blue, arrows). (C) Fluorescent confocal microscope image of all three channels overlaid showing *S. typhimurium* distribution throughout the mucus gel matrix and infecting the epithelial cells.

CHAPTER 5

FUTURE APPLICATIONS AND CONCLUSION

5.1 Development of a probiotic encapsulation and delivery vehicle using PSIM

The scalable mucus extraction process established in this work can enable development of delivery vehicles for orally ingested therapies. The intrinsic properties of mucus make this biomaterial an ideal candidate for oral delivery. We hypothesize that the intact sol-gel transition of mucus will protect a therapeutic compound or live probiotic bacteria from the harsh acidic environment of the stomach. We tested this concept by adding a droplet of PSIM (20 mg/ml) at pH 7 on top of a droplet of 20 mM HEPES buffer at pH 4 (Figure 5.1). Fluorescently labeled (Cy5) Sambucus nigra agglutinin (SNA) lectins were mixed in the PSIM solution for fluorescence microscopic visualization. A distinct ring of PSIM was formed with the aggregated PSIM on the outside. No aggregation was observed in the center of the ring. Cy5 lectin stain was also localized in the aggregated region with slight diffusion of possibly unbound lectin towards the center of the ring. This test indicates a feasibility of PSIM bead formation with an aggregated shell that forms a protective barrier against gastric acid and the desired therapeutic in the core of the bead (Figure 5.2A). We have demonstrated previously that PSIM is a solution at pH 7 but formed a gel at pH 4 and undergoes spontaneous sol-gel transition with change in the pH (Figure 5.2B). This property will be ideal for release of the encapsulated therapeutics in the neutral pH conditions present in the small and large intestines. To demonstrate the encapsulation, green, fluorescent polystyrene microbeads were mixed in PSIM (20 mg/ml) at pH 7. The mixture was gently pipetted into a bath containing 20 mM HEPES buffer at pH 4 forming a cross-linked spherical bead (Figure 5.2C). Fluorescent confocal microscopy showed

embedded GFP expressing polystyrene microbeads in the matrix of the PSIM beads (Figure 5.2D). This concept can be applied for encapsulation, gastric protection, and delivery of probiotic bacteria to the intestines.

To streamline this process a microfluidic platform can be utilized that will enable encapsulation of the probiotic bacteria in PSIM (pH 7) using a flow focusing channel containing a buffer solution at pH 4 (Figure 5.2E). After the beads are formed, they will pass through another flow focusing junction where the beads will be exposed to a buffer solution at pH 2. The beads can be collected while immersed in the pH 2 buffer solution. Lyophilization of the beads can be tested for long-term storage of the encapsulated probiotic bacteria. Further validation will be required to test if the beads are actually forming core-shell regions. Furthermore, the viability of the encapsulated probiotic bacteria can be tested by solubilizing the beads in a buffer solution at pH7. PSIM can be expected for good tolerance in the intestines since the mucin macromolecules are highly abundant in the lumen. To be clinically applicable, PSIM should be tested for presence of any endotoxins and other immunostimulatory antigens. Information on the exact biochemical composition of PSIM can lead to large-scale clinical applications.

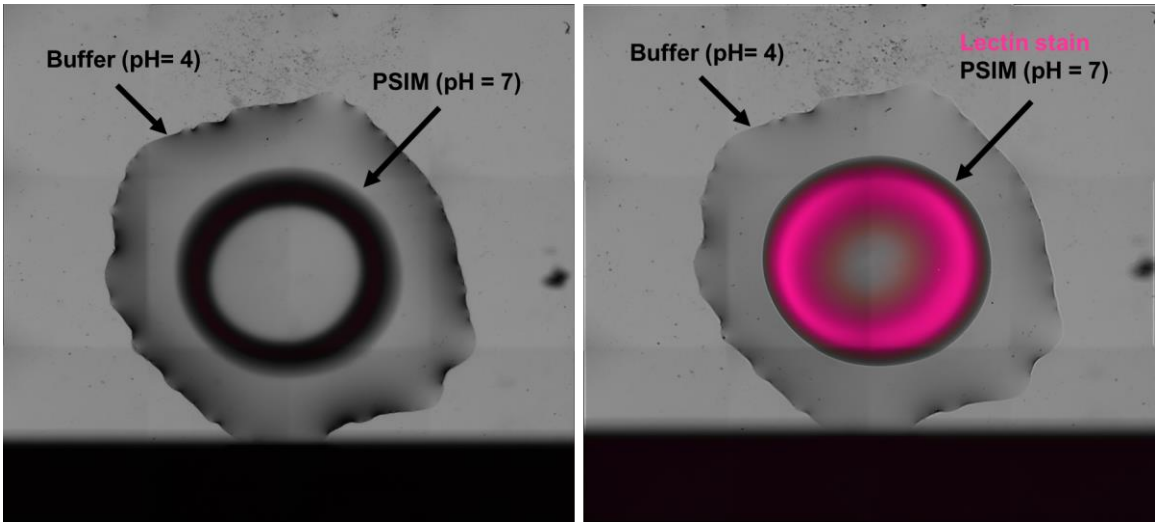

Figure 5.1 PSIM ring formation in low pH. Microscopic images of PSIM droplet (pH 7) interacting with a 20 mM HEPES buffer droplet (pH 4) and forming a ring with aggregated mucus at the periphery and PSIM solution in the core.

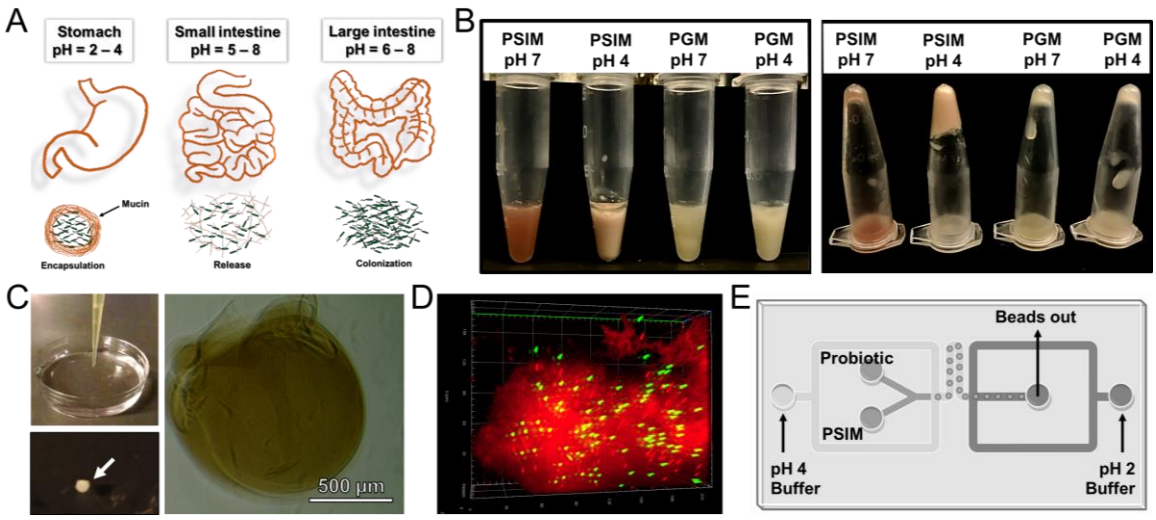

Figure 5.2 Conceptual design of core-shell particles of PSIM for probiotic encapsulation. (A) Schematic of the hypothesized PSIM beads that encapsulate probiotic bacteria in the core, protects the bacteria from gastric acid and releases the bacteria in the neutral environment of the intestines by reversible gel to sol transition. (B) Demonstration of sol (pH 7) to gel (pH 4) transition of PSIM (80 mg/ml) compared to commercially available porcine gastric mucin (PGM) that does not undergo sol-gel transition in response to pH change. (C) PSIM bead formation by gently pipetting 10 µl of PSIM (pH 7) into a bath of 20 mM HEPES buffer (pH 4). (D) GFP expressing polystyrene beads (1 µm size) embedded in Cy5 lectin stained PSIM gel matrix. (E) Proposed microfluidic device for streamlining probiotic encapsulation, uniform sized bead formation, and collection of PSIM beads at pH 2 that is similar to pH in the gastric lumen.

5.2 Creation of a two-layer mucus barrier relevant to the large intestine mucus barrier

Large intestines are the biggest reservoir of bacteria in the human body. The mucus layer protects underlying tissue from coming in direct with the bacteria. The most intriguing feature of the mucus layer in the large intestine is the structural organization into a two-layer system. The inner layer is tightly bound to the epithelium and is devoid of bacteria. The outer layer is loosely attached and is colonized by commensal bacteria. The exact mechanisms of how this structural layering is achieved in vivo are still being discovered. Consequently, it has been challenging to recreate the two-layer mucus barrier of the large intestine in vitro. Development of an in vitro model that mimics this essential feature of a healthy mucus barrier can provide significant insights into the factors that can lead to pathological conditions of large intestines. We have demonstrated before that PSIM forms structurally stable layers on top of transwell membranes in Chapter 2. The structure of the PSIM can be controlled by changing PSIM concentration, addition of multivalent cations, and changing pH. Since the pH in the intestines is maintained close to neutral, we utilized the change in PSIM concentration and Ca^{2+} ion concentration to create multiple layers with structural differences. Since the inner mucus layer is known to be more cross-linked and impenetrable to bacteria, we used a combination of high PSIM concentration (100 mg/ml) and high Ca^{2+} concentration (100 mM) to create this layer (Figure 5.3A). A 50 µL solution of PSIM in 20 mM HEPES buffer was added to the apical compartment of a transwell insert (3 µm pore size) and 100 mM $CaCl_2$ solution in 20mM HEPES buffer was added to the basolateral compartment of a 24 well plate. After incubation at 37^{o}C in a humidified incubator for 12 hours, 100 µL solution of PSIM (20 mg/ml) was added on top of the

preformed mucus layer. After incubation at 37ºC in a humidified incubator for 12 hours, the transwell membranes were carefully separated from the inserts and immersed in 10 % Formalin solution for 30 minutes. The fixed mucus layers were embedded in optimum cutting temperature (OCT) matrix and cryo-frozen by immersing in liquid Nitrogen. The frozen samples were sectioned into 20 µm thick slices using a cryostat. Fluorescently labeled (Cy5) Sambucus nigra agglutinin (SNA) lectins were mixed in the PSIM solution prior to gel formation to facilitate imaging after cryo-sectioning. The combination of high PSIM concentration (100 mg/ml) and gradient of Ca^{2+} ions from the basolateral compartment lead to formation of highly cross-linked mucus gel layer (Figure 5.3A). The gel layer was structurally stable and could be visualized microscopically by fluorescent microscopy. By adding PSIM solution at low concentration (20 mg/ml) on top of the first layer formed a structurally distinct outer mucus layer (Figure 5.3B). Fluorescent microscopy showed a clear interface between the two layers along with difference in the structure of both layers. The inner layer showed large areas of dense aggregates identified by bright fluorescence indicating higher density and cross-linking. The outer layer had branched structure and no bright fluorescent aggregates indicating the absence of Ca^{2+} induced crosslinking and therefore a loose structure. The results show that the two-layer structure of mucus barrier present in the large intestine can be captured by using PSIM.

Several challenges remain to make this system more physiological. The transwell platform does not allow the reduction in the height of the mucus layer formed. The viscoelastic properties and height of the inner and outer mucus layer needs to be tuned to match the in vivo properties of the mucus layers. This can be done by 1. Systematic testing of PSIM and Ca^{2+} concentrations, 2. Using methods like Particle tracking microrheology to measure the

viscoelastic properties of the gel layers formed, and 3. Creating tools to precisely control the thickness of the gel layers formed while still allowing the apical and basolateral interactions of PSIM and Ca^{2+} ions.

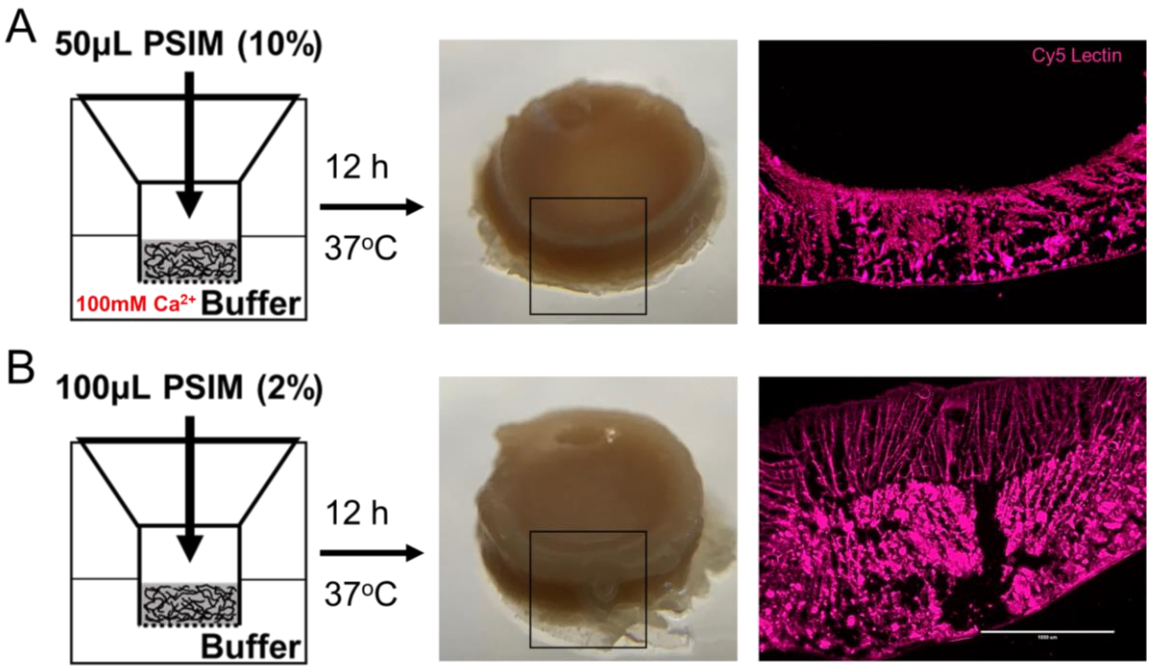

Figure 5.3 Two-layer mucus barrier formation using PSIM. (A) Schematic of the inner layer formation by using high concentration of PSIM in the apical compartment and high concentration of Ca^{2+} ions in the basolateral compartment (Left). After incubation, a structurally stable mucus gel layer formed (Middle) which was visualized using fluorescent microscopy (Right). (B) Schematic of the outer layer formation by using low concentration of PSIM on top of the preformed inner layer in the apical compartment and HEPES buffer solution without Ca^{2+} ions in the basolateral compartment (Left). After incubation, structurally stable mucus gel layers formed (Middle) which were visualized using fluorescent microscopy (Right).

5.3 Microfluidic platform for dynamic mucus barrier formation using PSIM

The mucus lining along the gastrointestinal tract is the outermost and largest interface in the body that protects the epithelium, regulates the selective transport of nutrients, and maintains symbiosis in presence of microbes (Figure 5.4). Goblet cells constitute about 4-12% of epithelium in the small intestine and up to 20% in the large intestine, which correlates with the properties and height of the mucus barrier. In human intestines, the turn-over rate of the entire mucus layer is close to 1 hour meaning that the mucus layer is essentially flowing at a very low rate. The secreted mucin biopolymers regulate barrier function via in situ biochemical and biophysical interactions with the luminal content that periodically fluctuates. Mimicking the mucus layer that is constantly replenishing and dynamically responsive to changes in surrounding environment (pH and ionic concentration) has not been realized in most commonly used in vitro models of human intestines. In vitro mucus barrier model that replenishes continually and is responsive to luminal content can serve as an enabling tool for understanding the interactions and transport of orally administrated drug compounds as well as bacteria across the protective mucus barrier in vivo.

To achieve this a simple microfluidic design was developed that enables flow of luminal content and PSIM in parallel. The microfluidic design was prepared using Adobe Illustrator software. A single microfluidic channel with Y-shaped inlets and outlets was printed on a 250 μm thick poly-dimethyl siloxane (PDMS) sheet using Graphtec plotter cutter. The PDMS sheet with the channel was bound onto a glass slide and covered with a thick PDMS sheet using oxygen plasma treatment for 2 minutes and a platform with multiple channels

on a single platform was created (Figure 5.5A). The channel layer was covered on top with a 3 mm thick PDMS layer with the inlet and outlet ports punched prior to oxygen plasma bonding for 2 minutes. All surfaces must be kept clean by washing in 70 % Ethanol and allowing the ethanol to air dry without touching the surface. The syringes containing PSIM or buffer solution were connected to the inlet ports using polypropylene tubing with 1 mm inner diameter. The flow was controlled using Harvard apparatus syringe pumps. The channels were filled with 20 mM HEPES buffer at pH 7 before connecting the inlet and outlet tubing to prevent air bubble formation. The exclusive presence of laminal flow profile in microfluidic devices prevents mixing and enables the study of diffusion across the interface between the two phases (Figure 5.5B). The device was tested by flowing a solution of food coloring dyes (blue and red) at a flow rate of 10 µl/min. A distinct interface was formed at the center of the main flow channel.

To demonstrate this concept with luminal content and mucus, PSIM in 20 mM HEPES buffer at a physiological concentration (20 mg/ml) and pH 7 was flown from one inlet and luminal content (20 mM HEPES buffer) with changing Ca^{2+} concentrations was flown from the other at a flow rate of 10 µl/min. We hypothesized that at the interface where the luminal content came in direct contact with PSIM, a diffusive barrier would form due to Ca^{2+} induced aggregation and cross-linking of mucus. Indeed, a visible barrier formed that changed in real time in response to Ca^{2+} concentration in the luminal content (Figure 5.6A). The thickness of the mucus gel layer increased by increasing the Ca^{2+} concentration in the luminal compartment (Figure 5.6B). At 5mM Ca^{2+}, mucus gel layer did not form in the entire channel. Increasing the Ca^{2+} concentration to 25 mM significantly increased the

thickness of the layer. Further increase in the Ca^{2+} concentration to 100 mM caused a 3-fold increase in the gel layer thickness compared to 25 mM Ca^{2+}. Increasing gel layer thickness caused reduction in the diffusion of FITC dextran (20 kDa) (Figure 5.6C). At 5 mM Ca^{2+} FITC dextran diffused across the interface and there was no difference in the GFP intensity in the luminal half and the mucus layer. At 25 mM and 100 mM Ca^{2+} a significant reduction in GFP intensity was measured in the mucus layer suggesting that the Ca^{2+} induced cross-linking of mucus at the interface acts as a barrier for molecular diffusion. In our preliminary testing, mucus aggregates also formed in the presence of most physiologically relevant and multivalent cationic species like Mg^{2+}, Zn^{2+}, Fe^{2+}, and Fe^{3+}. Most of these cations including calcium are present in foods and supplements ingested by humans on a regular basis. Therefore, the role these cations in the barrier function and nutrient absorption across the intestinal mucus barrier can be systematically explored using the microfluidic platform. The ease of imaging will enable systematic characterization of transport behavior of fluorescently labelled carbohydrates, amino acids, lipids, food grade nanoparticles, and live bacteria across the mucus barrier while changing pH and ionic concentrations.

Currently, the microfluidic device requires both the luminal content flow and PSIM to flow at equal flow velocity for the interface to form at the center of the device. Setting the flow rate at 10 10 µl/min in both the flow streams also ensured proper clearance of the device for operation until 1 hour. Under the current operating parameters, the flow velocity is two orders of magnitude higher than the physiological replenishing rate of mucus (hourly turnover). However, reducing the flow rate close to the physiological range caused

accumulation of aggregates, disruption of the gel layer interface and clogging of the device. Also. It may be ideal to have a stable static mucus barrier and flowing luminal content which will enable consistent quantification of diffusion across the mucus layer. However, stopping the mucus flow also leads to accumulation of aggregates, disruption of the gel layer interface and clogging of the device. One solution for this problem is to optimize the mucus flow rate as close to physiological as possible without clogging the device for at least 30 minutes. Matching the flow rate of luminal content with the optimized mucus flow rate will ensure a uniform interface formation that will also enable consistent measurement of diffusion across the gel layer formed at the interface. Another solution for this problem is to quantify the diffusion exclusively in the region of the gel interface. Since the gel interface once formed remains static irrespective of the flow rates of the luminal content or the PSIM. This strategy is more feasible for particle of micrometer scale and bacteria but may not be suitable for small molecule diffusion. Additional work is required in this direction.

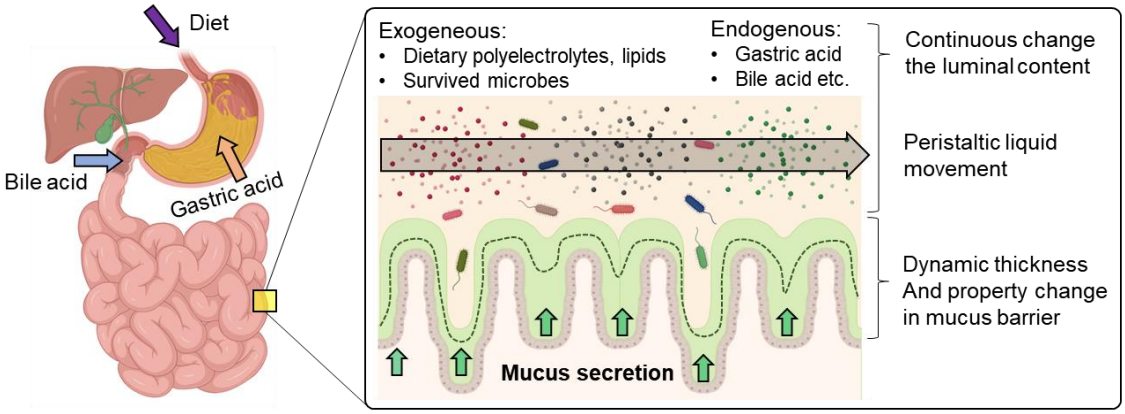

Figure 5.4 Luminal environment of the intestines is highly complex and dynamically evolving. Schematic showing the complex environment in the lumen of the intestinal tract including endogenously secreted gastric acid, bile salts, enzymes, and the resident microbiota. The lumen is also exposed to exogenous factors such as dietary molecules and pathogenic bacteria. The continuous secretion of the mucus and peristaltic movement of the luminal contents help in physically protecting the underlying tissue and clearance of the harmful luminal content continually.

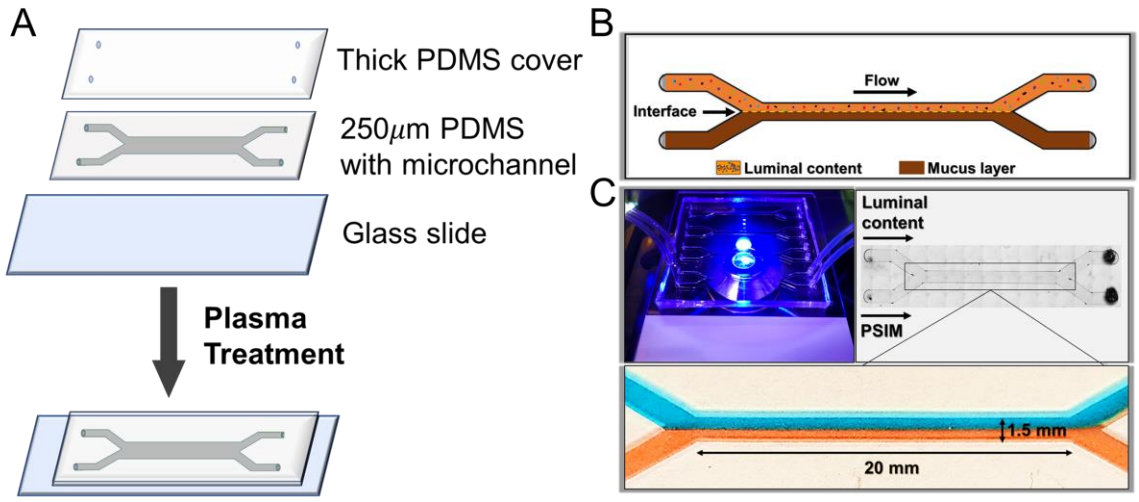

Figure 5.5 Dynamically responsive mucus barrier in a microfluidic platform. (A) Schematic of the microfluidic device fabrication process. (B) Schematic of the conceptual flow regimes in the 2-inlet microfluidic device. (C) Digital images of the microfluidic device in operation, microscopic image of the flow channels and food coloring dye blue and red forming an interface in the central microfluidic channel.

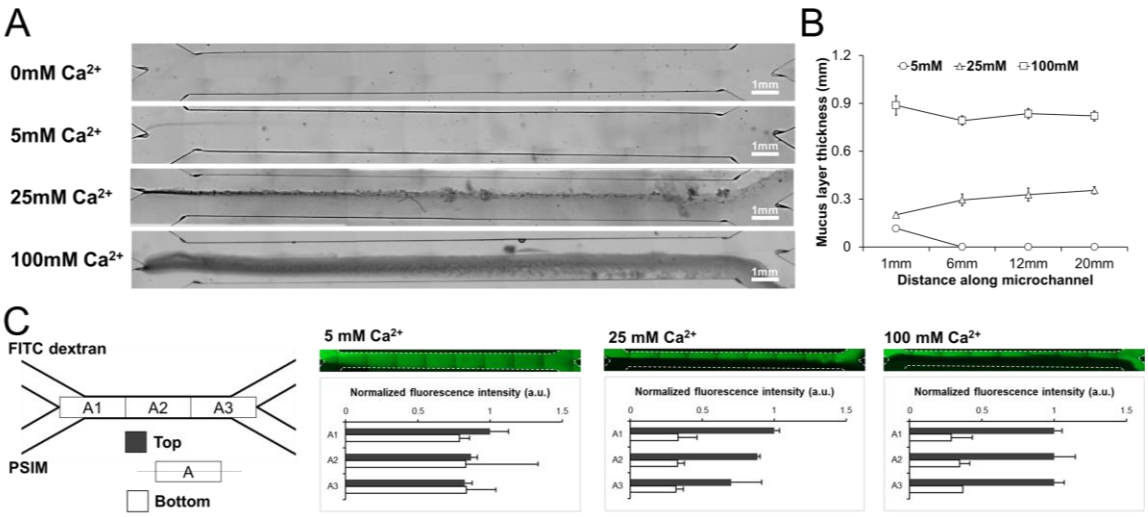

Figure 5.6 Regulation of molecular diffusion via PSIM gel formation at the lumen-mucus interface. (A) Microscopic images of Ca^{2+} dependent PSIM gel interface forming in the central microchannel. (B) Thickness of the gel interface increases with increasing Ca^{2+} concentration. (C) Diffusion of FITC dextran (20 kDa) dye is reduced with increasing gel layer thickness.

5.4 'Intestine mucosal barrier on a chip' for real time host-microbe interaction

To mimic intestinal physiology, two microfluidic designs were developed to combine a flow channel for luminal content, a flow channel for replenishing mucus layer and epithelial cell layer (Figure 5.7). This way bacteria can be cocultured with epithelial cell surface in presence or absence of mucus layer. Continuous removal of culture medium will prevent bacterial overgrowth. Due to the planar design of the microfluidic platform, interactions of bacteria with mucus gel and epithelial cells can be captured in real time. The devices were designed to specifically include 1. Resident immune cells embedded in extracellular matrix to mimic the innate immune responses, 2. Endothelial cell layer with a separate flow channel for capturing transmigration of effector cells into the extracellular matrix following a chemokine gradient. The devices were developed using a simple and cost-effective strategy that eliminated the use of microfabrication related instruments and cost involved.

The microfluidic design was prepared using Adobe Illustrator software. A single microfluidic channel with Y-shaped inlets and outlets was printed on a 500 μm thick poly-dimethyl siloxane (PDMS) sheet using Graphtec plotter cutter. The PDMS sheet with the channel was bound onto a glass slide and covered with a thick PDMS sheet using oxygen plasma treatment for 2 minutes and a platform with two devices on a single glass slide was created (Figure 5.8A). In a biosafety cabinet, the PDMS pieces cut out from the sheet were placed back in their position except the rectangular piece designated for collagen gel layer formation. Rat tail collagen (Type 1) solution (8 mg/ml) and 10x concentrated cell culture medium (w/ Phenol red) were placed on ice. The collagen solution and the 10x medium

were mixed in a proportion of 9-parts collagen and 1-part 10x medium and mixed gently to prevent any air bubble formation while keep the solution on ice at all times. The mixed solution (25 μl) was gently pipetted in the vacant rectangular piece making sure that no air bubble form and the solution is in contact with all the corners. For embedding immune cells in the collagen gel, the immune cell pellet should be formed by centrifugation and then resuspended using the collagen-medium solution. Depending on the efficiency of mixing, the collagen-medium solution will start to turn opaque at room temperature in 5-10 minutes indicating the collagen gel formation. To speed up the gel formation, the collagen-medium solution can be incubated in a humidified incubator at 37^{o}C with constant monitoring of the gel. The gel should not be left for too long at room temperature or 37^{o}C incubator as the dehydration of gel will affect the sealing of the collagen gel to the top PDMS and bottom glass surface. After gel formation, the PDMS pieces inserted in the main channels were gently removed (Figure 5.8B). This layer containing the collagen gel and the flow channel on the glass slide should not be taken out of the biosafety cabinet to maintain sterility and should not be exposed to plasma treatment. The channel layer was covered on top with a 3 mm thick PDMS layer with the inlet and outlet ports punched prior to oxygen plasma bonding for 2 minutes. While binding ensure the alignment of the inlet and outlet ports with the channels and are should be taken to not disturb the collagen gel layer. All surfaces must be kept clean by washing in 70 % Ethanol and allowing the ethanol to air dry without touching the surface inside a biosafety cabinet. For cell seeding and culture 200 μl pipet tips were inserted in the inlet and outlet ports and the medium level was maintained by gravity driven flow (Figure 5.8B). For flow experiments, the syringes containing cell suspensions, PSIM and cell culture medium solution were connected to the

inlet ports using polypropylene tubing with 1 mm inner diameter. The flow was controlled using Harvard apparatus syringe pumps. The channels were filled with cell culture medium before connecting the inlet and outlet tubing to prevent air bubble formation.

To test the stability of the cell-free collagen layer (Figure 5.9A), gravity-driven flow was used to perfuse phosphate buffer solution (PBS) containing 1 µg/ml of FITC dextran (20 kDa) and TRITC dextran (155 kDa). The devices were imaged over time for GFP and RFP fluorescence to quantify the rate of diffusion of these molecules across the collagen gel layer (Figure 5.9B). FITC dextran diffusion was significantly faster compared to TRITC dextran over time indicating that the rate of diffusion is size-dependent. Differences in the rate of diffusion of the two differently sized molecules also suggest that there is no leakage around the edges of the collagen gel. Additionally, the diffusion appeared to be uniform along the entire length of the collagen gel. FITC dextran (20 kDa) diffused across the entire width of the collagen gel reaching close to steady state in 4 hours suggesting that the cells can be embedded in the collagen gel since the nutrients can easily diffuse across the gel layer.

Immune (THP-1) cells embedded in the collagen gel under static conditions remained viable for more than 7 days (Figure 5.10A). The cell culture medium was replaced every other day. Cell viability was confirmed by blue, fluorescent live cell tracker (Hoechst 33342). Coculture of immune cells with live bacteria was tested by introducing red fluorescent protein (RFP) expressing E. coli Nissle 1917 strain in the luminal channel.

Fluorescence microscopy was used to track the growth of bacteria over time confirming the ability of real time imaging in the microfluidic platform (Figure 5.10B).

To establish the epithelial cell layer, epithelial (HT-29) cells were seeded on one edge of the gel by seeding 10^5 cells per device, setting the device vertical so that suspended cells settle on the collagen gel surface and incubated at 37^{o}C and 5% CO_2 in a humidified incubator. Cell culture medium was changed daily, and coverage of the epithelia cells was confirmed by brightfield imaging (Figure 5.11A). Epithelial cells covered the entire surface of the collagen gel in 3-5 days. The cell layer was fixed by perfusing 10% Formalin solution and incubating at room temperature for 30 minutes. To confirm the formation of tight epithelial barrier, HT-29 cells were stained with EPCAM-1 (Red) and nuclei (Blue). The epithelial cells formed a 3D structure with well-defined epithelial cell junctions (Figure 5.11B). To mimic the physiological complexity of intestines, PSIM gel layer was reconstituted in the main channel along with green fluorescent protein (GFP)-expressing bacteria suspended in cell culture medium (McCoy's 5A) supplemented with 20 mM Ca^{2+}. To demonstrate continuously replenishing luminal content, flow was maintained at 3 µl/min. Calcium induced aggregation created a distinct separation between the epithelial cell layer and the GFP bacteria flowing across the luminal side (Figure 5.11C top). By stopping the flow, mucus barrier was disrupted that caused the bacteria to fill the entire channel and came in direct contact with the epithelial cells (Figure 5.11C bottom).

Similarly, to establish endothelial cell layer after epithelial cell attachment, endothelial (HUVEC) were seeded on the other edge of the gel by seeding 10^5 cells per device, setting

the device vertical so that suspended cells settle on the collagen gel surface and incubated at 37^{o}C and 5% CO_2 in a humidified incubator. Collagen gel successfully created a partition between the top Y-inlet channel and the straight channel on the bottom (Figure 5.12A). Epithelial cells formed a uniform layer on the top edge of the collagen layer and expressed epithelial cell adhesion molecule - 1 (EPCAM-1) after 3 days of culture (Figure 5.12B). Endothelial cells formed an interconnected cell layer on the bottom edge of the collagen gel confirmed by platelet and endothelial cell adhesion molecule - 1 (PECAM-1) expression. Immune cells can be directly injected into the channel on endothelial side. Mucus and bacteria can be injected into the Y-shaped inlets. Cell viability and differentiation can be quantified using fluorescent confocal microscopy and flow cytometry.

The microfluidic mucosal barrier model provides a high throughput platform to test hypothesis related to efficacy and immune compatibility of probiotics and therapeutics. Simple chip design allows for real time monitoring of multiple species of bacteria co-cultured with human derived epithelial and endothelial cells. Continuously replenishing luminal content and the mucus gel layer can enhance the physiological relevance of this model. Additional work is needed to confirm the sealed epithelial cell layer formation. Cell seeding for epithelial, immune, and endothelial cells also needs to be adjusted to reflect the physiological structure of the intestines. Different methods will be required to quantify the permeability of the epithelial cell barrier such as dye-based methods or advance methods to measure trans-epithelial electrical resistance (TEER). We found that HT-29 cells start to form 3D aggregates after long-term culture. Other cell lines such as Caco-2 can be tested

for better results with cell coverage and forming a sealed epithelial barrier. Additionally, methods can be explored for covalent cross-linking of the collagen gel with the bottom glass slide and the top PDMS cover for preventing leakage on the edges for long-term studies. Also, immune cells showed limited migration in the collagen gel at the concentration of collagen tested. Therefore, further tuning the collagen gel to enable immune cell activity will enhance the functionality and applicability of this device. Since the thickness of the collagen cannot be reduced further due to technical reasons, more advanced methods can be tested to achieve vascularization of the collagen gel by endothelial cells. This will enable capturing the phenomena of immune cell trafficking from the immune cell channel to the site of epithelial cell injury in the microfluidic platform. The assembly of the microfluidic chip is such that the cells can be retrieved for downstream analysis including flow cytometry, DNA, RNA, and protein quantification. Secreted molecules such as cytokines and chemokines can be easily retrieved for quantification by collecting and replacing the medium over time.

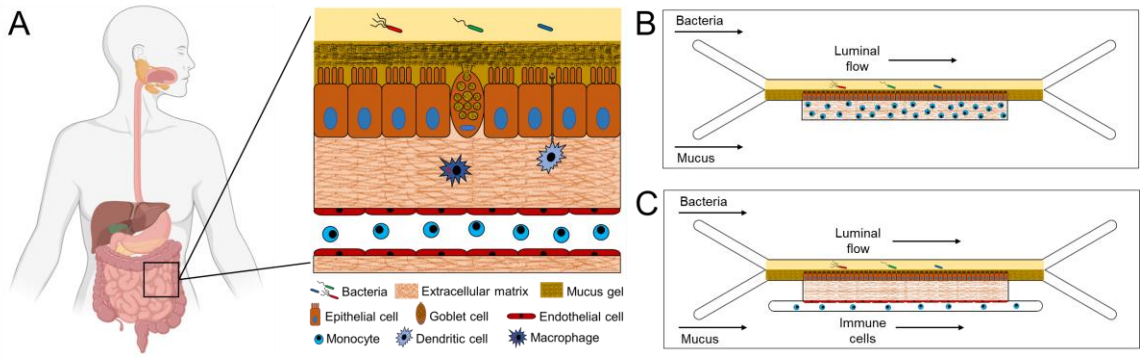

Figure 5.7 Microfluidic platform to reconstitute the mucosal and immunological function of the intestines. (A) Schematic of the physiological structure and the cells present at the mucosal interface. Mucus layer, epithelial barrier and the cells of innate immune cells are in constant communication with the intestinal microbiota. (B) A microfluidic chip design to incorporate bacteria, mucus, epithelial, and immune cells in a physiological manner. (C) A microfluidic chip design that incorporates an additional channel for adding endothelial cell layer with the cells of intestinal mucosa.

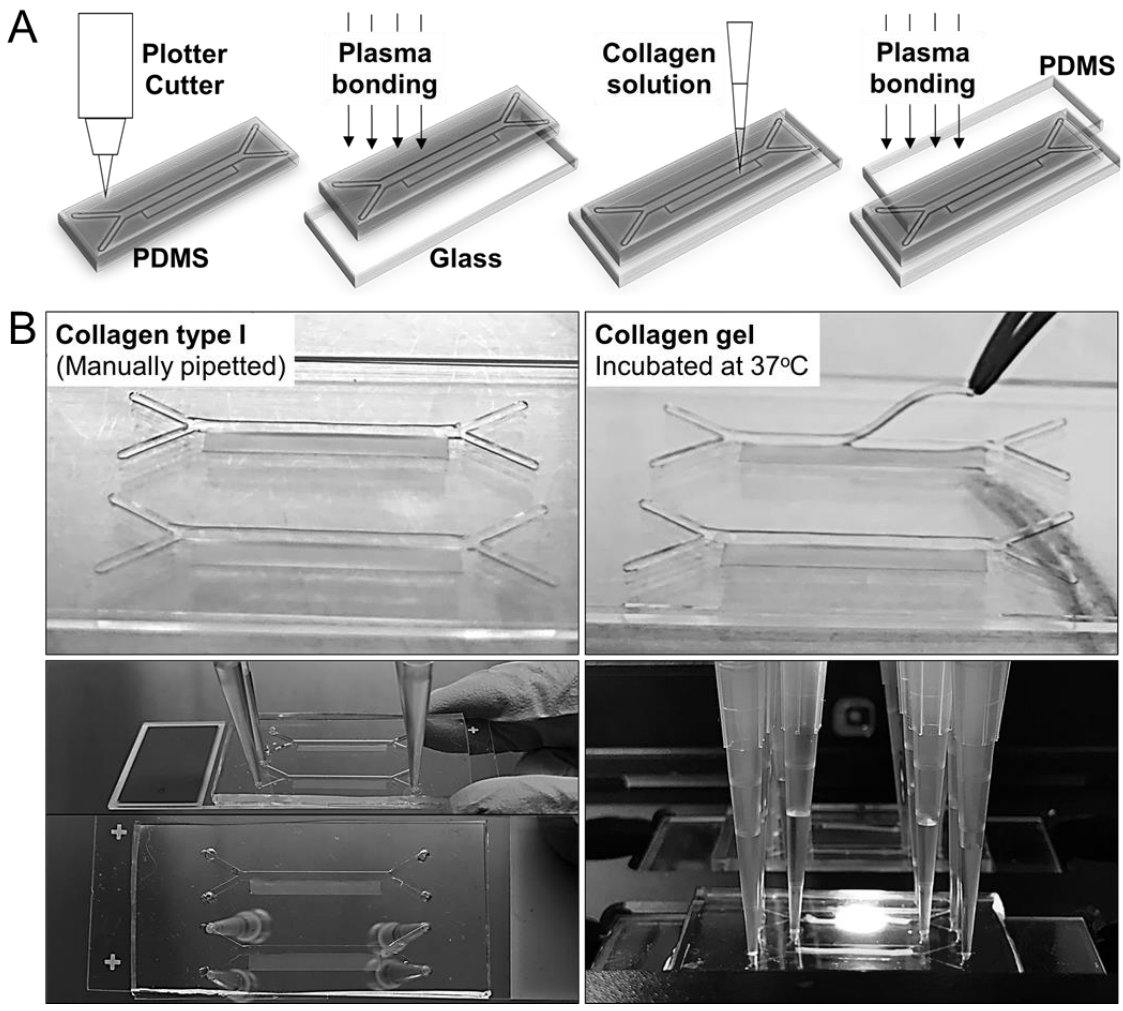

Figure 5.8 Fabrication of the microfluidic platform containing the collagen gel for supporting epithelial cell layer and embedded immune cells. (A) Schematic of the steps involved in the fabrication of the microfluidic chip. (B) A key step in the fabrication process is the manual addition of the collagen solution, and careful removal of the thin PDMS piece from the central channel. The planar design enables real-time imaging of the interactions occurring in the device.

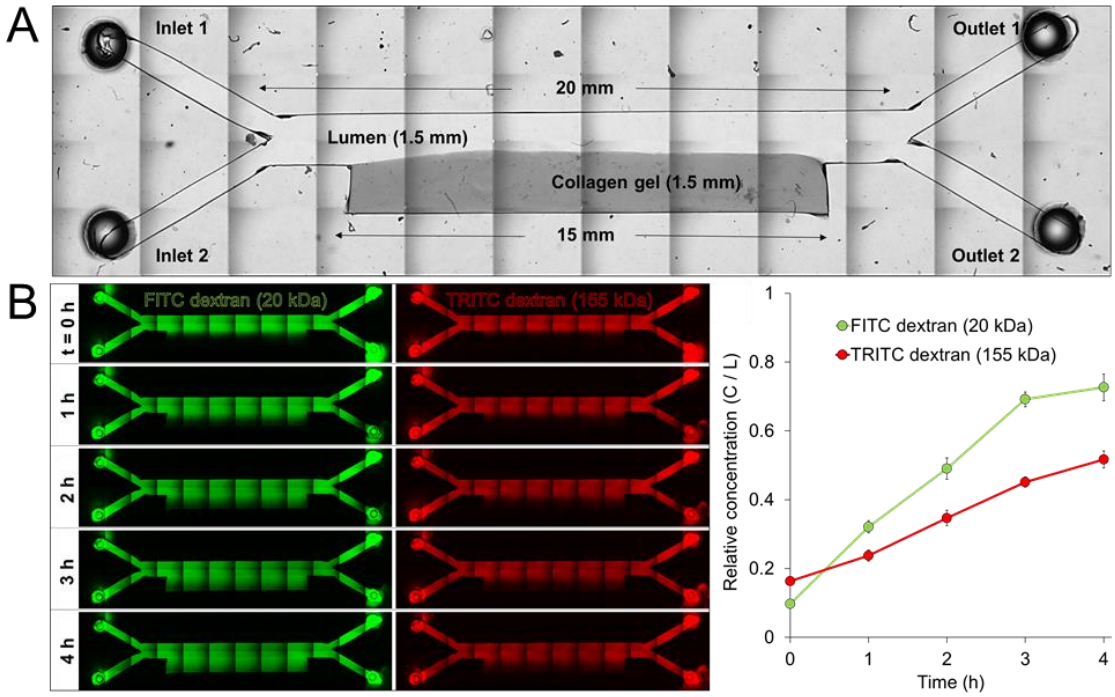

Figure 5.9 Testing the stability of the collagen gel and quantifying diffusion across the gel layer. (A) Brightfield microscope image shows a stable collagen gel layer formed in the rectangular region. The luminal channel is accessible to inlet and outlet flow. (B) Fluorescent microscope images showing the diffusion of two different sizes of dextran molecules. The rate of molecular diffusion was quantified by measuring the fluorescence intensity over time showing that diffusion was dependent on the size of the molecules tested.

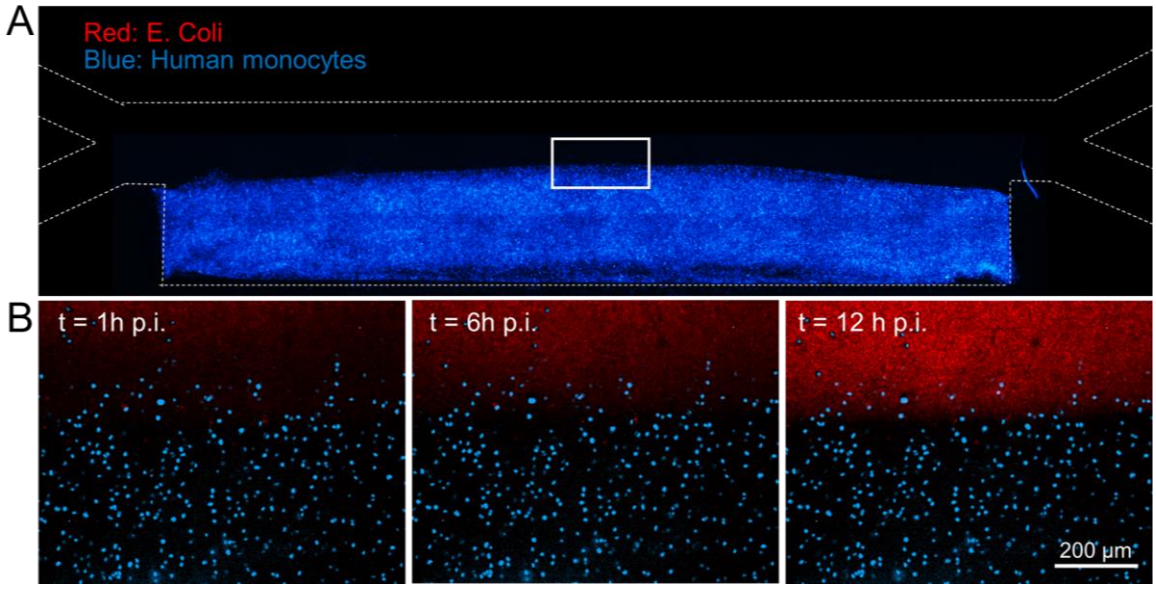

Figure 5.10 Testing viability of embedded immune cells and coculture with live bacteria. (A) Fluorescent microscope image of THP-1 cells embedded in the collagen and stained with blue live cell tracker. (B) RFP expressing E. coli Nissle 1917 cocultured with embedded THP-1 cells. Bacteria growth and interaction with the immune cells was captured over time.

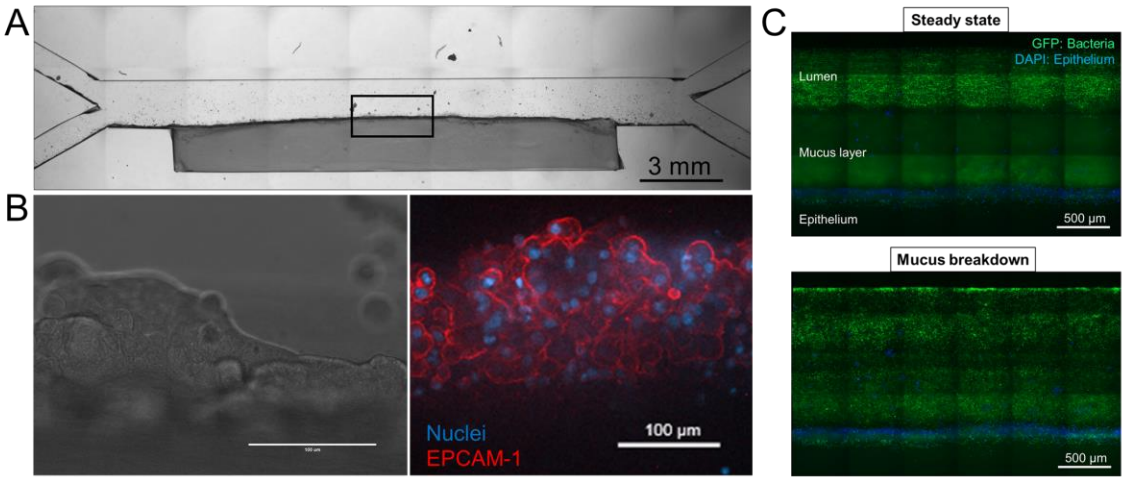

Figure 5.11 Demonstrating epithelial and mucus layer formation and coculture with live bacteria. (A) Brightfield microscope image of the microfluidic device showing the HT-29 epithelial cell layer covering the entire surface of the collagen gel. (B) High magnification image shows 3D growth of epithelial cells and the fluorescent microscope image shows the formation of epithelial cell junctions (EPCAM-1). (C) Fluorescent microscope images show the maintenance of steady state by flowing the mucus layer and the luminal content at equal flow rate of 3 µl/min. Presence of 20 mM Ca2+ in the luminal content enable the formation of a distinct interface separating the bacteria (GFP S. typhimurium) and the mucus layer. The underlying epithelial layer (blue) is prevented from bacterial infection. Disrupting the flow of mucus caused infiltration of bacteria into the mucus layer and epithelial cell infection.

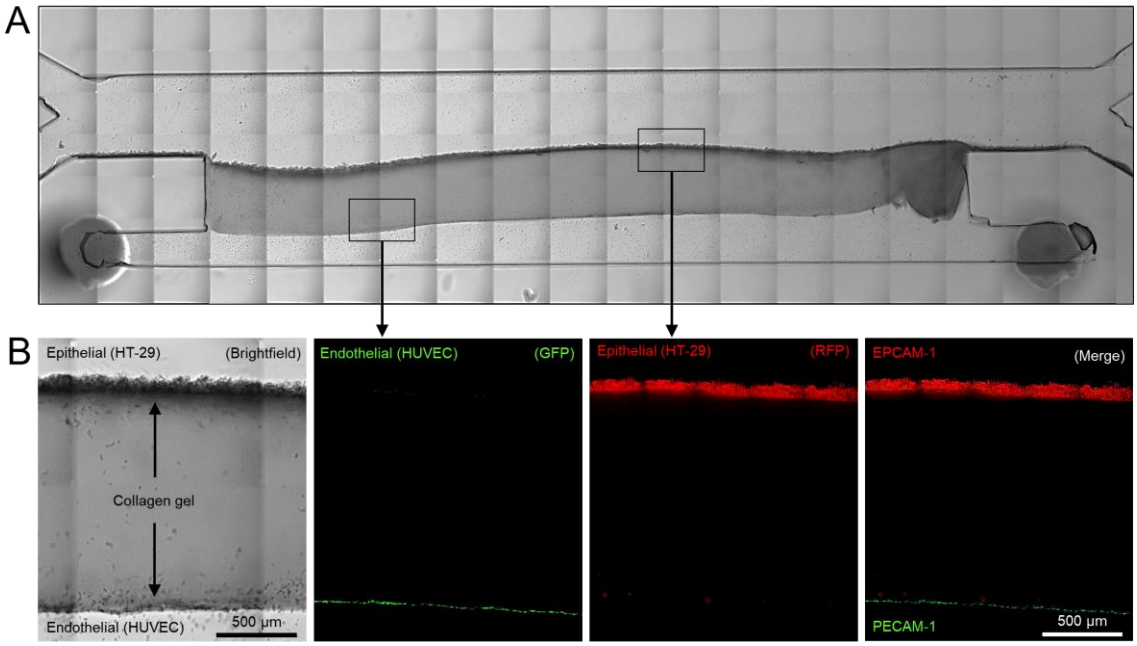

Figure 5.12 Demonstrating epithelial and endothelial layer formation in a single microfluidic device. (A) Brightfield microscope image showing the collagen gel separating the epithelial (Top) and the endothelial (Bottom) channels. (B) High magnification images showing the formation of uniform epithelial (HT-29) and endothelial (HUVEC) cell layers after three days of culture. Immunostaining of the fixed cells show that epithelial cells expressed EPCAM-1 (Red) and the endothelial cells expressed PECAM-1 (Green) indicating the formation of cellular junctions.

5.5 Incorporation of primary gut organoids and immune cells for 'Personalized Medicine' applications

Primary stem cell-derived organoids contain all the different types of cells present in the epithelial cell layer in vivo including absorptive enterocytes, mucus secreting goblet cells, Paneth cells, enteroendocrine cells, and microfold cells. Presence of these cell types enable testing of specific hypotheses in vitro depending on the specialized function of the respective cell type. The discovery of stem cell marker Lgr5 and commercial technology development in the recent times have simplified the extraction of stem cells from freshly excised tissues and the growth of these stem cells into three-dimensional (3D) organoids (Figure 5.13A). These organoids are grown embedded in the extracellular matrix (ECM) like Matrigel and form an enclosed structure with the lumen on the inside of the 3D structure that is difficult to access for stimulation (Figure 5.13B). However, these organoids can be dissociated to into single cells and re-seeded in commonly used platforms including transwells, ECM derived scaffolds, and microfluidic platforms. This way in vivo like epithelial monolayers can be formed that are accessible on both apical and basolateral sides for drug discovery, studying transport or molecular secretion from the cells after stimulation. To develop personalized models, the methods for recreating the mucosal barrier presented in the thesis using immortal cell line for epithelial barrier can be easily replaced with the primary epithelial cells derived from stem cell organoids (Figure 5.13B). Additionally, the immortalized cell lines can be replaced by peripheral blood derived mononuclear cells (PBMCs). PBMCs constitute a diverse population of the immune cells that represent the effector cells during an immune response to immunomodulatory molecules or infectious agents like bacteria, viruses, fungi, and parasites present in the

lumen of the intestines. By donor matching the epithelial and immune cells in the in vitro platforms described in this thesis can serve as personalized models for real time testing of the efficacy and safety of probiotic bacteria and the fecal microbiota transplant (FMT) in the treatment of gastro-intestinal disorders.

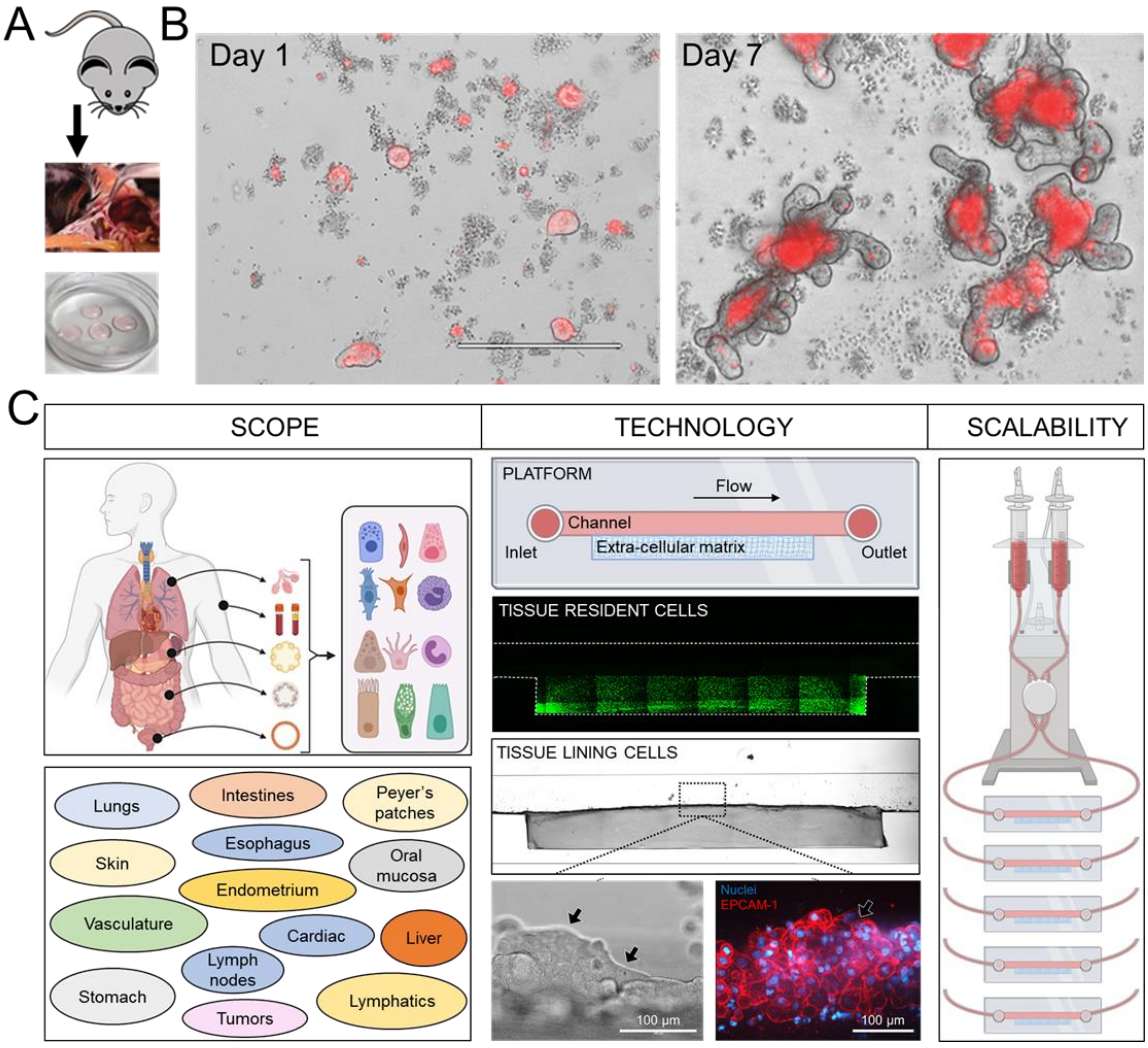

Figure 5.13 Intestinal stem cell isolation and growth into 3D organoids. (A) Small intestines excised from transgenic mice expressing red fluorescent protein variant (DsRed-Express) under the direction of the mouse doublecortin (Dcx) promoter using a commercial isolation kit and protocol (Stemcell Technologies Inc.). Cells are embedded in a dome of Matrigel matrix. (B) 3D buds start to originate from individual stem cells after 1 day of culture. After 7 days of culture crypt and villous structure form with a lumen at the center of the organoids that contain dead cell debris. (C) Schematic of a 'single translational platform' for personalized models of human organs on a microfluidic chip.

5.6 Overall conclusion

In the first part of the thesis, a high throughput method to extract natural mucus was developed that will stimulate broad aspects of mucus barrier research. Using mucus extracted with this process, we have shown that the local ionic environment plays an important role in regulating the biophysical properties of the mucus barrier. Integration of the extracted mucus with an epithelial cell layer lead to the development of the mucosal barrier model of the intestines in vitro. Using the mucosal barrier model, we demonstrated the role of flagellar motility in promoting bacterial infection and inducing pro-inflammatory cytokine and chemokine production from epithelial and immune cells. Mucosal barrier model was further used to elucidate that depending on the dosage, probiotics can be beneficial against pathogenic infection, but insufficient dosage and presence of mucus induce hypervirulence in *S. typhimurium* and higher inflammatory response. Finally, advanced applications of the mucus biomaterial in developing translational platforms ranging from therapeutic delivery to micro-physiological models using microfluidics have been described. The techniques presented here will help uncover the mechanisms behind the effects of environmental molecules on biophysical properties of mucus. The in vitro mucus barrier model is functional and can be tuned to match physiological thicknesses and densities like native mucus. We envision that these models will serve as high throughput tools for understanding the role of mucus barrier in nutrient absorption, host-microbiome interactions, and drug absorption. A better understanding of mucosal barriers and their interaction with the local environment has potential to improve treatment of intestinal diseases and other mucosal barrier organs.

ADDITIONAL FIGURES

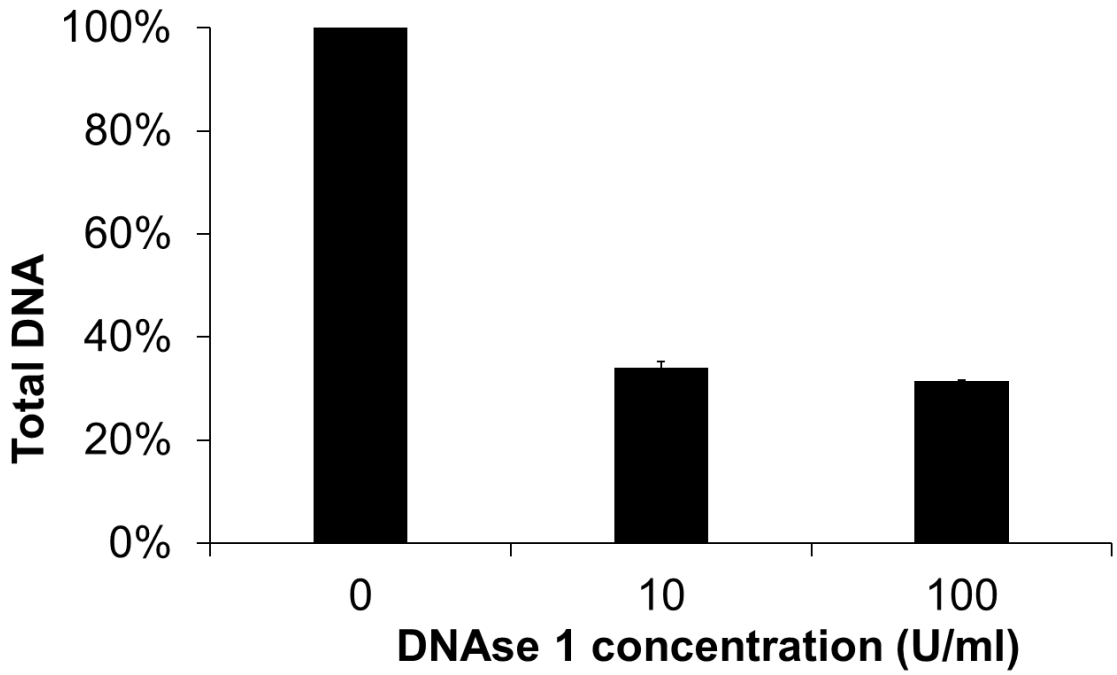

Figure 2.S1. Quantification and removal of total DNA post PSIM extraction. Change in total DNA after DNAse treatment of PSIM at room temperature for 10 hours compared to the untreated PSIM.

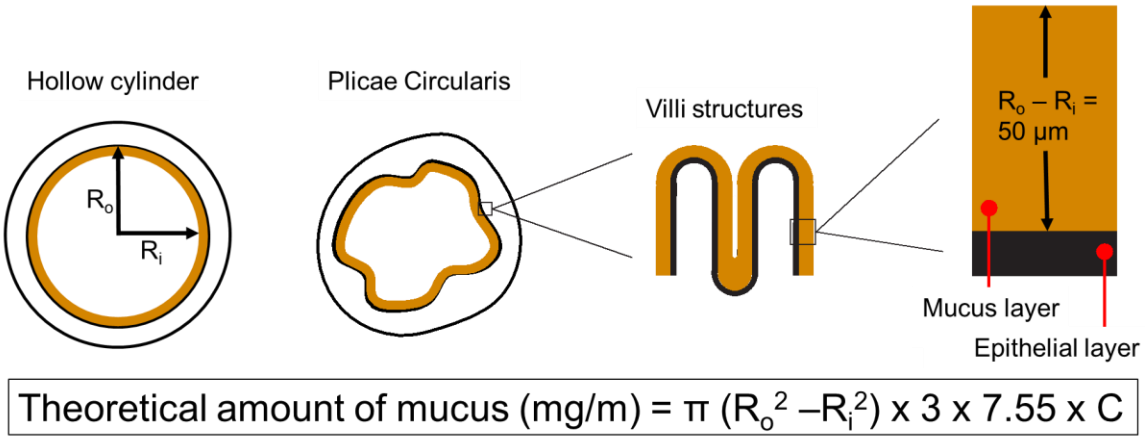

Figure 2.S2. Theoretical quantification of total mucus on the luminal surface of the pig intestines. Schematic representation of gross small intestinal (SI) morphology and microstructure showing the components that contribute to increase in the surface area of the small intestine. In the equation for mucus amount, π (R_o^2 –R_i^2) is the cross-sectional surface area of a hollow cylinder, and plicae circularis and villi structures increased the cross-sectional area by factors of 3 and 7.55, respectively. The theoretical amount of mucus per meter length was based on an outer radius (R_o) of 12.5 mm, an inner radius (R_i) of 12.45 mm, and pig small intestinal mucus concentration of 20 mg/ml.

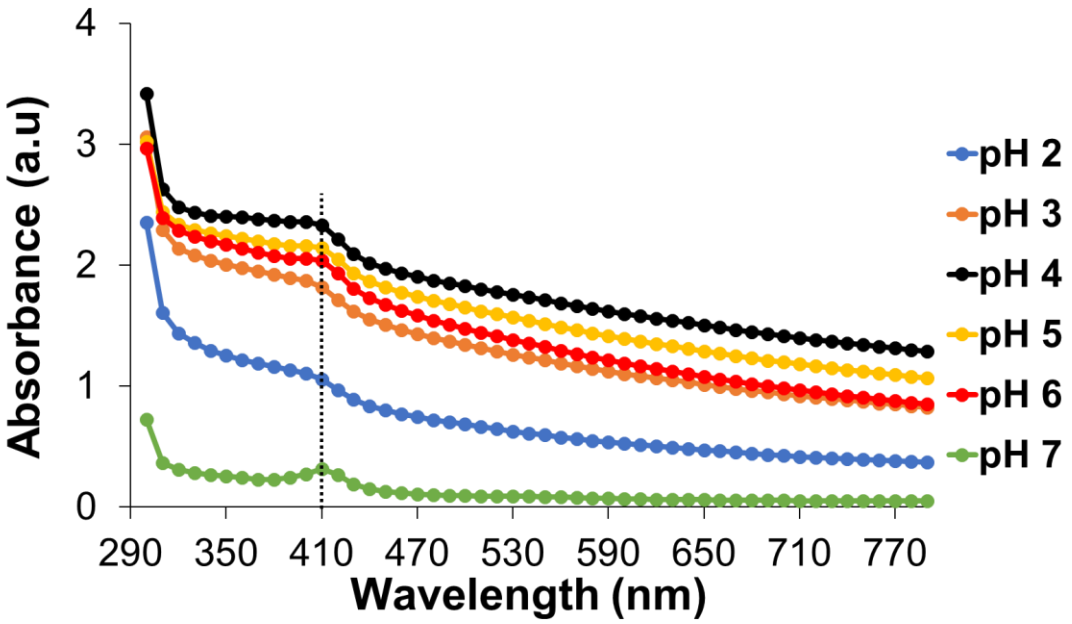

Figure 2.S3. Absorbance spectra of 2 % (w/v) PSIM in the pH range 2-7. Data was plotted as an average of three independent intestine samples from different pigs.

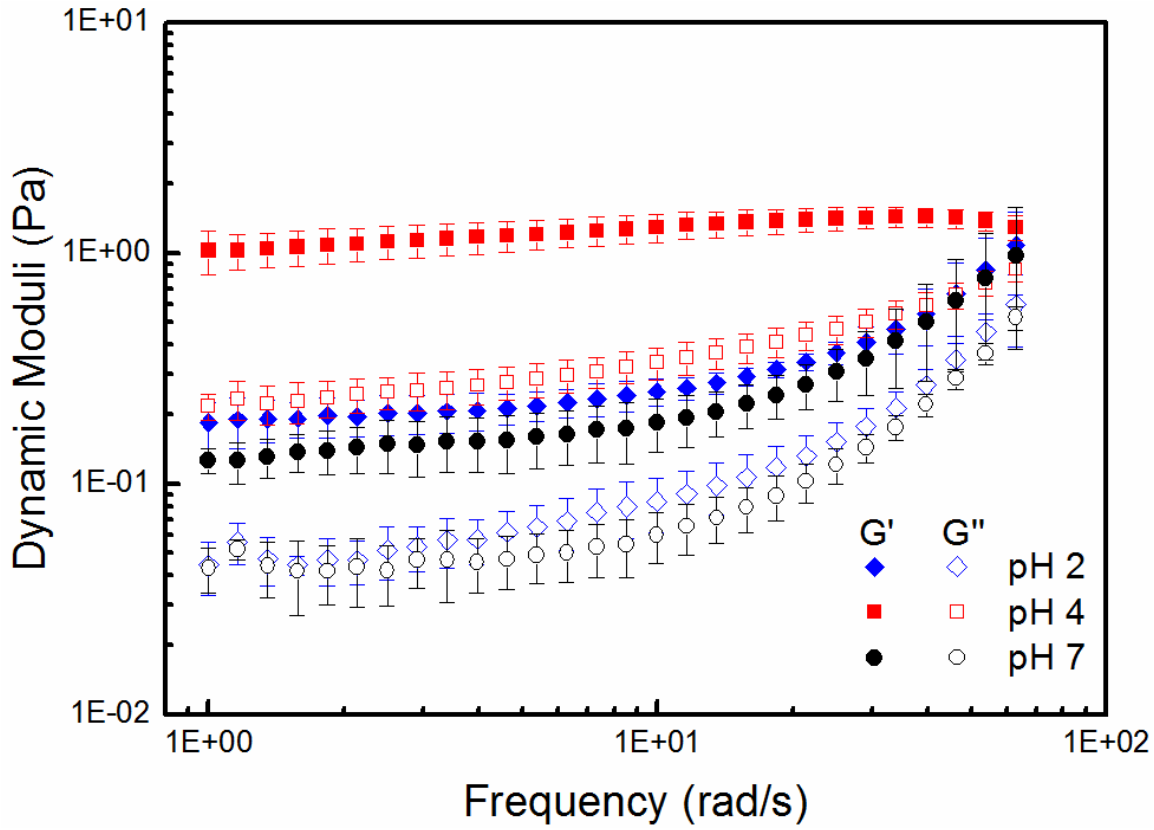

Figure 2.S4. Rheological data for the change in dynamic moduli (G′ and G″) of PSIM (2% w/v). The measurements were performed in the frequency range 1-68.3rad/s at 37°C (N = 3 PSI).

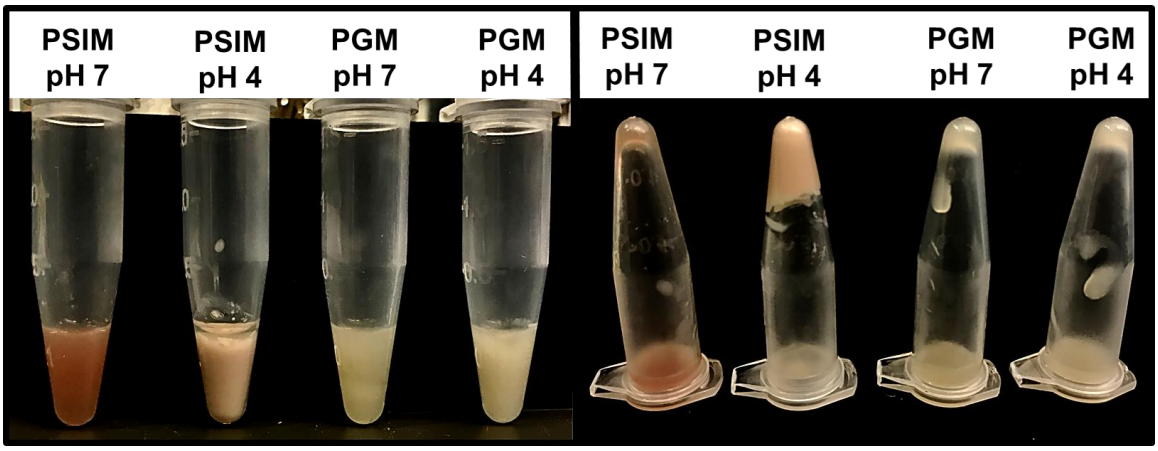

Figure 2.S5. Gross image of PSIM compared to Porcine gastric mucin (Type II, Sigma Aldrich). The freeze-dried samples were solubilized in 20mM HEPES solution at a concentration of 8% (w/v), and at values of 7 and 4 respectively.

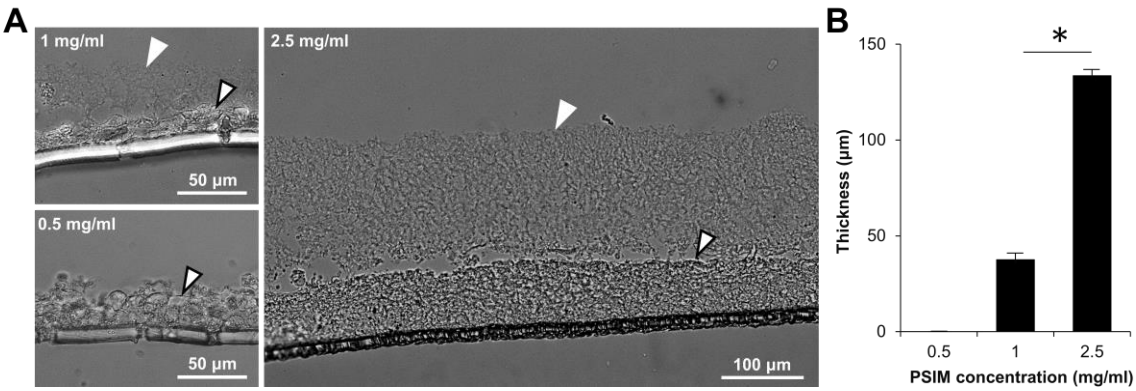

Figure 3.S1. Mucus layer thickness is concentration dependent. (A) Brightfield micrographs of histological sections with epithelial layer (black border arrows) and mucus layer (white arrows). (B) Mucus layer thickness increased with PSIM concentration.

BIBLIOGRAPHY

1. Allen, A.; Bell, A.; Mantle, M.; Pearson, J. P., The Structure and Physiology of Gastrointestinal Mucus. In *Mucus in Health and Disease—II*, Chantler, E. N.; Elder, J. B.; Elstein, M., Eds. Springer US: Boston, MA, 1982; pp 115-133.

2. Cone, R. A., Barrier properties of mucus. *Adv Drug Deliv Rev* **2009,** *61* (2), 75-85.

3. Johansson, M. E.; Sjovall, H.; Hansson, G. C., The gastrointestinal mucus system in health and disease. *Nat Rev Gastroenterol Hepatol* **2013,** *10* (6), 352-61.

4. Donaldson, G. P.; Lee, S. M.; Mazmanian, S. K., Gut biogeography of the bacterial microbiota. *Nature reviews. Microbiology* **2016,** *14* (1), 20-32.

5. Vighi, G.; Marcucci, F.; Sensi, L.; Di Cara, G.; Frati, F., Allergy and the gastrointestinal system. *Clinical and experimental immunology* **2008,** *153 Suppl 1* (Suppl 1), 3-6.

6. Round, J. L.; Mazmanian, S. K., The gut microbiota shapes intestinal immune responses during health and disease. *Nature reviews. Immunology* **2009,** *9* (5), 313-323.

7. Tano De La Hoz, M. F.; Flamini, M. A.; Diaz, A. O., Comparative Analysis of the Morphology, Ultrastructure, and Glycosylation Pattern of the Jejunum and Ileum of the Wild Rodent Lagostomus maximus. *Anat Rec (Hoboken)* **2016,** *299* (5), 630-42.

8. Carr, K. E.; Toner, P. G., Morphology of the Intestinal Mucosa. In *Pharmacology of Intestinal Permeation I*, Csáky, T. Z., Ed. Springer Berlin Heidelberg: Berlin, Heidelberg, 1984; pp 1-50.

9. Lacy, E. R., Functional Morphology of the Large Intestine. In *Comprehensive Physiology*, John Wiley & Sons, Inc.: 2010.

10. Nguyen, T. L. A.; Vieira-Silva, S.; Liston, A.; Raes, J., How informative is the mouse for human gut microbiota research? *Disease models & mechanisms* **2015,** *8* (1), 1-16.

11. Kim, H. J.; Ingber, D. E., Gut-on-a-Chip microenvironment induces human intestinal cells to undergo villus differentiation. *Integr Biol-Uk* **2013,** *5* (9), 1130-1140.

12. Chen, Y.; Lin, Y.; Davis, K. M.; Wang, Q.; Rnjak-Kovacina, J.; Li, C.; Isberg, R. R.; Kumamoto, C. A.; Mecsas, J.; Kaplan, D. L., Robust bioengineered 3D functional human intestinal epithelium. *Sci Rep* **2015,** *5*, 13708.

13. Wang, Y.; Gunasekara, D. B.; Reed, M. I.; DiSalvo, M.; Bultman, S. J.; Sims, C. E.; Magness, S. T.; Allbritton, N. L., A microengineered collagen scaffold for generating

a polarized crypt-villus architecture of human small intestinal epithelium. *Biomaterials* **2017,** *128* (Supplement C), 44-55.

14. Kim, H. J.; Huh, D.; Hamilton, G.; Ingber, D. E., Human gut-on-a-chip inhabited by microbial flora that experiences intestinal peristalsis-like motions and flow. *Lab Chip* **2012,** *12* (12), 2165-2174.

15. Kim, H. J.; Li, H.; Collins, J. J.; Ingber, D. E., Contributions of microbiome and mechanical deformation to intestinal bacterial overgrowth and inflammation in a human gut-on-a-chip. *P Natl Acad Sci USA* **2016,** *113* (1), E7-E15.

16. Marzorati, M.; Vanhoecke, B.; De Ryck, T.; Sadaghian Sadabad, M.; Pinheiro, I.; Possemiers, S.; Van den Abbeele, P.; Derycke, L.; Bracke, M.; Pieters, J.; Hennebel, T.; Harmsen, H. J.; Verstraete, W.; Van de Wiele, T., The HMI module: a new tool to study the Host-Microbiota Interaction in the human gastrointestinal tract in vitro. *BMC microbiology* **2014,** *14*, 133.

17. Shah, P.; Fritz, J. V.; Glaab, E.; Desai, M. S.; Greenhalgh, K.; Frachet, A.; Niegowska, M.; Estes, M.; Jäger, C.; Seguin-Devaux, C.; Zenhausern, F.; Wilmes, P., A microfluidics-based in vitro model of the gastrointestinal human–microbe interface. *Nature Communications* **2016,** *7*, 11535.

18. Fogh, J.; Fogh, J. M.; Orfeo, T., One hundred and twenty-seven cultured human tumor cell lines producing tumors in nude mice. *Journal of the National Cancer Institute* **1977,** *59* (1), 221-6.

19. Pinto, M.; Robine, S.; Appay, M. D., *Enterocyte-like differentiation and polarization of the human colon carcinoma cell line CACO-2 in culture*. 1983; Vol. 47, p 323-330.

20. Zweibaum, A.; Pinto, M.; Chevalier, G.; Dussaulx, E.; Triadou, N.; Lacroix, B.; Haffen, K.; Brun, J. L.; Rousset, M., Enterocytic differentiation of a subpopulation of the human colon tumor cell line HT-29 selected for growth in sugar-free medium and its inhibition by glucose. *Journal of cellular physiology* **1985,** *122* (1), 21-9.

21. Lesuffleur, T.; Barbat, A.; Luccioni, C.; Beaumatin, J.; Clair, M.; Kornowski, A.; Dussaulx, E.; Dutrillaux, B.; Zweibaum, A., Dihydrofolate reductase gene amplification-associated shift of differentiation in methotrexate-adapted HT-29 cells. *The Journal of Cell Biology* **1991,** *115* (5), 1409-1418.

22. Lesuffleur, T.; Porchet, N.; Aubert, J. P.; Swallow, D.; Gum, J. R.; Kim, Y. S.; Real, F. X.; Zweibaum, A., Differential expression of the human mucin genes MUC1 to MUC5 in relation to growth and differentiation of different mucus-secreting HT-29 cell subpopulations. *Journal of cell science* **1993,** *106 (Pt 3)*, 771-83.

23. Hilgendorf, C.; Spahn-Langguth, H.; Regardh, C. G.; Lipka, E.; Amidon, G. L.; Langguth, P., Caco-2 versus Caco-2/HT29-MTX co-cultured cell lines: permeabilities via diffusion, inside- and outside-directed carrier-mediated transport. *J Pharm Sci* **2000,** *89* (1), 63-75.

24. Kleinman, H. K.; Luckenbill-Edds, L.; Cannon, F. W.; Sephel, G. C., Use of extracellular matrix components for cell culture. *Analytical biochemistry* **1987,** *166* (1), 1-13.

25. Walter, E.; Janich, S.; Roessler, B. J.; Hilfinger, J. M.; Amidon, G. L., HT29-MTX/Caco-2 Cocultures as an in Vitro Model for the Intestinal Epithelium: In Vitro–in Vivo Correlation with Permeability Data from Rats and Humans. *Journal of Pharmaceutical Sciences* **1996,** *85* (10), 1070-1076.

26. Artursson, P., Epithelial transport of drugs in cell culture. I: A model for studying the passive diffusion of drugs over intestinal absorptive (Caco-2) cells. *J Pharm Sci* **1990,** *79* (6), 476-82.

27. Gullberg, E.; Leonard, M.; Karlsson, J.; Hopkins, A. M.; Brayden, D.; Baird, A. W.; Artursson, P., Expression of Specific Markers and Particle Transport in a New Human Intestinal M-Cell Model. *Biochemical and Biophysical Research Communications* **2000,** *279* (3), 808-813.

28. des Rieux, A.; Fievez, V.; Theate, I.; Mast, J.; Preat, V.; Schneider, Y. J., An improved in vitro model of human intestinal follicle-associated epithelium to study nanoparticle transport by M cells. *European journal of pharmaceutical sciences : official journal of the European Federation for Pharmaceutical Sciences* **2007,** *30* (5), 380-91.

29. Antunes, F.; Andrade, F.; Araujo, F.; Ferreira, D.; Sarmento, B., Establishment of a triple co-culture in vitro cell models to study intestinal absorption of peptide drugs. *Eur J Pharm Biopharm* **2013,** *83* (3), 427-35.

30. Larhed, A. W.; Artursson, P.; Gråsjö, J.; Björk, E., Diffusion of Drugs in Native and Purified Gastrointestinal Mucus. *Journal of Pharmaceutical Sciences* **1997,** *86* (6), 660-665.

31. Yu, J.; Carrier, R. L.; March, J. C.; Griffith, L. G., Three dimensional human small intestine models for ADME-Tox studies. *Drug Discov Today* **2014,** *19* (10), 1587-94.

32. Boegh, M.; Foged, C.; Müllertz, A.; Mørck Nielsen, H., Mucosal drug delivery: barriers, in vitro models and formulation strategies. *Journal of Drug Delivery Science and Technology* **2013,** *23* (4), 383-391.

33. Kočevar-Nared, J.; Kristl, J.; Šmid-Korbar, J., Comparative rheological investigation of crude gastric mucin and natural gastric mucus. *Biomaterials* **1997,** *18* (9), 677-681.

34. Boegh, M.; Baldursdottir, S. G.; Mullertz, A.; Nielsen, H. M., Property profiling of biosimilar mucus in a novel mucus-containing in vitro model for assessment of intestinal drug absorption. *Eur J Pharm Biopharm* **2014,** *87* (2), 227-35.

35. Boegh, M.; Garcia-Diaz, M.; Mullertz, A.; Nielsen, H. M., Steric and interactive barrier properties of intestinal mucus elucidated by particle diffusion and peptide permeation. *Eur J Pharm Biopharm* **2015,** *95* (Pt A), 136-43.

36. Duval, K.; Grover, H.; Han, L.-H.; Mou, Y.; Pegoraro, A. F.; Fredberg, J.; Chen, Z., Modeling Physiological Events in 2D vs. 3D Cell Culture. *Physiology (Bethesda, Md.)* **2017,** *32* (4), 266-277.

37. Sung, J. H.; Yu, J.; Luo, D.; Shuler, M. L.; March, J. C., Microscale 3-D hydrogel scaffold for biomimetic gastrointestinal (GI) tract model. *Lab Chip* **2011,** *11* (3), 389-92.

38. Esch, M. B.; Sung, J. H.; Yang, J.; Yu, C.; Yu, J.; March, J. C.; Shuler, M. L., On chip porous polymer membranes for integration of gastrointestinal tract epithelium with microfluidic 'body-on-a-chip' devices. *Biomedical microdevices* **2012,** *14* (5), 895-906.

39. Costello, C. M.; Jia, H. P.; Shaffiey, S.; Yu, J. J.; Jain, N. K.; Hackam, D.; March, J. C., Synthetic Small Intestinal Scaffolds for Improved Studies of Intestinal Differentiation. *Biotechnol Bioeng* **2014,** *111* (6), 1222-1232.

40. Costello, C. M.; Sorna, R. M.; Goh, Y. L.; Cengic, I.; Jain, N. K.; March, J. C., 3-D Intestinal Scaffolds for Evaluating the Therapeutic Potential of Probiotics. *Mol Pharmaceut* **2014,** *11* (7), 2030-2039.

41. DeCicco RePass, M. A.; Chen, Y.; Lin, Y.; Zhou, W.; Kaplan, D. L.; Ward, H. D., Novel Bioengineered Three-Dimensional Human Intestinal Model for Long-Term Infection of Cryptosporidium parvum. *Infection and Immunity* **2017,** *85* (3).

42. Shaban, L.; Chen, Y.; Fasciano, A. C.; Lin, Y.; Kaplan, D. L.; Kumamoto, C. A.; Mecsas, J., A 3D intestinal tissue model supports Clostridioides difficile germination, colonization, toxin production and epithelial damage. *Anaerobe* **2018,** *50*, 85-92.

43. Kasendra, M.; Tovaglieri, A.; Sontheimer-Phelps, A.; Jalili-Firoozinezhad, S.; Bein, A.; Chalkiadaki, A.; Scholl, W.; Zhang, C.; Rickner, H.; Richmond, C. A.; Li, H.; Breault, D. T.; Ingber, D. E., Development of a primary human Small Intestine-on-a-Chip using biopsy-derived organoids. *Scientific Reports* **2018,** *8* (1), 2871.

44. Workman, M. J.; Gleeson, J. P.; Troisi, E. J.; Estrada, H. Q.; Kerns, S. J.; Hinojosa, C. D.; Hamilton, G. A.; Targan, S. R.; Svendsen, C. N.; Barrett, R. J., Enhanced Utilization of Induced Pluripotent Stem Cell–Derived Human Intestinal Organoids Using Microengineered Chips. *Cellular and Molecular Gastroenterology and Hepatology* **2018,** *5* (4), 669-677.e2.

45. Turner, J. R., Intestinal mucosal barrier function in health and disease. *Nat Rev Immunol* **2009,** *9* (11), 799-809.

46. Lieleg, O.; Ribbeck, K., Biological hydrogels as selective diffusion barriers. *Trends Cell Biol* **2011,** *21* (9), 543-51.

47. Alipour, M.; Zaidi, D.; Valcheva, R.; Jovel, J.; Martinez, I.; Sergi, C.; Walter, J.; Mason, A. L.; Wong, G. K.; Dieleman, L. A.; Carroll, M. W.; Huynh, H. Q.; Wine, E., Mucosal Barrier Depletion and Loss of Bacterial Diversity are Primary Abnormalities in Paediatric Ulcerative Colitis. *J Crohns Colitis* **2016,** *10* (4), 462-71.

48. Ijssennagger, N.; van der Meer, R.; van Mil, S. W., Sulfide as a Mucus Barrier-Breaker in Inflammatory Bowel Disease? *Trends Mol Med* **2016,** *22* (3), 190-9.

49. Swidsinski, A.; Weber, J.; Loening-Baucke, V.; Hale, L. P.; Lochs, H., Spatial Organization and Composition of the Mucosal Flora in Patients with Inflammatory Bowel Disease. *Journal of Clinical Microbiology* **2005,** *43* (7), 3380-3389.

50. Ehre, C.; Ridley, C.; Thornton, D. J., Cystic fibrosis: An inherited disease affecting mucin-producing organs. *The International Journal of Biochemistry & Cell Biology* **2014,** *52* (Supplement C), 136-145.

51. Krishn, S. R.; Kaur, S.; Smith, L. M.; Johansson, S. L.; Jain, M.; Patel, A.; Gautam, S. K.; Hollingsworth, M. A.; Mandel, U.; Clausen, H.; Lo, W. C.; Fan, W. T.; Manne, U.; Batra, S. K., Mucins and associated glycan signatures in colon adenoma-carcinoma sequence: Prospective pathological implication(s) for early diagnosis of colon cancer. *Cancer Lett* **2016,** *374* (2), 304-14.

52. Velcich, A.; Yang, W.; Heyer, J.; Fragale, A.; Nicholas, C.; Viani, S.; Kucherlapati, R.; Lipkin, M.; Yang, K.; Augenlicht, L., Colorectal Cancer in Mice Genetically Deficient in the Mucin Muc2. *Science* **2002,** *295* (5560), 1726-1729.

53. Bansil, R.; Celli, J. P.; Hardcastle, J. M.; Turner, B. S., The Influence of Mucus Microstructure and Rheology in Helicobacter pylori Infection. *Front Immunol* **2013,** *4*, 310.

54. Kleessen, B.; Kroesen, A. J.; Buhr, H. J.; Blaut, M., Mucosal and Invading Bacteria in Patients with Inflammatory Bowel Disease Compared with Controls. *Scandinavian Journal of Gastroenterology* **2002,** *37* (9), 1034-1041.

55. Ambort, D.; Johansson, M. E.; Gustafsson, J. K.; Nilsson, H. E.; Ermund, A.; Johansson, B. R.; Koeck, P. J.; Hebert, H.; Hansson, G. C., Calcium and pH-dependent packing and release of the gel-forming MUC2 mucin. *Proc Natl Acad Sci U S A* **2012,** *109* (15), 5645-50.

56. Tytgat, K. M.; Buller, H. A.; Opdam, F. J.; Kim, Y. S.; Einerhand, A. W.; Dekker, J., Biosynthesis of human colonic mucin: Muc2 is the prominent secretory mucin. *Gastroenterology* **1994,** *107* (5), 1352-63.

57. Dekker, J.; Rossen, J. W. A.; Büller, H. A.; Einerhand, A. W. C., The MUC family: an obituary. *Trends in Biochemical Sciences* **2002,** *27* (3), 126-131.

58. Atuma, C.; Strugala, V.; Allen, A.; Holm, L., The adherent gastrointestinal mucus gel layer: thickness and physical state in vivo. *American Journal of Physiology - Gastrointestinal and Liver Physiology* **2001,** *280* (5), G922-G929.

59. Vaishnava, S.; Yamamoto, M.; Severson, K. M.; Ruhn, K. A.; Yu, X.; Koren, O.; Ley, R.; Wakeland, E. K.; Hooper, L. V., The antibacterial lectin RegIIIγ promotes the spatial segregation of microbiota and host in the intestine. *Science (New York, N.Y.)* **2011,** *334* (6053), 255-258.

60. Cornick, S.; Tawiah, A.; Chadee, K., Roles and regulation of the mucus barrier in the gut. *Tissue Barriers* **2015,** *3* (1-2), e982426.

61. Tlaskalova-Hogenova, H.; Stepankova, R.; Kozakova, H.; Hudcovic, T.; Vannucci, L.; Tuckova, L.; Rossmann, P.; Hrncir, T.; Kverka, M.; Zakostelska, Z.; Klimesova, K.; Pribylova, J.; Bartova, J.; Sanchez, D.; Fundova, P.; Borovska, D.; Srutkova, D.; Zidek, Z.; Schwarzer, M.; Drastich, P.; Funda, D. P., The role of gut microbiota (commensal bacteria) and the mucosal barrier in the pathogenesis of inflammatory and autoimmune diseases and cancer: contribution of germ-free and gnotobiotic animal models of human diseases. *Cell Mol Immunol* **2011,** *8* (2), 110-20.

62. Faderl, M.; Noti, M.; Corazza, N.; Mueller, C., Keeping bugs in check: The mucus layer as a critical component in maintaining intestinal homeostasis. *IUBMB Life* **2015,** *67* (4), 275-85.

63. Johansson, M. E.; Phillipson, M.; Petersson, J.; Velcich, A.; Holm, L.; Hansson, G. C., The inner of the two Muc2 mucin-dependent mucus layers in colon is devoid of bacteria. *Proc Natl Acad Sci U S A* **2008,** *105* (39), 15064-9.

64. Birchenough, G. M.; Nystrom, E. E.; Johansson, M. E.; Hansson, G. C., A sentinel goblet cell guards the colonic crypt by triggering Nlrp6-dependent Muc2 secretion. *Science* **2016,** *352* (6293), 1535-42.

65. Kamphuis, J. B. J.; Mercier-Bonin, M.; Eutamène, H.; Theodorou, V., Mucus organisation is shaped by colonic content; a new view. *Scientific Reports* **2017,** *7* (1), 8527.

66. Celli, J. P.; Turner, B. S.; Afdhal, N. H.; Ewoldt, R. H.; McKinley, G. H.; Bansil, R.; Erramilli, S., Rheology of Gastric Mucin Exhibits a pH-Dependent Sol−Gel Transition. *Biomacromolecules* **2007,** *8* (5), 1580-1586.

67. Lafitte, G.; Söderman, O.; Thuresson, K.; Davies, J., PFG-NMR diffusometry: A tool for investigating the structure and dynamics of noncommercial purified pig gastric mucin in a wide range of concentrations. *Biopolymers* **2007,** *86* (2), 165-175.

68. Bansil, R.; Turner, B. S., Mucin structure, aggregation, physiological functions and biomedical applications. *Current Opinion in Colloid & Interface Science* **2006,** *11* (2-3), 164-170.

69. Barz, B.; Turner, B. S.; Bansil, R.; Urbanc, B., Folding of pig gastric mucin non-glycosylated domains: a discrete molecular dynamics study. *J Biol Phys* **2012,** *38* (4), 681-703.

70. Cao, X.; Bansil, R.; Bhaskar, K. R.; Turner, B. S.; LaMont, J. T.; Niu, N.; Afdhal, N. H., pH-dependent conformational change of gastric mucin leads to sol-gel transition. *Biophysical Journal* **1999,** *76* (3), 1250-1258.

71. Sellers, L. A.; Allen, A.; Morris, E. R.; Ross-Murphy, S. B., The rheology of pig small intestinal and colonic mucus: weakening of gel structure by non-mucin components. *Biochimica et Biophysica Acta (BBA) - General Subjects* **1991,** *1115* (2), 174-179.

72. Yang, N.; Garcia, M. A.; Quinton, P. M., Normal mucus formation requires cAMP-dependent HCO3- secretion and Ca2+-mediated mucin exocytosis. *J Physiol* **2013,** *591* (18), 4581-93.

73. Raynal, B. D.; Hardingham, T. E.; Sheehan, J. K.; Thornton, D. J., Calcium-dependent protein interactions in MUC5B provide reversible cross-links in salivary mucus. *J Biol Chem* **2003,** *278* (31), 28703-10.

74. Verdugo, P.; Aitken, M.; Langley, L.; Villalon, M. J., Molecular mechanism of product storage and release in mucin secretion. II. The role of extracellular Ca++. *Biorheology* **1987,** *24* (6), 625-33.

75. Fallingborg, J., Intraluminal pH of the human gastrointestinal tract. *Danish medical bulletin* **1999,** *46* (3), 183-96.

76. Yildiz, H. M.; Speciner, L.; Ozdemir, C.; Cohen, D. E.; Carrier, R. L., Food-associated stimuli enhance barrier properties of gastrointestinal mucus. *Biomaterials* **2015,** *54*, 1-8.

77. Fordtran, J. S.; Locklear, T. W., Ionic constituents and osmolality of gastric and small-intestinal fluids after eating. *The American journal of digestive diseases* **1966,** *11* (7), 503-21.

78. Di Maio, S.; Carrier, R. L., Gastrointestinal contents in fasted state and post-lipid ingestion: In vivo measurements and in vitro models for studying oral drug delivery. *Journal of Controlled Release* **2011,** *151* (2), 110-122.

79. Starkey, B. J.; Snary, D.; Allen, A., Characterization of gastric mucoproteins isolated by equilibrium density-gradient centrifugation in caesium chloride. *The Biochemical journal* **1974,** *141* (3), 633-9.

80. Bell, A. E.; Sellers, L. A.; Allen, A.; Cunliffe, W. J.; Morris, E. R.; Ross-Murphy, S. B., Properties of Gastric and Duodenal Mucus: Effect of Proteolysis, Disulfide Reduction, Bile, Acid, Ethanol, and Hypertonicity on Mucus Gel Structure. *Gastroenterology* **1985,** *88* (1), 269-280.

81. Bhaskar, K. R.; Gong, D. H.; Bansil, R.; Pajevic, S.; Hamilton, J. A.; Turner, B. S.; LaMont, J. T., Profound increase in viscosity and aggregation of pig gastric mucin at low pH. *The American journal of physiology* **1991,** *261* (5 Pt 1), G827-32.

82. Li, L.; Lieleg, O.; Jang, S.; Ribbeck, K.; Han, J., A microfluidic in vitro system for the quantitative study of the stomach mucus barrier function. *Lab Chip* **2012,** *12* (20), 4071-9.

83. Li, L. D.; Crouzier, T.; Sarkar, A.; Dunphy, L.; Han, J.; Ribbeck, K., Spatial configuration and composition of charge modulates transport into a mucin hydrogel barrier. *Biophys J* **2013,** *105* (6), 1357-65.

84. Ho, S. B.; Takamura, K.; Anway, R.; Shekels, L. L.; Toribara, N. W.; Ota, H., The Adherent Gastric Mucous Layer Is Composed of Alternating Layers of MUC5AC and MUC6 Mucin Proteins. *Digestive Diseases and Sciences* **2004,** *49* (10), 1598-1606.

85. Veronika J. Schömiga, B. T. K., Christoph Scholza, Konstantinia Bidmonb, Oliver Lielegb and Sonja Berensmeier, An optimized purification process for porcine gastric mucin with preservation of its native functional properties. *RSC Advances* **2016,** *6*, 44932.

86. Lai, S. K.; O'Hanlon, D. E.; Harrold, S.; Man, S. T.; Wang, Y.-Y.; Cone, R.; Hanes, J., Rapid transport of large polymeric nanoparticles in fresh undiluted human mucus. *Proceedings of the National Academy of Sciences* **2007,** *104* (5), 1482-1487.

87. Marshall, T.; Allen, A., The isolation and characterization of the high-molecular-weight glycoprotein from pig colonic mucus. *The Biochemical journal* **1978,** *173* (2), 569-78.

88. Mantle, M.; Allen, A., Isolation and characterization of the native glycoprotein from pig small-intestinal mucus. *The Biochemical journal* **1981,** *195* (1), 267-75.

89. Sellers, L. A.; Allen, A.; Morris, E. R.; Ross-Murphy, S. B., The rheology of pig small intestinal and colonic mucus: weakening of gel structure by non-mucin components. *Biochimica et biophysica acta* **1991,** *1115* (2), 174-9.

90. Davies, J. R.; Wickstrom, C.; Thornton, D. J., Gel-forming and cell-associated mucins: preparation for structural and functional studies. *Methods Mol Biol* **2012,** *842*, 27-47.

91. Georgiades, P.; Pudney, P. D. A.; Thornton, D. J.; Waigh, T. A., Particle tracking microrheology of purified gastrointestinal mucins. *Biopolymers* **2014,** *101* (4), 366-377.

92. Georgiades, P.; di Cola, E.; Heenan, R. K.; Pudney, P. D.; Thornton, D. J.; Waigh, T. A., A combined small-angle X-ray and neutron scattering study of the structure of purified soluble gastrointestinal mucins. *Biopolymers* **2014,** *101* (12), 1154-64.

93. Schömig, V. J.; Käsdorf, B. T.; Scholz, C.; Bidmon, K.; Lieleg, O.; Berensmeier, S., An optimized purification process for porcine gastric mucin with preservation of its native functional properties. *RSC Advances* **2016,** *6* (50), 44932-44943.

94. Schoemig, V.; Isik, E.; Martin, L.; Berensmeier, S., Solid liquid liquid extraction of porcine gastric mucins from homogenized animal material. *RSC Advances* **2017,** *7* (63), 39708-39717.

95. Helander, H. F.; Fändriks, L., Surface area of the digestive tract – revisited. *Scandinavian Journal of Gastroenterology* **2014,** *49* (6), 681-689.

96. Varum, F. J.; Veiga, F.; Sousa, J. S.; Basit, A. W., Mucus thickness in the gastrointestinal tract of laboratory animals. *J Pharm Pharmacol* **2012,** *64* (2), 218-27.

97. Turner, J. R., Intestinal mucosal barrier function in health and disease. *Nat Rev Immunol* **2009,** *9* (11), 799-809.

98. McGuckin, M. A.; Eri, R.; Simms, L. A.; Florin, T. H.; Radford-Smith, G., Intestinal barrier dysfunction in inflammatory bowel diseases. *Inflammatory bowel diseases* **2009,** *15* (1), 100-13.

99. König, J.; Wells, J.; Cani, P. D.; García-Ródenas, C. L.; MacDonald, T.; Mercenier, A.; Whyte, J.; Troost, F.; Brummer, R.-J., Human Intestinal Barrier Function in Health and Disease. *Clin Transl Gastroenterol* **2016,** *7* (10), e196-e196.

100. Johansson, M. E. V.; Larsson, J. M. H.; Hansson, G. C., The two mucus layers of colon are organized by the MUC2 mucin, whereas the outer layer is a legislator of host-microbial interactions. *P Natl Acad Sci USA* **2011,** *108*, 4659-4665.

101. Johansson, M. E.; Gustafsson, J. K.; Sjoberg, K. E.; Petersson, J.; Holm, L.; Sjovall, H.; Hansson, G. C., Bacteria penetrate the inner mucus layer before inflammation in the dextran sulfate colitis model. *PLoS One* **2010,** *5* (8), e12238.

102. Sovran, B.; Lu, P.; Loonen, L. M.; Hugenholtz, F.; Belzer, C.; Stolte, E. H.; Boekschoten, M. V.; van Baarlen, P.; Smidt, H.; Kleerebezem, M.; de Vos, P.; Renes, I.

B.; Wells, J. M.; Dekker, J., Identification of Commensal Species Positively Correlated with Early Stress Responses to a Compromised Mucus Barrier. *Inflammatory bowel diseases* **2016,** *22* (4), 826-40.

103. Marteyn, B.; Gazi, A.; Sansonetti, P., Shigella: a model of virulence regulation in vivo. *Gut Microbes* **2012,** *3* (2), 104-120.

104. Croxen, M. A.; Law, R. J.; Scholz, R.; Keeney, K. M.; Wlodarska, M.; Finlay, B. B., Recent advances in understanding enteric pathogenic Escherichia coli. *Clin Microbiol Rev* **2013,** *26* (4), 822-880.

105. Hering, N. A.; Fromm, A.; Kikhney, J.; Lee, I.-F. M.; Moter, A.; Schulzke, J. D.; Bücker, R., Yersinia enterocolitica Affects Intestinal Barrier Function in the Colon. *The Journal of Infectious Diseases* **2015,** *213* (7), 1157-1162.

106. Furter, M.; Sellin, M. E.; Hansson, G. C.; Hardt, W. D., Mucus Architecture and Near-Surface Swimming Affect Distinct Salmonella Typhimurium Infection Patterns along the Murine Intestinal Tract. *Cell Rep* **2019,** *27* (9), 2665-2678.e3.

107. Sansonetti, P. J., War and peace at mucosal surfaces. *Nature Reviews Immunology* **2004,** *4*, 953.

108. Lee, S. H., Intestinal Permeability Regulation by Tight Junction: Implication on Inflammatory Bowel Diseases. *Intestinal Research* **2015,** *13* (1), 11-18.

109. Kucharzik, T.; Hudson, J. T., 3rd; Lügering, A.; Abbas, J. A.; Bettini, M.; Lake, J. G.; Evans, M. E.; Ziegler, T. R.; Merlin, D.; Madara, J. L.; Williams, I. R., Acute induction of human IL-8 production by intestinal epithelium triggers neutrophil infiltration without mucosal injury. *Gut* **2005,** *54* (11), 1565-1572.

110. Bain, C. C.; Bravo-Blas, A.; Scott, C. L.; Gomez Perdiguero, E.; Geissmann, F.; Henri, S.; Malissen, B.; Osborne, L. C.; Artis, D.; Mowat, A. M., Constant replenishment from circulating monocytes maintains the macrophage pool in the intestine of adult mice. *Nature Immunology* **2014,** *15*, 929.

111. Iliev, I. D.; Spadoni, I.; Mileti, E.; Matteoli, G.; Sonzogni, A.; Sampietro, G. M.; Foschi, D.; Caprioli, F.; Viale, G.; Rescigno, M., Human intestinal epithelial cells promote the differentiation of tolerogenic dendritic cells. *Gut* **2009,** *58* (11), 1481-1489.

112. Leon, C. G.; Tory, R.; Jia, J.; Sivak, O.; Wasan, K. M., Discovery and Development of Toll-Like Receptor 4 (TLR4) Antagonists: A New Paradigm for Treating Sepsis and Other Diseases. *Pharmaceutical Research* **2008,** *25* (8), 1751-1761.

113. Hayashi, F.; Smith, K. D.; Ozinsky, A.; Hawn, T. R.; Yi, E. C.; Goodlett, D. R.; Eng, J. K.; Akira, S.; Underhill, D. M.; Aderem, A., The innate immune response to bacterial flagellin is mediated by Toll-like receptor 5. *Nature* **2001,** *410* (6832), 1099-103.

114. Hoshino, K.; Takeuchi, O.; Kawai, T.; Sanjo, H.; Ogawa, T.; Takeda, Y.; Takeda, K.; Akira, S., Cutting Edge: Toll-Like Receptor 4 (TLR4)-Deficient Mice Are Hyporesponsive to Lipopolysaccharide: Evidence for TLR4 as the Lps Gene Product. *The Journal of Immunology* **1999,** *162* (7), 3749-3752.

115. Mazzucchelli, L.; Hauser, C.; Zgraggen, K.; Wagner, H.; Hess, M.; Laissue, J. A.; Mueller, C., Expression of interleukin-8 gene in inflammatory bowel disease is related to the histological grade of active inflammation. *The American Journal of Pathology* **1994,** *144* (5), 997-1007.

116. Neurath, M. F., Cytokines in inflammatory bowel disease. *Nat Rev Immunol* **2014,** *14* (5), 329-42.

117. Crum-Cianflone, N. F., Salmonellosis and the gastrointestinal tract: more than just peanut butter. *Curr Gastroenterol Rep* **2008,** *10* (4), 424-431.

118. Eng, S.-K.; Pusparajah, P.; Ab Mutalib, N.-S.; Ser, H.-L.; Chan, K.-G.; Lee, L.-H., Salmonella: A review on pathogenesis, epidemiology and antibiotic resistance. *Frontiers in Life Science* **2015,** *8* (3), 284-293.

119. Garcia Rodriguez, L. A.; Ruigomez, A.; Panes, J., Acute gastroenteritis is followed by an increased risk of inflammatory bowel disease. *Gastroenterology* **2006,** *130* (6), 1588-94.

120. Porter, C. K.; Tribble, D. R.; Aliaga, P. A.; Halvorson, H. A.; Riddle, M. S., Infectious gastroenteritis and risk of developing inflammatory bowel disease. *Gastroenterology* **2008,** *135* (3), 781-6.

121. Gradel, K. O.; Nielsen, H. L.; Schonheyder, H. C.; Ejlertsen, T.; Kristensen, B.; Nielsen, H., Increased short- and long-term risk of inflammatory bowel disease after salmonella or campylobacter gastroenteritis. *Gastroenterology* **2009,** *137* (2), 495-501.

122. Nevola, J. J.; Laux, D. C.; Cohen, P. S., In vivo colonization of the mouse large intestine and in vitro penetration of intestinal mucus by an avirulent smooth strain of Salmonella typhimurium and its lipopolysaccharide-deficient mutant. *Infection and immunity* **1987,** *55* (12), 2884-90.

123. McCormick, B. A.; Stocker, B. A.; Laux, D. C.; Cohen, P. S., Roles of motility, chemotaxis, and penetration through and growth in intestinal mucus in the ability of an avirulent strain of Salmonella typhimurium to colonize the large intestine of streptomycin-treated mice. *Infection and immunity* **1988,** *56* (9), 2209-17.

124. Vimal, D. B.; Khullar, M.; Gupta, S.; Ganguly, N. K., Intestinal mucins: the binding sites for Salmonella typhimurium. *Molecular and cellular biochemistry* **2000,** *204* (1-2), 107-17.

125. Hallstrom, K.; McCormick, B., Salmonella Interaction with and Passage through the Intestinal Mucosa: Through the Lens of the Organism. *Frontiers in Microbiology* **2011,** *2* (88).

126. Linden, S. K.; Sutton, P.; Karlsson, N. G.; Korolik, V.; McGuckin, M. A., Mucins in the mucosal barrier to infection. *Mucosal Immunology* **2008,** *1* (3), 183-197.

127. Wang, Y.; Gunasekara, D. B.; Reed, M. I.; DiSalvo, M.; Bultman, S. J.; Sims, C. E.; Magness, S. T.; Allbritton, N. L., A microengineered collagen scaffold for generating a polarized crypt-villus architecture of human small intestinal epithelium. *Biomaterials* **2017,** *128*, 44-55.

128. Noel, G.; Baetz, N. W.; Staab, J. F.; Donowitz, M.; Kovbasnjuk, O.; Pasetti, M. F.; Zachos, N. C., A primary human macrophage-enteroid co-culture model to investigate mucosal gut physiology and host-pathogen interactions. *Scientific reports* **2017,** *7*, 45270-45270.

129. Leonard, F.; Collnot, E. M.; Lehr, C. M., A three-dimensional coculture of enterocytes, monocytes and dendritic cells to model inflamed intestinal mucosa in vitro. *Molecular pharmaceutics* **2010,** *7* (6), 2103-19.

130. Kim, H. J.; Huh, D.; Hamilton, G.; Ingber, D. E., Human gut-on-a-chip inhabited by microbial flora that experiences intestinal peristalsis-like motions and flow. *Lab on a chip* **2012,** *12* (12), 2165-74.

131. Behrens, I.; Stenberg, P.; Artursson, P.; Kissel, T., Transport of Lipophilic Drug Molecules in a New Mucus-Secreting Cell Culture Model Based on HT29-MTX Cells. *Pharmaceutical Research* **2001,** *18* (8), 1138-1145.

132. Mahler, G. J.; Shuler, M. L.; Glahn, R. P., Characterization of Caco-2 and HT29-MTX cocultures in an in vitro digestion/cell culture model used to predict iron bioavailability. *The Journal of Nutritional Biochemistry* **2009,** *20* (7), 494-502.

133. Wang, Y.; Kim, R.; Sims, C. E.; Allbritton, N. L., Building a Thick Mucus Hydrogel Layer to Improve the Physiological Relevance of In Vitro Primary Colonic Epithelial Models. *Cellular and Molecular Gastroenterology and Hepatology* **2019,** *8* (4), 653-655.e5.

134. Sontheimer-Phelps, A.; Chou, D. B.; Tovaglieri, A.; Ferrante, T. C.; Duckworth, T.; Fadel, C.; Frismantas, V.; Sutherland, A. D.; Jalili-Firoozinezhad, S.; Kasendra, M.; Stas, E.; Weaver, J. C.; Richmond, C. A.; Levy, O.; Prantil-Baun, R.; Breault, D. T.; Ingber, D. E., Human Colon-on-a-Chip Enables Continuous In Vitro Analysis of Colon Mucus Layer Accumulation and Physiology. *Cellular and Molecular Gastroenterology and Hepatology* **2019**.

135. Celli, J.; Gregor, B.; Turner, B.; Afdhal, N. H.; Bansil, R.; Erramilli, S., Viscoelastic Properties and Dynamics of Porcine Gastric Mucin. *Biomacromolecules* **2005,** *6* (3), 1329-1333.

136. Lieleg, O.; Lieleg, C.; Bloom, J.; Buck, C. B.; Ribbeck, K., Mucin biopolymers as broad-spectrum antiviral agents. *Biomacromolecules* **2012,** *13* (6), 1724-32.

137. Wheeler, K. M.; Cárcamo-Oyarce, G.; Turner, B. S.; Dellos-Nolan, S.; Co, J. Y.; Lehoux, S.; Cummings, R. D.; Wozniak, D. J.; Ribbeck, K., Mucin glycans attenuate the virulence of Pseudomonas aeruginosa in infection. *Nature Microbiology* **2019**.

138. Sharma, A.; Kwak, J.-G.; Kolewe, K. W.; Schiffman, J. D.; Forbes, N. S.; Lee, J., In vitro reconstitution of an intestinal mucus layer shows that cations and pH control the pore structure that regulates its permeability and barrier function. *ACS Applied Bio Materials* **2020,** 3, 5, 2897–2909.

139. Chow, J. C.; Young, D. W.; Golenbock, D. T.; Christ, W. J.; Gusovsky, F., Toll-like Receptor-4 Mediates Lipopolysaccharide-induced Signal Transduction. *Journal of Biological Chemistry* **1999,** *274* (16), 10689-10692.

140. Mosberg, J. A.; Lajoie, M. J.; Church, G. M., Lambda red recombineering in Escherichia coli occurs through a fully single-stranded intermediate. *Genetics* **2010,** *186* (3), 791-9.

141. Kamada, N.; Chen, G. Y.; Inohara, N.; Núñez, G., Control of pathogens and pathobionts by the gut microbiota. *Nat Immunol* **2013,** *14* (7), 685-690.

142. Gillis, C. C.; Hughes, E. R.; Spiga, L.; Winter, M. G.; Zhu, W.; Furtado de Carvalho, T.; Chanin, R. B.; Behrendt, C. L.; Hooper, L. V.; Santos, R. L.; Winter, S. E., Dysbiosis-Associated Change in Host Metabolism Generates Lactate to Support Salmonella Growth. *Cell Host Microbe* **2018,** *23* (1), 54-64.e6.

143. Diard, M.; Sellin, Mikael E.; Dolowschiak, T.; Arnoldini, M.; Ackermann, M.; Hardt, W.-D., Antibiotic Treatment Selects for Cooperative Virulence of Salmonella Typhimurium. *Current Biology* **2014,** *24* (17), 2000-2005.

144. Stecher, B.; Hapfelmeier, S.; Müller, C.; Kremer, M.; Stallmach, T.; Hardt, W.-D., Flagella and Chemotaxis Are Required for Efficient Induction of Salmonella enterica Serovar Typhimurium Colitis in Streptomycin-Pretreated Mice. *Infection and Immunity* **2004,** *72* (7), 4138.

145. Stecher, B.; Barthel, M.; Schlumberger, M. C.; Haberli, L.; Rabsch, W.; Kremer, M.; Hardt, W. D., Motility allows S. Typhimurium to benefit from the mucosal defence. *Cellular microbiology* **2008,** *10* (5), 1166-80.

146. Natsui, M.; Kawasaki, K.; Takizawa, H.; Hayashi, S. I.; Matsuda, Y.; Sugimura, K.; Seki, K.; Narisawa, R.; Sendo, F.; Asakura, H., Selective depletion of neutrophils by a monoclonal antibody, RP-3, suppresses dextran sulphate sodium-induced colitis in rats. *Journal of gastroenterology and hepatology* **1997,** *12* (12), 801-8.

147. Zhou, G. X.; Liu, Z. J., Potential roles of neutrophils in regulating intestinal mucosal inflammation of inflammatory bowel disease. *Journal of Digestive Diseases* **2017,** *18* (9), 495-503.

148. Hafez, M. M., Upregulation of Intestinal Mucin Expression by the Probiotic Bacterium E. coli Nissle 1917. *Probiotics and antimicrobial proteins* **2012,** *4* (2), 67-77.

149. Gareau, M. G.; Sherman, P. M.; Walker, W. A., Probiotics and the gut microbiota in intestinal health and disease. *Nat Rev Gastroenterol Hepatol* **2010,** *7*.

150. Abraham, B. P.; Quigley, E. M. M., Probiotics in Inflammatory Bowel Disease. *Gastroenterology clinics of North America* **2017,** *46* (4), 769-782.

151. El Hage, R.; Hernandez-Sanabria, E.; Van de Wiele, T., Emerging Trends in "Smart Probiotics": Functional Consideration for the Development of Novel Health and Industrial Applications. *Frontiers in microbiology* **2017,** *8*, 1889.

152. Derwa, Y.; Gracie, D. J.; Hamlin, P. J.; Ford, A. C., Systematic review with meta-analysis: the efficacy of probiotics in inflammatory bowel disease. *Alimentary pharmacology & therapeutics* **2017,** *46* (4), 389-400.

153. Brugiroux, S.; Beutler, M.; Pfann, C.; Garzetti, D.; Ruscheweyh, H.-J.; Ring, D.; Diehl, M.; Herp, S.; Lötscher, Y.; Hussain, S.; Bunk, B.; Pukall, R.; Huson, D. H.; Münch, P. C.; McHardy, A. C.; McCoy, K. D.; Macpherson, A. J.; Loy, A.; Clavel, T.; Berry, D.; Stecher, B., Genome-guided design of a defined mouse microbiota that confers colonization resistance against Salmonella enterica serovar Typhimurium. *Nature Microbiology* **2016,** *2* (2), 16215.

154. Mimura, T.; Rizzello, F.; Helwig, U.; Poggioli, G.; Schreiber, S.; Talbot, I. C.; Nicholls, R. J.; Gionchetti, P.; Campieri, M.; Kamm, M. A., Once daily high dose probiotic therapy (VSL#3) for maintaining remission in recurrent or refractory pouchitis. *Gut* **2004,** *53* (1), 108.

155. Ekmekciu, I.; Fiebiger, U.; Stingl, K.; Bereswill, S.; Heimesaat, M. M., Amelioration of intestinal and systemic sequelae of murine Campylobacter jejuni infection by probiotic VSL#3 treatment. *Gut Pathog* **2017,** *9*, 17-17.

156. Selinger, C. P.; Bell, A.; Cairns, A.; Lockett, M.; Sebastian, S.; Haslam, N., Probiotic VSL#3 prevents antibiotic-associated diarrhoea in a double-blind, randomized, placebo-controlled clinical trial. *Journal of Hospital Infection* **2013,** *84* (2), 159-165.

157. Gaudier, E.; Michel, C.; Segain, J.-P.; Cherbut, C.; Hoebler, C., The VSL# 3 Probiotic Mixture Modifies Microflora but Does Not Heal Chronic Dextran-Sodium Sulfate–Induced Colitis or Reinforce the Mucus Barrier in Mice. *The Journal of Nutrition* **2005,** *135* (12), 2753-2761.

158. Macfarlane, S.; Woodmansey, E. J.; Macfarlane, G. T., Colonization of mucin by human intestinal bacteria and establishment of biofilm communities in a two-stage continuous culture system. *Appl Environ Microbiol* **2005,** *71* (11), 7483-92.

159. Ekmekciu, I.; von Klitzing, E.; Fiebiger, U.; Neumann, C.; Bacher, P.; Scheffold, A.; Bereswill, S.; Heimesaat, M. M., The Probiotic Compound VSL#3 Modulates Mucosal, Peripheral, and Systemic Immunity Following Murine Broad-Spectrum Antibiotic Treatment. *Frontiers in Cellular and Infection Microbiology* **2017,** *7* (167).

160. Sharma, A.; Raman, V.; Lee, J.; Forbes, N. S., Mucus blocks probiotics but increases penetration of motile pathogens and induces TNF-α and IL-8 secretion. *Biotechnology and Bioengineering* **2020,** *; 117:* 2540– 2555.

161. Yurist-Doutsch, S.; Arrieta, M.-C.; Tupin, A.; Valdez, Y.; Antunes, L. C. M.; Yen, R.; Finlay, B. B., Nutrient Deprivation Affects Salmonella Invasion and Its Interaction with the Gastrointestinal Microbiota. *PLoS One* **2016,** *11* (7), e0159676-e0159676.

162. Nissle, A., Weiteres über Grundlagen und Praxis der Mutaflorbehandlung. *Dtsch Med Wochenschr* **1925,** *51* (44), 1809-1813.

163. Nissle, A., Ueber die Grundlagen einer neuen ursächlichen Bekämpfung der pathologischen Darmflora1. *Dtsch Med Wochenschr* **1916,** *42* (39), 1181-1184.

164. Schultz, M., Clinical use of E. coli Nissle 1917 in inflammatory bowel disease. *Inflammatory bowel diseases* **2008,** *14* (7), 1012-8.

165. Scaldaferri, F.; Gerardi, V.; Mangiola, F.; Lopetuso, L. R.; Pizzoferrato, M.; Petito, V.; Papa, A.; Stojanovic, J.; Poscia, A.; Cammarota, G.; Gasbarrini, A., Role and mechanisms of action of Escherichia coli Nissle 1917 in the maintenance of remission in ulcerative colitis patients: An update. *World J Gastroenterol* **2016,** *22* (24), 5505-5511.

166. Yang, Y.; Yang, Y.; Ou, B.; Xia, P.; Zhou, M.; Li, L.; Zhu, G., The flagellin hypervariable region is a potential flagella display domain in probiotic Escherichia coli strain Nissle 1917. *Archives of Microbiology* **2016,** *198* (7), 603-610.

167. Marteau, P.; Seksik, P.; Jian, R., Probiotics and intestinal health effects: a clinical perspective. *British Journal of Nutrition* **2007,** *88* (S1), s51-s57.

168. von Sonnenburg, F.; Tornieporth, N.; Waiyaki, P.; Lowe, B.; Peruski, L. F., Jr.; DuPont, H. L.; Mathewson, J. J.; Steffen, R., Risk and aetiology of diarrhoea at various tourist destinations. *Lancet (London, England)* **2000,** *356* (9224), 133-4.

169. Yates, J., Traveler's diarrhea. *American family physician* **2005,** *71* (11), 2095-100.